FIBER LASER WELDING OF NICKEL-BASED SUPERALLOY INCONEL 718

by

Omudhohwo Emaruke Oshobe

A Thesis submitted to the Faculty of Graduate Studies of

The University of Manitoba

in partial fulfilment of the requirements of the degree of

MASTER OF SCIENCE

Department of Mechanical and Manufacturing Engineering

University of Manitoba

Winnipeg

Abstract

Inconel 718 (IN 718) is widely used in applications, such as aircraft and power turbine components. Recently, fiber laser welding has become an attractive joining technique in industry for fabrication and repair of service-damaged components. However, a major limitation in the laser welding of IN 718 is that liquation cracking occurs. In the present work, autogenous fiber laser welding of IN 718 was used to study the effects of welding parameters and different pre-weld heat treatments on liquation cracking. Contrary to previous studies, a dual effect of heat input on cracking is observed. A rarely reported effect of heat input is attributed to process instability. Liquation cracking increases with pre-weld heat treatment temperatures that increase grain size and/or, possibly, intregranular boron segregation. The study shows that pre-weld heat treatment at 950^{o}C can be used for repair welding of IN 718 without significant loss in cracking resistance.

Acknowledgement

First of all, I will like to express my appreciation to my supervisor, Dr. O.A Ojo, for giving me the opportunity to work on this project and his instructions, suggestions and invaluable guidance throughout this study.

The financial support of NSERC and Standard Aero Ltd. is gratefully acknowledged. I will also like to thank the staff of Standard Aero Ltd. for performing the welds used for this project.

I have to express my gratitude to lab technicians, Don Mardis, John van Dorp and Mike Boswick for their continual assistance in the lab.

Special thanks go to Dr. N.L Richards and Dr. J. Beddoes for their helpful discussions and advice.

I want to say thanks to my friends/colleagues, James Arthur, Osoba Lawrence, Mark Amegadzie, Juhaina Hunedy, Mojtaba Montarezi, Oyedele Ola, Richard Akpreku Buckson, Ioannis Polyzois, Kwadwo Poku Owusu, John Dohie and Emmanuel Otchere Abrokwah, for their helpful conversation, constructive criticisms and for lending a helping hand when needed.

Many thanks go to Juliet Blouin and her wonderful family for giving me a home away from home. Finally, I would like to extend my heartfelt appreciation to my closest friends, Ioannis Polyzois, Juhaina Hunedy, Rekha Chaudhari and especially to my family for their unremitting support and encouragement.

Table of Contents

List of Figures

List of Tables

List of Copyrighted Materials for which Permission was Obtained

Figure 2.1: Source – "Welding Metallurgy" (2nd Ed) by Sindo Kuo. Reprinted with permission from the Global Rights Department, John Wiley & Sons, Inc. (June 04, 2012).

Figure 2.2: Source – "Welding Metallurgy" (2nd Ed) by Sindo Kuo. Reprinted with permission from the Global Rights Department, John Wiley & Sons, Inc. (June 04, 2012).

Figure 2.3: Source – "Welding Metallurgy" (2nd Ed) by Sindo Kuo. Reprinted with permission from the Global Rights Department, John Wiley & Sons, Inc. (June 04, 2012).

Figure 2.7: Source – "Analysis of Welded Structures" (1st Ed) by Koichi Masubuchi. Reprinted with permission from the author Koichi Masubuchi (May 08, 2012).

1 Introduction

1.1 Background

Inconel 718 (IN 718) is a γ" precipitation-hardened nickel-based superalloy [1]. The superalloy has been the workhorse in the jet gas turbine field for the past 60 years and accounts for a significant portion of superalloy production and usage [2, 3]. IN 718 has found use in high temperature applications, such as turbine disk blades, cases, tubes, fasteners, stators, seals, shafts, space shuttle rocket engines and compressors due to its excellent corrosion resistance and mechanical strength at high temperatures (up to 650^{o}C) [4, 5, 6, 7, 8]. The fabrication techniques used to produce the alloy and the operational conditions affect the life of IN 718 components. In some cases, the use of a simple single cast component instead of a welded assembly significantly saves on costs, but the cast material has generally poorer properties and is more difficult to weld than wrought material owing to its inhomogeneous nature [1, 7, 9]. Improved fabrication and repair techniques for the alloy are of interest because turbine engines and their components are subjected to fatigue cracking and extensive wear [2, 10], which can lead to failure. The increase in cost of superalloys and high cost of manufacturing turbine components fosters research on repair methods that use fusion welding rather than replacing failed parts to restore structural integrity [10, 11].

Laser welding has an ever growing role in the manufacturing industry, such as the aerospace industry [12, 13]. High power laser welding is becoming wide-spread and one of the latest developments is the fiber laser which has a high power laser range [12, 14].

Laser welding has been lately promoted over other conventional welding processes due to its advantages, such as high quality joining with deep penetration at high speeds, as well as low heat input, which minimizes deterioration of mechanical properties, cold cracking and distortion [13, 15, 16, 17, 18]. High brightness fiber lasers are well-received because they have superior beam quality, high efficiency, a flexible fiber optic delivery system and lower operating cost [19, 20, 21].

1.2 Motivation and Purpose of Study

Several studies have been carried out in the past on welding of wrought and cast IN 718. Previous studies have shown that liquation cracking in the area around the weld, heat-affected zone (HAZ), is highly influenced by welding parameters (heat input) and metallurgical factors. HAZ liquation cracking, which occurs in welded superalloys, has been attributed to the metallurgical factors, such as material composition and pre-weld heat treatment conditions [22, 23, 24]. Currently, laser welding research involves investigation on the influence of process parameters on the occurrence of cracking in welded alloys [4]. There is limited information on high power fiber laser beam welding because the process is new; hence, its influence on microstructure of welded alloys is not yet fully understood [12].

It is prudent to apply proven effective joining techniques in safety demanding industries, like the aerospace industry. The lack of database of fiber laser welding motivated this research to investigate and gain more understanding of the process. The present study

investigates the influence of heat input, a factor of welding parameters –fiber laser power and welding speed, on susceptibility to HAZ liquation cracking of welded wrought IN 718. This research also involves a study of the effect of pre-weld heat treatment on HAZ cracking susceptibility in wrought and cast IN 718.

1.3 Research Method

The microstructure of IN 718 is examined using optical and electron microscopes before and after it is subjected to pre-weld heat treatments. Fiber laser bead-on-plate welding, using various powers and speeds, is performed on IN 718 material that had been previously heat-treated. The welds are sectioned transversely to produce 10 cross-sections, which are then prepared using standard metallographic methods. Subsequently, general examination using optical microscopes is carried out on the prepared specimens of the welds to determine geometry. This is followed by more detailed microstructural examination of the 10 cross-sections of each weld using a scanning electron microscope to determine total crack lengths (TCL) and microstructural changes in the different weld regions.

1.4 Findings

Fiber laser welding carried out with 2.5kW laser power shows that increase in heat input reduces HAZ cracking and produces good quality welds. In contrast, welding at higher

levels of power, which also increases heat input, results in increase in HAZ cracking and poor quality of welds. The latter effect of heat input on cracking is attributable to the phenomenon of process instability. The result of the research shows that HAZ cracking in IN 718 alloy during fiber laser welding can be minimized by subjecting the alloy to pre-weld heat treatment that ,possibly, minimizes non-equilibrium intergranular boron segregation and inhibits grain growth in fine grained material.

1.5 Scope of Work

This thesis comprises of six chapters:

- Chapter one outlines the motivation and a brief description of this investigation.
- Chapter two provides relevant literature on the research topic, in addition, the objectives of the study are detailed.
- Chapter three outlines the experimental methods used.
- Chapter four contains the results and the discussion of results in this study.
- Chapter five and six include the conclusions and the suggestions for future work respectively.

2 Literature Review

2.1 Background

Some of the ways that alloying elements increase strength of metals are by solid solution strengthening and precipitation hardening. Solid solution hardening involves the introduction of solute atoms to occupy positions in the solvent-atom lattice (solid solution), which results in an alloy stronger than the pure metal [25]. Alloying elements can also promote precipitation of particles. Precipitation strengthening occurs when secondary phase particles are coherently precipitated in a finely distributed fashion in an alloy matrix after isothermal treatment at relatively low temperatures [25]. Alloys are often referred to as “ superalloys ” based on their maintenance of unusually superior strength and corrosion resistance at elevated temperatures [26]. They hold complex precipitation strengthening mechanisms that are needed to provide high temperature strength in service, which encourages their use in applications of relatively severe mechanical stress and where surface stability is required [26, 27]. Superalloys, therefore, are the primary materials used to produce gas turbines that drive jet aircraft. There is continued production of superalloys for medium and high temperature sections of turbines as well as other new applications such as petrochemical equipment, nuclear reactors and power plants [26].

Superalloys are available in cast (solidified ingot) and wrought (heat treated and processed into sheets or plates) forms [28]. Superalloys need to be joined for fabrication of intricate shapes and repair. Superalloys can be joined by arc, electron and laser beam

fusion welding processes [28]. The welding of these alloys is problematic due to their highly-alloyed nature and inherent capability of precipitation hardening [27]. Strengthening mechanisms often interact in a damaging manner with thermal conditions and stresses generated during welding or subsequent high temperature service [27]. Strain-age cracking occurs when rapid hardening (aging) develops due to fast precipitation and coarsening of hardening particles during cooling and heating, respectively. The developed strains that follow are transferred from the weld to the material, which cause cracks [27]. Weld defects and other forms of cracking, such as liquation cracking, can occur due to the welding method and material composition.

Precipitation-strengthened nickel-based superalloys are generally strengthened by the γ'(Ni_3Al,Ti) and γ''(**Ni_3Nb**) precipitates. γ'(Ni_3Al,Ti) precipitation-strengthened superalloys, Rene 41, Udimet 700 (with higher amounts of precipitation than IN 718), Inconel X-750 and Waspalloy (with similar amounts of precipitation as IN 718) are prone to strain-age cracking, which makes it difficult to produce satisfactory parts [1, 7]. The major factors that favour the use of IN 718 include: that it is less prone to cracking (more weldable) and has high strength stability at elevated temperatures.

A review of the literature on the metallurgy and the roles of the alloying elements of IN 718 has been summarized. The ways in which superalloys are produced, common fusion welding methods and previously studied methods used for welding IN 718 are reviewed. Consideration is taken for literature on the effect of welding on the microstructure of

alloys, theories used to describe weld microstructure, such as solidification, constitutional liquation, liquation cracking and reported factors that affect liquation cracking.

2.2 Metallurgy of Inconel 718 (IN 718)

The search for a solution-strengthened non-age hardenable alloy steered the development of IN 718, which lead to further improvement of gas-turbine jet propelled aircraft, and IN 718 has played a continual role in the jet age [1, 7, 29]. IN 718 was produced in the late 1950's and introduced, in the early 1960's by H.L Eiselstein/Huntington, to an alloy division of the International Nickel Company (INCO) [7, 30, 31]. The alloy is currently used in cast, wrought and powder form [7, 30, 31]. There is a lesser amount of aluminium (Al) and titanium (Ti) in IN 718, which cause precipitation hardening by the γ" **(**Ni_3Nb) phase instead of the γ' phase (Ni_3 Al, Ti) [14]. Weldability and stability are apparently due to the sluggishness of precipitation, aging response and transformation kinetics of the coherent strengthening phase γ" in the nickel-based alloy. This behaviour of γ" limits strengthening during welding, which relaxes weld-induced stresses and preventing strain-age cracking during post weld aging heat treatment [7, 30, 32, 33, 34]. The alloy has reasonably good resistance to fusion-zone (FZ) cracking and comparable sensitivity to cracking in the HAZ, like other chromium (Cr)/nickel (Ni) and Cr-iron (Fe) alloys [1].

IN 718 was designed for high temperature and pressure applications that require high strength and long term metallurgically stable alloys at 650^{o}C to 760^{o}C [1]. It has also

found use in cryogenic temperatures for space shuttle engines [7]. However, when application temperatures rise above 650^{o}C, the alloy strength deteriorates [3, 7, 32].

2.2.1 Microstructural Phases in IN 718

IN 718 has different phases which can be identified by characteristic morphology or temperature of formation if the thermal history of the alloy is known [35]. The phases normally found in the γ matrix of IN 718 are disk-shaped γ" (Ni_3Nb), spheroidal γ' (Ni_3Al, Ti), needle/plate-like δ phase, discrete metal-carbide (MC) particles and round, island-like Laves phase [35, 36].

The major strengthening phases are the γ" and γ' phases, which strengthen the alloy by producing coherency strains in the γ matrix [31]. The alloy is known to have exceptionally high strength from cryogenic to intermediate temperatures, in considering the relatively low volume fraction of strengthening precipitates and their sluggish precipitation kinetics [7, 32]. In a fully strengthened condition, the amount of precipitates is just about 19wt% of which γ" and γ' have been reported to be 15wt% and 4wt% respectively [32].

Gamma Matrix (γ)

IN 718 is made of a face centered cubic (FCC) nickel-based austenitic matrix phase called gamma (γ) which contains alloying elements, such as Ni, Cr, Fe and

molybdenum(Mo) for strength and stability. The γ matrix is a base on which the other phases are formed.

Gamma double prime (γ") Phase

The metastable γ" phase is the principal strengthening phase in IN 718 since its body centered tetragonal (BCT) crystal lattice structure offers a higher coherency strain than γ' [32, 36, 37]. γ" is a DO_2 ordered Ni_3Nb phase with a lattice parameter ratio c/a =2.04 and it strengthens the alloy due to strains that arise from the tetragonal distortion of its lattice, which is a mismatch with the FCC γ matrix [32, 37, 38] . The precipitation of the γ" phase bestows a fully strengthened microstructure and acceptable ductility. During isothermal aging, γ" is precipitated at a temperature range of approximately 704°C - 899°C with a peak at 760°C for the shortest time of 7 minutes [30, 31]. Upon ingot solidification, γ" is precipitated in the alloy within the cooling temperature range of 815°C - 704°C [31]. Inconel 718 is stable at 600°C during long thermal exposure, but deterioration of its creep and tensile strengths can occur at higher temperatures due to:

1. rapid coarsening of the γ" phase at the range of 640°C - 760°C and possible loss of coherency,
2. coarsening and partial dissolution of γ" and γ' above 760°C decrease the volume fraction of these precipitates and

3. the accompanied transformation of metastable γ" and γ' to stable δ above 843^{o}C [3, 7, 26, 32, 36].

γ" precipitates have an average diameter of 600 angstrom and thickness of 50 - 90 angstrom in a fully heat treated condition [32].

Gamma prime (γ') Phase:

The γ' phase (Ni_3Al, Ti) is the secondary strengthening phase in IN 718 [32]. γ' is an LI_2 ordered intermetallic compound with an FCC crystal structure. It also produces a coherency strain with the matrix and is richer in Al than γ". Upon ingot solidification, the precipitation of γ' occurs below 704^{o}C and during isothermal aging from 593^{o}C - 704^{o}C [31]. It has been suggested that the solvus temperature for γ' in IN 718 is between 843^{o}C - 871^{o}C [32]. Its shape is related to the matrix-lattice mismatch. Hagel and Beattie [39] observed that the γ' phase appears as a sphere at a 0.2% lattice mismatch, becomes cubes at lattice mismatch around 0.5%-1.0% and then is in plate form at mismatch above approximately 1.25%.

Delta (δ) Phase

The equilibrium δ phase is a stable, Ni_3Nb, intermetallic with an orthorhombic (DO_a ordered) crystal structure [32]. The δ phase is sometimes considered undesirable because it is incoherent with the γ matrix and, therefore, is not an effective strengthener [29]. The

approximate range of temperatures in which the δ phase precipitates is 843^{o}C - 982 °C [35] in the form of platelets and its precipitation precedes the γ" and γ' phases at temperatures below 900^{o}C [26, 40]. The δ phase precipitates on grain boundaries (intergranularly), twin boundaries and intragranularly in association with stacking faults located within pre-existing γ" or Laves phase particles [1, 40]. The maximum precipitation rate of the δ phase is achieved at 900^{o}C [41]. In the absence of other grain boundary particles, such as carbides, the alternative nucleation of the δ phase in a uniform manner effectively controls and refines grain size, which affects material strength and ductility [1, 41]. The presence of globular δ phase at grain boundary inhibits long-range grain boundary sliding [26]. The dissolution temperature range of the δ phase is 925^{o}C-1010^{o}C [10].

Laves Phase

The brittle, topologically close pack (TCP) Laves phase can be represented as A_2B, where "A" atoms are primarily Ni, Fe, and Cr, and the "B" atoms are Nb, Mo, and Ti, i.e. $(Fe,Ni,Cr)_2$ (Nb, Mo, Ti) [34]. This phase forms as a result of the segregation of "B" atoms into liquid region (interdendritic) in between solidified material (dendrite) during cast solidification [1, 7]. Therefore, the Laves phase, like carbides, is a terminal solidification product formed on the grain boundary of IN 718 [42, 43]. This phase is detrimental to fatigue properties as well as the weldability of IN 718 [1, 7]. The Laves phase and Nb-rich MC carbides precipitate within a cooling temperature range of about

1260^{o}C - 1093^{o}C during solidification [31]. The hot isosatic pressing (HIP) solution temperature of the Laves phase is around 1191^{o}C [7]. The amount of the Laves phase in cast IN 718 can be used as an indicator of the degree of alloying elements homogeneity [1, 9] in IN 718 material.

Carbides

Refractory and reactive elements, Nb and Ti, combine with carbon (C) and nitrogen (N) to form MC phase particles [26, 28]. The carbides exhibit an FCC crystal structure and are promoted by the strong tendency of the forming elements to segregate into the liquid during solidification, which causes carbide distribution typically along the interdendritic and solidification grain boundary regions [29] i.e. localized areas that solidify last. The MC carbides and/or carbonitride can also be precipitated at grain boundaries during processing [26]. Their morphology is usually cubic, irregular or "Chinese script" shape. "Chinese script" morphology could suggest that formation of MC carbide occurred by eutectic-type transformation during the later stage of solidification [26]. The MC and titanium nitride (TiN) phases are considered stable at low temperatures [1, 28]. Their temperature stability is useful for grain refinement during processing and globular carbides prevent grain boundary sliding, which is beneficial for good rupture life and ductility [26, 28, 41]. In IN 718, titanium carbide (TiC) has a higher stability temperature than NbC [44].

2.2.2 Roles of Alloying Elements of IN 718

The chemical composition range of IN 718 is given in Table 2.1 [1, 36]. The principal alloying elements are Ni, Fe and Cr. Other alloying elements are Al, Mo, Nb and Ti. In addition, impurity elements, such as boron (B), sulphur (S) and phosphorus (P) [45] are present.

The following are intentional additions [26, 29]:

i. Ni, Cr, Fe and Mo for solid solution strengthening. These elements differ from the Ni atom by 1-13% in atomic diameter and preferable make up FCC matrix.

ii. Al, Ti and Nb for precipitation strengthening. These elements partition to form Ni_3X particles, where X represents these alloying elements.

iii. Cr and Al for oxidation resistance. These elements are formers of adherent, diffusion resistant oxides.

iv. Cr for hot corrosion resistance.

v. B, C for resistant to creep and stress rupture. These elements segregate to boundaries where they could form grain boundary phases.

Table 2.1 : Chemical Composition of IN 718

Element	wt%
Nickel (Ni)	50.00 - 55.00
Chromium (Cr)	17.00 - 21.00
Iron (Fe)	Balance
Niobium (Nb)	4.75 - 5.50
Molybdenum (Mo)	2.80 - 3.30
Aluminum (Al)	0.20 - 0.80
Titanium (Ti)	0.65 - 1.15
Manganese (Mn)	0.35 max
Silicon (Si)	0.35 max
Boron (B)	0.006max
Carbon (C)	0.08max
Sulphur (S)	0.15max
Magnesium (Mg)	Residual

Nickel and Iron

It is known that the austenite matrix of IN 718 is nickel-based and also contains Fe. The ratio of these elements also determine the cost and useful temperature of the alloy: a higher Fe addition reduces cost and improves formability, but reduces high temperature stability by limiting the degree to which the alloy can be strengthened [26]. Nickel is capable of dissolving a high amount of alloying elements, which aids its primary aim of solid solution strengthening and also promotes the ductile austenitic phase [29, 45].

Chromium

Chromium primarily provides corrosion resistance; however, it is also a component of brittle intermetallic compounds, such as the Laves phase [45]. A reduction of Cr content from 17% to 12% and an increase of Nb content to 6% and Ti to 2% reduce the Laves phase formation in IN 718 [7]. Cr also provides some degree of solution strengthening since it is a substitutional atom in the FCC crystal lattice [45].

Aluminum and Titanium

The addition of Al and Ti improves creep strength since they promote the precipitation of the ordered γ' (Ni_3Ti and Ni_3Al) phase for hardening [29, 45]. Alloys containing 4 wt% of Al and Ti in their content are deemed difficult to weld because they are prone to strain-

age cracking as a result of γ' rapid precipitation mechanism [27] . In weldable alloys, like IN 718, there are lower Al and Ti contents [44]. Ti is a strong carbide former [45].

Niobium

The ultimate strength of alloys is reduced when there is a limited amount of Al and Ti in the alloying element content [44]. However, the addition of Nb results in an aging response by the γ" phase, which increases strength and minimizes strain-age cracking that readily occurs with increased amount of Al and Ti [1, 44] . Niobium is a strong carbide former and a major constituent in two eutectic reactions, the MC and Laves eutectic, during solidification of IN 718 [9, 42, 45]. An increase in Nb content increases these secondary phases including δ phase [10, 42].

Molybdenum

Molybdenum expands the crystal lattice of nickel-based γ matrix and hence it is solid solution strengthener in IN 718 [26]. Also, Mo improves the elevated temperature strength [45]. The addition of Mo is useful for increasing creep strength due to its low diffusivity in Ni [26, 29].

Silicon

Silicon (Si) is known to improve fluidity and acts as a deoxidizer in alloys; however, it can segregate during solidification, which results in the formation of low melting eutectics, like Laves-γ eutectic [45, 46]. Silicon increases the stability of the Laves phase in IN 718 [1].

Carbon

Carbon is a deoxidant and forms the primary MC phase particles useful for refinement of grains and stress rupture properties. About 0.05-0.2% of C affects the chemical stability of the matrix through the removal of refractory and reactive elements, Nb and Ti, respectively [26]. For instance, C removes metallic elements such as Cr, from solid solution, which can degrade corrosion resistance in some alloys [45]. The concentration level of Nb and Ti control the formation of carbide.

Sulphur, Phosphorus and Boron

Sulphur is a surface-active element and hence is a grain boundary weakening element [47, 26]. Boron is added for hot malleability and stress rupture [1]. The addition of B is vital for grain boundary modification to block tearing under creep loading [26]. Alloying

elements, S and P, form low melting-point compounds with Fe and Ni, which cause embrittlement.

Manganese and Magnesium

Manganese (Mn) promotes austenite formation, affects solidification cracking [45] and acts as a deoxider in Ni-Fe alloys [26]. The segregation of S can be mitigated by the addition of Mn [47, 48]. Magnesium (Mg) improves the forgeability of wrought alloys [26]. Magnesium has high affinity for S and, therefore, Mg improves stress rupture by combining with S, which is detrimental to the ductility of nickel alloys [26, 28, 49]. Magnesium modifies grain boundary phases and morphologies thereby improving stress-rupture strength [26].

2.2.3 Cast and Wrought IN 718

Processing carried out on material before welding can affect its cracking susceptibility during welding [44].

2.2.3.1 **Cast IN 718**

Conventional casting involves the placing of a molten alloy mix into a mould of a definite shape to cool and solidify. Solidification will be discussed in section 2.3.5. Typically, conventional cast IN 718 microstructure contains γ dendrites as well as a mixture of eutectic Laves phase, carbide and δ phase particles in the interdendrictic

regions and boundaries [34, 42, 50]. The mixture of phases is the result of high segregation of Nb and other major alloying elements, like Mo and Ti, which partition into these phases [34, 42, 50]. On the other hand, the dendritic regions contain more of other refractory metals. Therefore, exhaustive heat treatments, such as HIP, are sometimes necessary for microstructural homogenization of metallic elements [7]. HIP should be performed at an optimum temperature that is high enough to close pores, homogenize and improve strength without causing incipient melting of microconstituents, which will reduce fatigue capability [7, 26]. Precipitation reactions are highly dependent on Nb segregation and fast cooling rates can reduce re-precipitation of unwanted secondary phases [1, 44]. Ingot melting methods are used to reduce segregation in larger castings where localized inhomogenous areas occur due to the inability to control cooling rates during solidification [7]. Thermal processing alone is impracticable to homogenize cast IN 718 because hot working puts phases into the alloy solution, but the elemental constituents remain segregated and ready to precipitate the original phases present [9, 34, 42, 51]. Although cast alloys are more difficult to weld due to inhomogeneity, castings are intrinsically stronger than forgings at high temperature because an equiaxed coarse grained casting possesses higher temperature creep-rupture strength [28]. Micro-casting produces fewer defects and finer grain sizes that improve yield strength [7].

2.2.3.2 **Wrought IN 718**

To produce wrought alloy, ingots (large sized as-casted alloys) are normally converted to defined shaped billets prior to forging to refine the grain structure. Forging is done by a

variety of equipment to achieve further grain refinement [26, 28]. Improvements of this method lead to products of finer grain, which are suitable for applications in critical engine components [7]. Forging may form a stringer of carbides that makes such areas susceptible to cracking [51]. Homogenization is used to reduce segregation and eliminate brittle Laves phase precipitates in the as-cast or billet by static homogenization.

Wrought and cast material may need to be joined by methods, such as fusion welding. Like the other nickel-based superalloys, IN 718 is affected by defects, such as hot cracking i.e. HAZ liquation cracking during welding [4, 16].

2.3 Fusion Welding

Fusion welding involves the use of a heat source to cause melting and subsequent solidification forms a joint. The welding processes, such as tungsten inert gas (TIG), metal inert gas (MIG) , submerged arc, electron beam, plasma and laser welding have been used successfully in welding IN 718 [14, 52].

2.3.1 Gas and Arc Welding Processes

Gas and arc welding processes are well known and can be referred to as conventional fusion welding processes.

2.3.1.1 **Oxyacetylene Fusion Welding**

Oxyacetylene fusion welding utilizes a flame, produced by a mixture of acetylene and oxygen, to heat metals for melting and joining. A typical set up for this process is shown in Figure 2.1. It is difficult to focus the heat given off from the flame to a small area of the material being joined; hence, power density is low. Therefore, the flame requires a relatively long time for joining and high temperatures are maintained in that period, which could lead to microscopic porosity in nickel-based alloys [53, 54]. Low power density generally means oxyacetylene fusion welding has to be performed slowly to achieve melting, which results in a rather high total heat input per unit length of the weld and causes a large area of melting. Consequently, there is a large HAZ and severe distortion in the material.

2.3.1.2 **Tungsten Inert Gas and Plasma Arc Welding**

TIG welding, also known as gas tungsten arc welding (GTAW), uses an electric arc from a non-consumable tungsten electrode to produce the weld. The weld area is protected from atmospheric contamination by a shielding gas (usually an inert gas, such as argon), which is supplied through a shielding gas nozzle as shown in Figure 2.2. A filler metal is normally added, but there are cases were filler is not used (autogenous welding) [54]. TIG welding is often chosen due to its ability to meet key requirements of high precision and reliability [4, 17]. The main issue of this process is its dependence on manual skill for metal working and welding procedures [27].

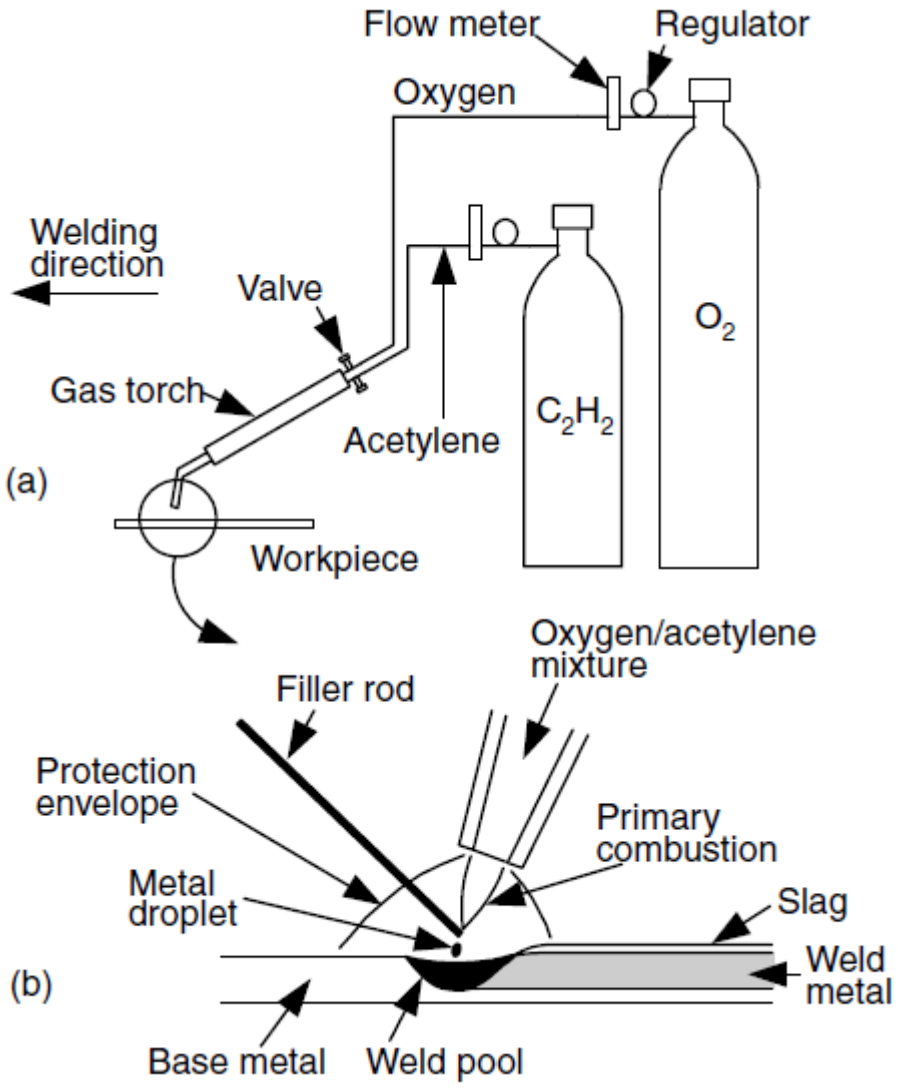

Figure 2.1: Oxyacetylene welding: (a) overall process (b) welding area enlarged [54]

Source:"Welding Metallurgy" (2nd Ed) by Sindo Kuo [54]. Reprinted with permission from the Global Rights Department, John Wiley & Sons, Inc. (June 04, 2012).

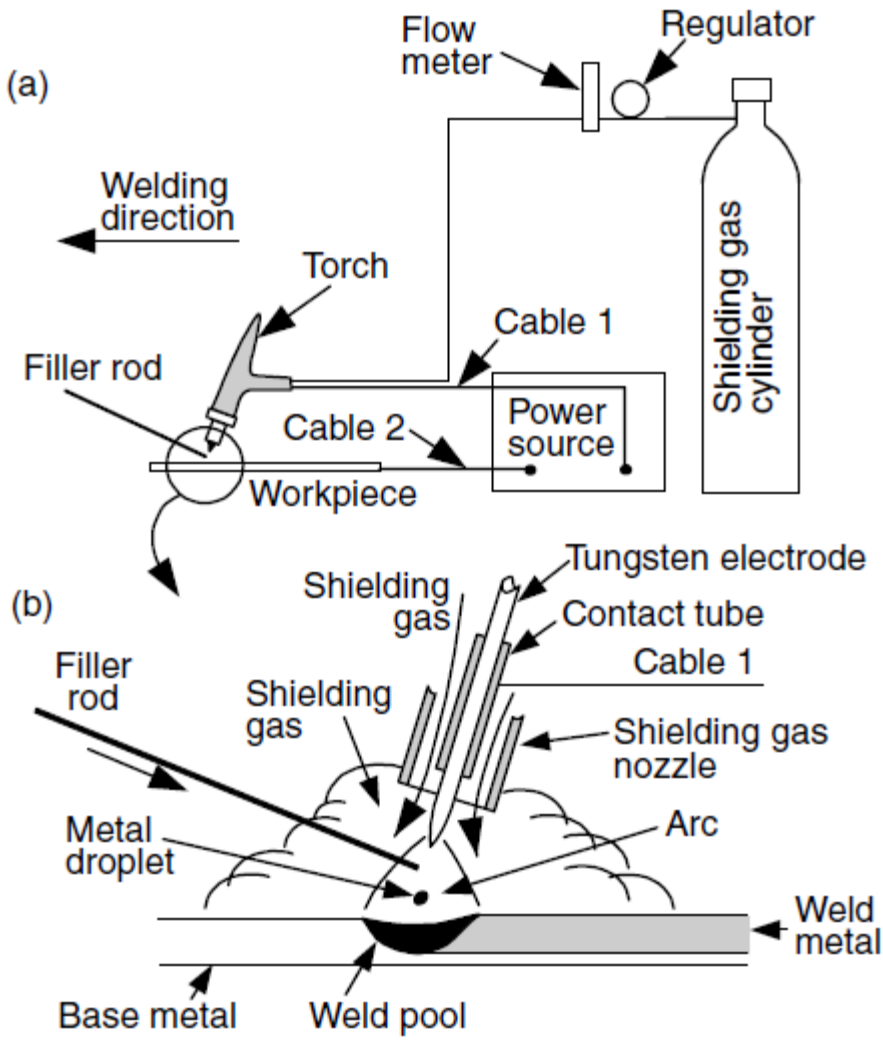

Figure 2.2: Gas-tungsten arc (a) overall process (b) welding area enlarged [54]

Source:"Welding Metallurgy" (2nd Ed) by Sindo Kuo [54]. Reprinted with permission from the Global Rights Department, John Wiley & Sons, Inc. (June 04, 2012).

Also, the short arc length can cause a welder to involuntarily contact the molten alloy with the electrode tip, thus contaminating the weld with tungsten [54]. For a single, welding pass over an alloy with no filler, this weld process is limited to thin sheets and can be done at slow welding speeds [54].

A similar process, plasma arc welding (PAW), uses a slightly different welding torch, which has additional orifice gas nozzle with a converging action for a more focused welding arc. However, the PAW torch is more complicated, requiring strict welding parameter configuration e.g. selection and setting of orifices and electrode tip position, and it is more expensive than GTAW [54].

2.3.1.3 **Metal Inert Gas Welding**

MIG welding is also known as gas-metal arc welding. An arc is established between a continuously fed filler wire and the metal being joined [54]. Shielding gas is often used and could be inert or non inert gas.

The skill requirement for MIG welding is not as high as that of TIG welding, but the MIG torch is bulky and is unsuitable for small area or corners that are difficult to reach [54].

2.3.1.4 **Submerged Arc Welding**

Submerged arc welding (SAW) is similar to other arc welding processes, such as MIG, where the melting and joining of metal is carried out by an arc established between a

consumable, filler-wire electrode and the metal being joined. In SAW, shielding is achieved by molten slag and granular flux supplied by a hopper, which travels with the torch. Therefore, the difference in this case is that the arc is submerged and thus invisible [54]. The submerging of the arc mitigates splashing of molten metal, which can cause spatters and heat loss from the process to the environment [54]. The shortcoming of this process is that it is limited to welding of flat or circumferential objects [54].

2.3.2 High Power Density Welding Processes

High power density welding processes are more recent and improved to attain higher power densities than those achieved by conventional gas and electric arc welding.

2.3.2.1 Electron Beam Welding

Electron beam welding (EBW) is a process whereby heating to cause joining is achieved by bombarding the alloy with electrons from an electron beam. This process is capable of achieving heat input far higher than conventional electric arc welding. The high intensity parallel beam of electrons allows for deeper penetration and narrow weld melts suitable for close tolerances, hence the EBW process has proven to be very reliable [4, 17]. EBW is one of the most demanded types of welding from the perspective of cracking [1]. A downside of EBW is the requirement for a vacuum and x-ray shielding [54].

2.3.2.2 **Laser Beam Welding (LBW)**

A laser device converts energy from a primary source into a beam of electromagnetic radiation at a specific frequency. The conversion is made possible by a medium (solid or gas), which is "pumped" or excited on a molecular or atomic scale to a high energy level. Excited molecules on transition to a lower energy level will emit a coherent, relatively monochromatic (singular frequency) form of light – a laser beam [55]. This is shown in Figure 2.3a. The laser is multi-reflected for amplification, directed and focused to a small spot size by optical means to achieve high power densities [54, 55]. Laser welding uses heat obtained from this concentrated laser beam to join alloys [55, 56].

Initially, the absorption of heat normally occurs through conduction and convection or radiation into the surrounding material [55, 57, 58]. Power density above $10^6 W/Cm^2$ is needed for deep penetration welding. The heat raises the material to temperatures that cause local melting and vaporization, the resultant vapour recoil pressure forms a deep conical column of vapour surrounded by molten metal, which is called a keyhole [55, 57, 59] (Figure 2.3b).

During welding, a balance between vapour pressure, surface tension and liquid hydrostatic forces has to be maintained to prevent keyhole collapses [57, 58]. The molten metal that surrounds the keyhole flows opposite to the welding direction, where it solidifies [55] to form the welded joint.

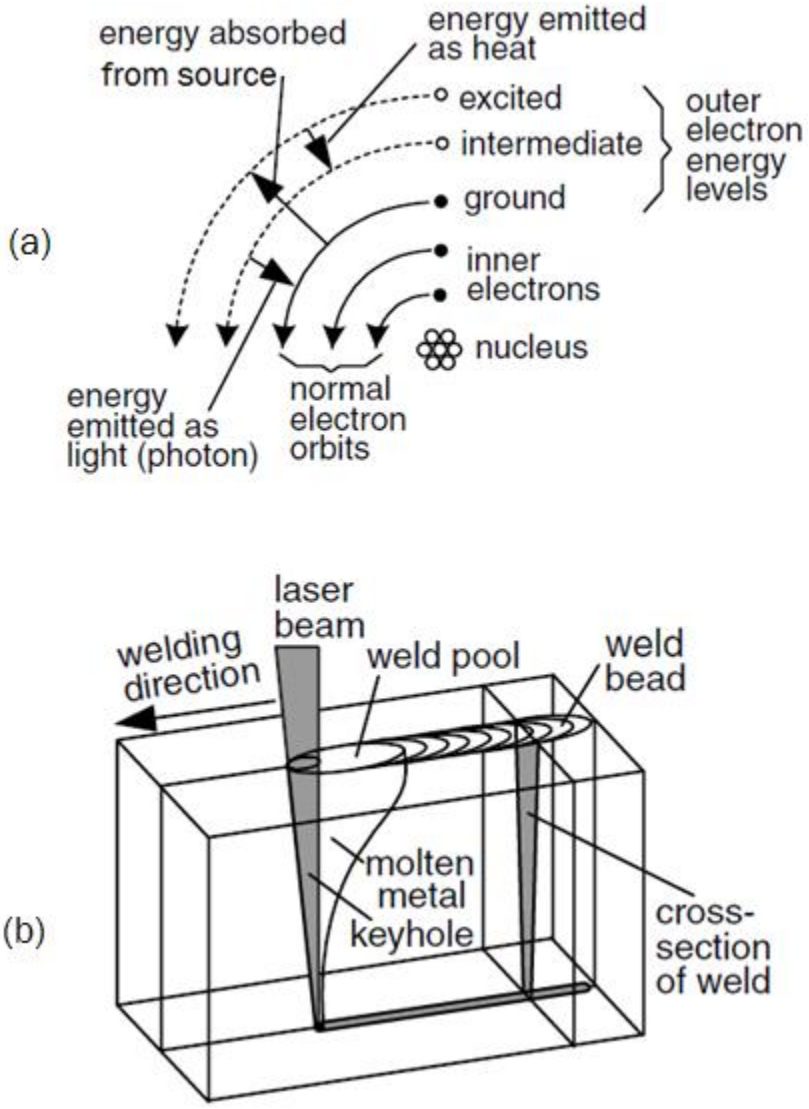

Figure 2.3 Laser welding: (a) energy absorption and emission during laser action (b) process courtesy [54]

Source:"Welding Metallurgy" (2nd Ed) by Sindo Kuo [54]. Reprinted with permission from the Global Rights Department, John Wiley & Sons, Inc. (June 04, 2012).

This high power density process requires no vacuum [14]. Shielding gases are used. Some advantages of high power density processes over conventional arc and gas welding include the following:

1. They are high quality joining techniques with deep penetration [18]. Such high energy density in keyhole mode enables the welding of thick sections with one pass at high speed, which reduces the welding time [60, 61] and this aids in improved productivity [62].
2. High energy density allows for minimal heat input, which results in reduced distortion, a narrow HAZ [61] and thus, the material properties of the metal that is being joined are less altered [55].
3. High power density increases the aspect ratio (depth/width), lowers heat input and results in faster solidification [13, 16, 63]
4. Typical high input energy density encourages a high cooling rate, which leads to a reduction of elemental inhomogeneity in weld joint [24].
5. Laser welding can be easily automated [61].
6. Laser welding has the capability to perform autogenous welding, unlike most other conventional welding processes [61].

Carbon dioxide laser welding

Carbon dioxide (CO_2) laser consists of a gas mixture of primarily nitrogen (N_2), helium (He) and a small percent of CO_2 as laser medium [54, 55]. Higher power can be achieved

by a CO_2 than a solid-state laser [54]. The focusing system of metallic optical mirrors, which are highly reflective, prevent beam attenuation before getting to the weld area [55]. This laser can be operated in continuous wave (CW) and a variety of pulsed wave (PW) modes. Enhanced pulses can achieve peak powers several times higher than CW ratings and typical laser emissions have a wavelength of 10.6μm [55]. The low density and high thermal diffusivity of the gas medium reduces the tendency to distort light that goes through it; therefore, this laser has good optical quality [55].

Neodymium-doped yttrium-aluminum-garnet laser welding

Neodymium-doped yttrium-aluminum-garnet (Nd:YAG) lasers are solid-state lasers consisting of a single crystal rod of YAG doped with small concentrations of transition elements or rare earth element, Nd [54, 55]. The crystal rod is surrounded by xeron or krypton lamps, which give out high-intensity lights to excite the electrons of dopant atoms. Lasing occurs when these excited electrons return to their normal energy state, emitting a beam at a wavelength of 1.06μm [54, 55]. It is a known issue that laser beams are highly reflected by the metal surface being welded, but the reflectivity is slightly lower with a YAG than CO_2 laser [54]. Therefore, YAG lasers utilize a transmissive optic lens system to focus the beam. Unlike mirrors, lenses are less reflective of the beam and their sensitivity to soiling by spattering causes beam attenuation and they are not easily maintained [55]. This laser can be operated in CW and PW modes [64]. The high power

YAG has multimode outputs with high divergence, so it is difficult to focus the beam and the laser must be near the work piece [55].

Nd:YAG laser welding with higher power and the use of fiber optics is becoming wide spread [14].

Fiber laser welding

Fiber laser welding is a new method of laser welding technique and is used in this research. Active fiber coils made of silica are used for high power. The active medium is the core of these fibers, which is doped with rare earth and pumped by multimode diodes [19]. The resulting laser emission, as a heat source, is transmitted through a passive fiber [19]. In comparison to old lasers, the beam is transported via optical fiber, which eliminates the need for an aligning optics system [12]. In addition to the typical advantages of laser welding, this process has some additional advantages, which include:

1. The power density of fiber laser is significantly higher than that of older lasers, even when used at high powers [12].
2. Fiber lasers offers low wavelength beam, which increase absorptivity by all metal [19] and therefore, can weld several types of materials of various thicknesses.
3. Fiber lasers offers high power with good beam absorption, energy efficiency and the fiber laser machine requires low maintenance [12].
4. Higher power enables deeper penetration [12].

5. The superior beam quality (i.e. focus ability [19]) facilitates the use of robots to perform welding and the use of longer focal lengths for easier utilization as well as flexibility [12].
6. Fiber lasers are more compact and robust, which aids ease of movement of the system and eliminates the need for large workstations to weld huge structures [12].
7. Fiber lasers have lower operating costs than CO_2 and YAG lasers [19, 21].

Usually, when considering the process of welding, weld defects can occur [12, 15]. Weld defects are explained in section 2.3.7. Different parameters are used during laser welding.

2.3.3 Welding Parameters

A typical laser welding set up is shown in Figures 2.4

2.3.3.1 **Focal Spot Size and Focal Point**

The focal spot size is the diameter of the focused beam on the work piece i.e. the area where the power is concentrated. Changing spot size alters power density, which is the magnitude of laser power divided by the area of focus, and therefore leads to changes in the weld geometry. With a small spot size, power density is increased [20, 65], which enables deep penetration keyhole mode even at high welding speeds [65, 66].

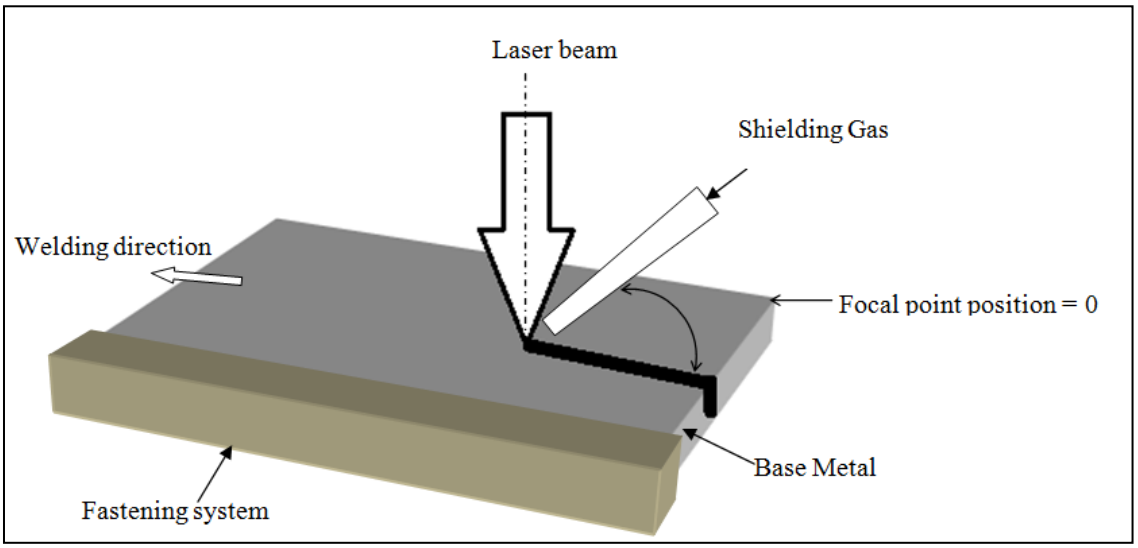

Figure 2.4 : Typical set up of a laser welding process [61, 67]

An increase in working distance results in an increase in spot size [58]. Contrarily, with large spot size, the laser beam is more diffused. Therefore, input energy distribution is spread out, which increases melting on the surface of the material, and weld penetration decreases [58]. This diffused beam results in a weld that is wide and shallow. Rush et al. [11] in the welding of another nickel-based alloy reported an optimum spot size range of 2.5 – 3 mm, which showed minimal cracking.

Focal point is the vertical position on the work-piece at which the laser is focused. Previous study by Heß et al. [12, 68] has shown that a focal point below the surface of the work-piece, for bead-on-plate welding, produces good quality welds.

2.3.3.2 **Welding Speed**

Welding speed is the travelling velocity of the laser beam on the alloy during joining. Weld becomes shallower with increase in the welding speed [19, 65]. Fiber laser welding is susceptible to oxidation due to high melting vapour pressure, which makes shielding difficult and this problem is aggravated at higher welding speeds [12].

2.3.3.3 **Welding Power**

In laser welding, high power levels, up to 30 kW, have shown great performance [12]. Katayama et al. [69] showed that weld penetration increases with power in laser welding.

Rush et al. [11] reported that a small spot size and high power result in deep penetration and narrow welds due to high power density.

2.3.3.4 **Beam Angle**

Beam angle is the angle at which the laser beam strikes the surface of the metal that is being joined. There are reports that this parameter can affect welding quality. Kawahito et al. [66] and Nguyen et al. [62] reported that welding with the beam or material tilted at an angle can reduce weld defects, such as spatters and non-uniformity of weld beads.

2.3.3.5 **Shielding Gas Flow Rate**

A plasma plume (ionic gas and metal) is produced during LBW, especially at high power levels, due to the ionization of atoms or molecules of the shielding gas and metal vapour by the laser [54, 55, 63, 67]. The presence of plasma is characteristic to keyhole welding since the power density is sufficient to vaporize metal [64]. Plasma is detrimental because it absorbs beam energy, which disrupts energy transfer to material, thus causing diminishing weld depth by keyhole collapsing [55, 70].

Shielding gas protects molten metal from oxidation and optimum control gas directed sideways of beam axis blows/deflects plasma away from the beam path [12, 55, 54]. The properties of the two common gases used in LBW, including fiber laser welding, are given in Table 2.2.

Plasma formation is more pronounced during continuous mode CO_2 welding with higher wavelengths, which easily ionizes both gases and metal [63, 69]. Therefore, He, is preferred for CO_2 welding due its higher ionization potential energy, which makes it less likely to be ionized; consequently, suppressing plasma formation and enabling deeper penetration welding [12, 54, 63, 67].

When welding with short wavelength lasers, such as YAG and fiber lasers, the shielding gas is not easily ionized. Kuo et al. [63] observed that only a small amount of metallic plasma is formed based on the thermal conductivity and density of shielding gas. The use of He with high thermal conductivity results in rapid cooling of metal vapour, which results in the formation of a smaller amount of metallic plasma [70]. However, the lower density of He gas prevents effective blowing away of metallic plasma and air, which become entrapped in the keyhole and result in pores. Therefore, a higher flow rate for an effective blow away is needed [64, 67]. A combination of He and Ar can be used [54], which can mitigate the expenses associated with using just He and the spattering associated with the use of Ar alone [67].

An overly high gas flow rate leads to keyhole collapse and when combined with high speed, which causes a fast cooling rate, more pores form in the weld due to rapid solidification that traps gas in solidifying melt [2, 61].

2.3.4 Weld Macrostructure

Due to the heat experienced by an alloy during joining, a welded joint consists of three distinct zones (Figure 2.5): the Fusion Zone (FZ), Heat affected Zone (HAZ) and unaffected base metal (BM) [54, 71]. The FZ melts due to the direct heat of the welding process. The HAZ is part of the base metal that experiences mechanical property and microstructure changes [56]. The structure and mechanical properties of the weld metal are as a result of the sequence in weld solidification [56]. When the welding parameters are not considered, the grain structure is thus determined by the BM [71]. This is because the initial solidification of grains, nucleation, is at the FZ/BM interface. The grains grow in parallel direction of heat flow and in favoured crystal orientation of BM, which is maintained since these faster growing grains hindering and stopping the growth of unfavourable crystals [56].

2.3.5 Solidification

The solidification of IN 718 can be explained by the theory of constitutional supercooling proposed by Chalmers et al. [54, 71, 72]. Thermal and solute diffusion conditions can lead to the breakdown of a single solidifying plane interface in to several solidifying cells or dendrites (Figure 2.6) [73, 74].

Table 2.2: Properties of shielding gases used in laser welding [67].

Properties	Shielding gas	
	Helium (He)	Argon (Ar)
Ionization potential (eV)	24.5	15.76
Th. Conductivity(W/mk)	0.1381	0.0159
Density (Kg/m^3)	0.178	1.784

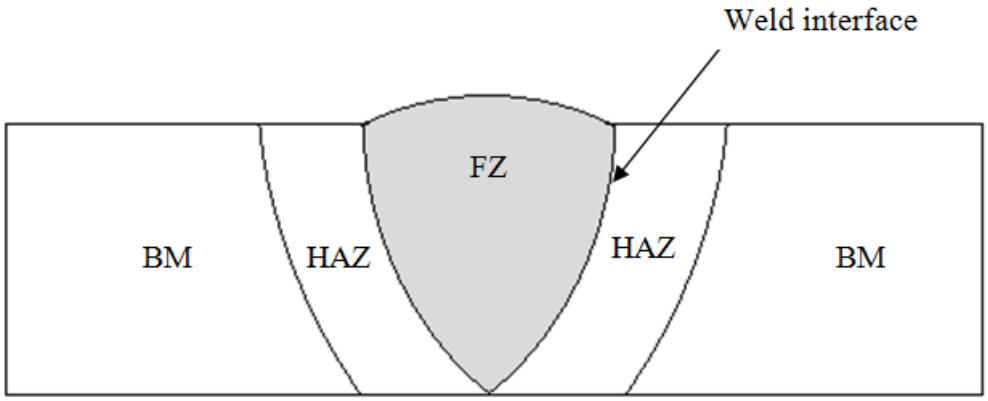

Figure 2.5: Macrostructure of typical fusion weld joint

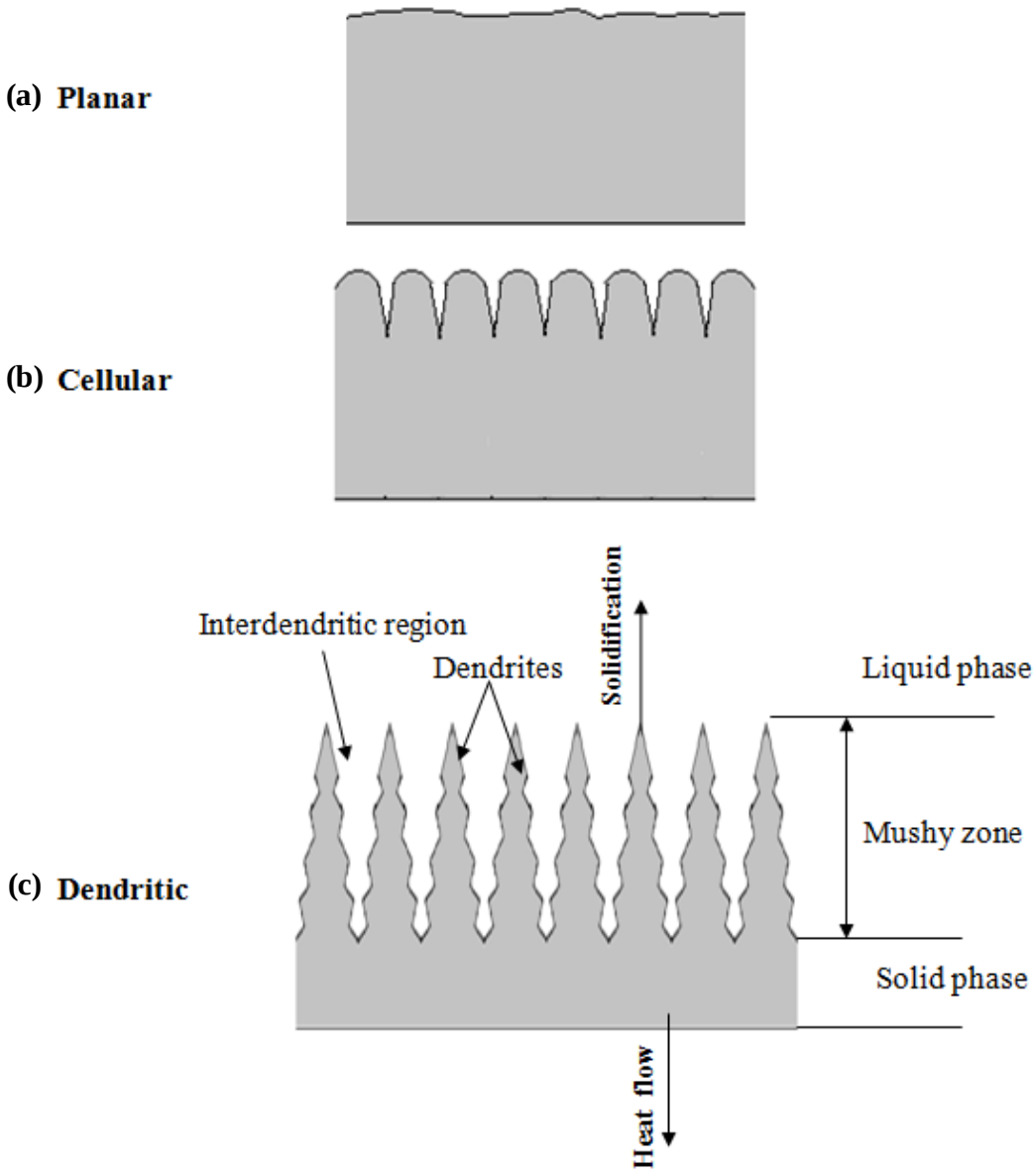

Figure 2.6: Solidification modes (a) planar (b) cellular (c) dendritic [73, 74]

According to the criterion for constitutional supercooling, a planar solid/liquid(S/L) growth is stable if [54, 71, 72]:

$$\frac{\mathbf{G}}{\mathbf{R}} > \frac{\mathbf{\Delta T}}{\mathbf{D_L}} \qquad \textbf{(1)}$$

where G = Temperature gradient at S/L interface, R = solidification front growth rate, $\Delta T = T_L - T_S$ = equilibrium solidification temperature range and D_L = diffusion coefficient of solute in liquid. Therefore, the ratio, G/R, determines the morphology of the S/L interface [71]. A high G/R ratio indicates a low degree of supercooling that favours a planar solidification mode [54]. In nickel-based superalloys, microsegregation of some alloying elements into solidifying liquid does occur during solidification, which results in increased extent of supercooling. This increased extent of supercooling causes a breakdown of S/L planar interfaces and solidification proceeds by the formation of many dendrites [28].

A typical dendritic solidification microstructure is shown in Figure 2.6. The equilibrium segregation coefficient, k, determines the extent and patterns of elemental segregation [74].

$$\boldsymbol{k = \frac{C_s}{C_l}} \qquad \textbf{(2)}$$

where, C_s and C_l are the compositions of solute and liquid at the S/L interface respectively. As IN 718 dendrite solidifies, Nb, Al, Ti with $k < 1$, which are more soluble in the liquid, are rejected from the solidifying dendrite and diffuse into the remaining liquid [9]. If solidification is slow, a continuous channel of high solute content

interdendritic region is formed [9, 28, 56]. While Ni, Cr and Fe, with k > 1, enrich the solidified dendrites [9].

In the differential thermal analysis of IN 718 by Knorovsky et al. [43], three solidification reactions are evident and occur in the following order:

1. Primary γ dendrite
2. γ/Nbc reaction
3. γ/Laves reaction

Reaction 2 and 3 occur later, therefore, this explains why MC carbides and Laves phase particles form in the interdendritic regions of IN 718 that solidifies last.

Welding is a complex process and involves solidification reactions that rapidly occur in contrast to those of equilibrium conditions [56] i.e. non-equilibrium solidification takes place during welding [71]. Weld microstructure can gradually change from a planar solidification mode at weld interface, to a cellular mode and then to a dendritic mode at the FZ center region [74]. This change is because G/R is maximun at weld interface and decreases toward the FZ centerline [75]. In high power density welding of austenitic alloy that solidifies in dendritic mode, initially, build up of solutes ahead of dendrites prevents further solute rejection by dendrite and less enriched interdendritic regions form [75]. Therefore, a microstruture that consists of a reduced dendritic microsegregation is produced.

2.3.6 Welding Residual Stresses

Welding residual stresses occur due to non-uniform temperature changes that are characteristic of the welding process [56]. These thermal stresses result because of thermal expansion during welding and subsequent shrinkage contraction strain of the solidifying melt in the presence of a cool base metal. [48, 56].

Figure 2.7 schematically shows the changes in temperature and stress in the x-direction for bead-on-plate welds. This is detailed in [56]. In front of the heat source for section A-A, the temperature and stress distribution are insignificant. At section B-B, which is across the heat source, the temperature distribution is steep. The weld metal is hot and has low yield strength, and therefore, exerts little stress on the HAZ and cooled base metal. However, thermal expansion of the heated HAZ metal near the fusion line causes compression stresses [48] because the cooler base metal restricts its expansion, which results in compressive stresses in the HAZ of both sides of the weld pool. The magnitude of the compressive stress is dependent on yield strength. Material of lower yield strength is closer to the heat source; therefore, the build up of compressive stress approaches a maximum with increasing distance from the heat source. This compressive stress is balanced by tensile stresses in the base metal. At section C-C the HAZ and the weld metal has cooled and can exert stress because it has achieved yield strength comparable to the base metal. Still cooling, the weld metal begins to contract [48]. The cooled base metal restricts shrinkage. The shrinkage induces tensile stresses in the weld metal, which has to be balanced out by compressive stresses that develop in the cooler base material.

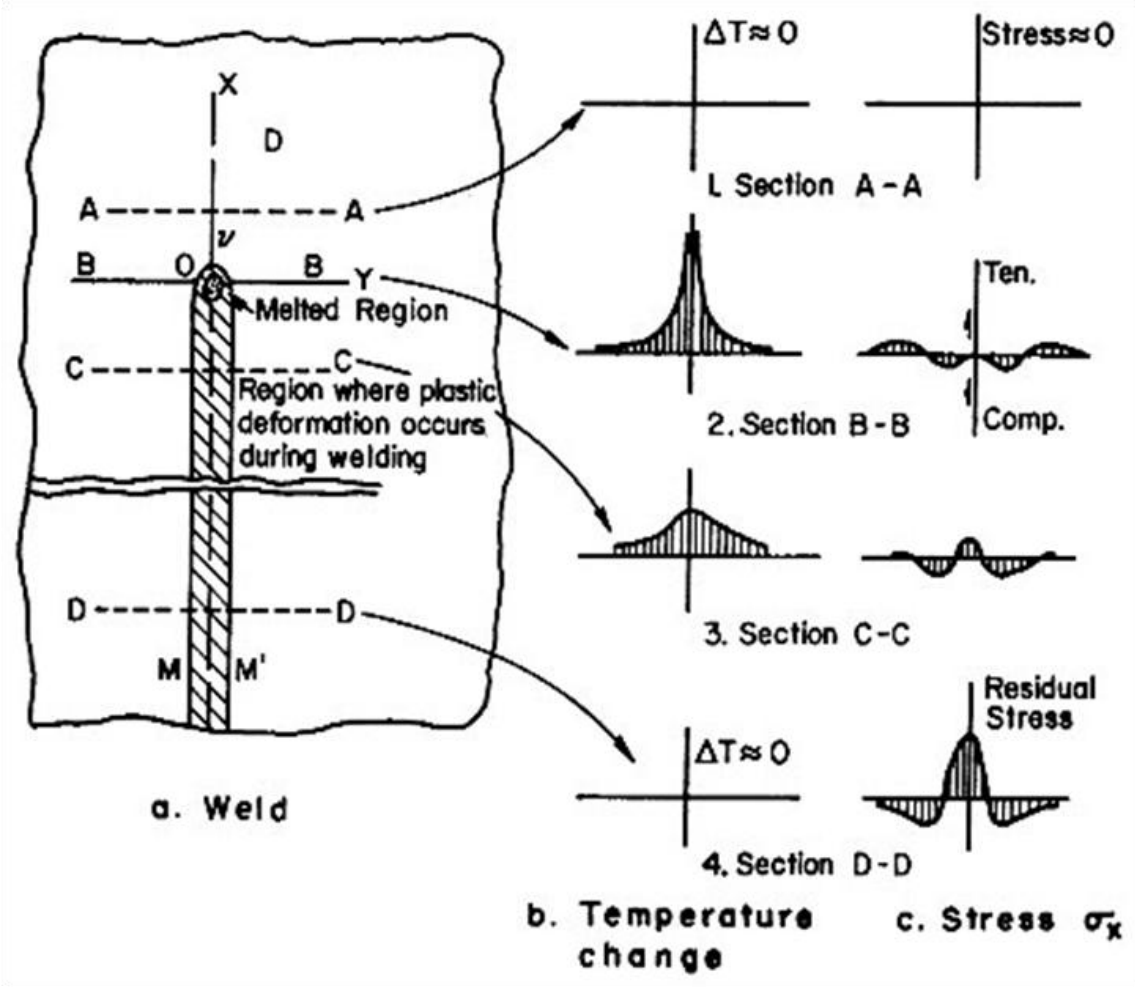

Figure 2.7: Stress and temperature distribution during welding [56]

Source:"Analysis of Welded Structures." (1st Ed) by Koichi Masubuchi [56]. Reprinted with permission from the author Koichi Masubuchi (May 08, 2012).

At section D-D where the whole joint has been further cooled to room temperature, temperature distribution across the joint is also insignificant. However, higher tensile stresses in the weld and HAZ, and compressive stress in the base material have developed. These residual stresses are unavoidable during welding; therefore, post-weld heat treatment is usually done to reduce residual stresses [48, 56]. If there is considerable expansion and weld shrinkage stress that exceed yield strength, cracking will occur [48].

2.3.7 Weld Defects

The types of weld defects are shown in Figure 2.8. The following are classification of weld joint defects [56]:

2.3.7.1 **Welding Process Related Defects**

These discontinuities are mainly geometrical and are related to the weld procedures used. In Figure 2.8a, it is shown that *undercuts* are visible notches or sharp recesses located at the junction of the FZ and base metal. They can be caused by shrinkage of base metal, FZ weld metal that does not wet the base metal or the melting away of the sidewall of the welding groove [55]. As also shown in Figure 2.8a, o*verlap*, occurs due to the spreading of FZ molten metal on base metal.

Underfill results from insufficient filling of weld pool (Figure 2.8b). They can also be formed if there are relatively large masses of FZ molten metal, such that the bead will tend to sag due to insufficient surface tension. [55].

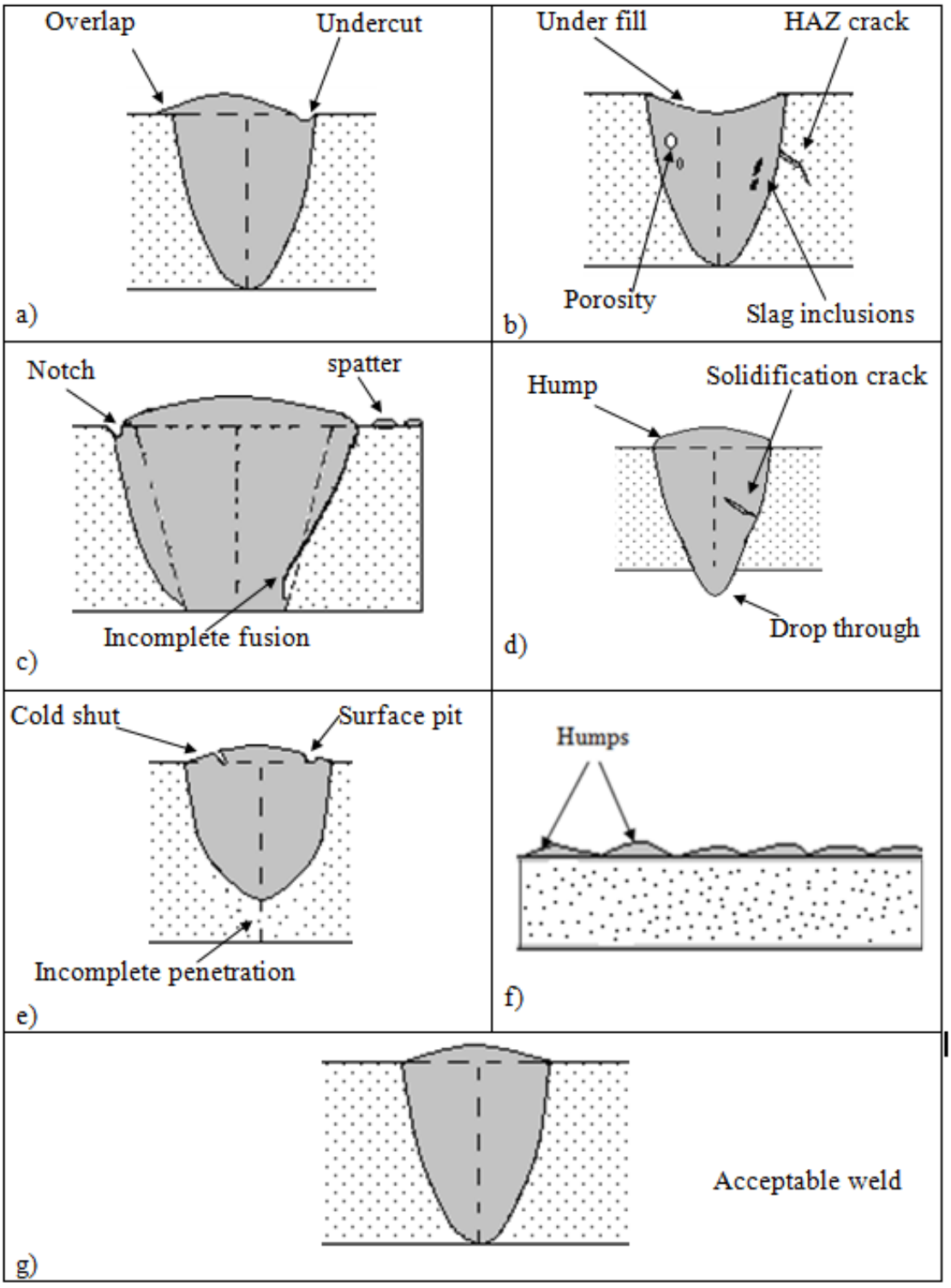

Figure 2.8: Schematic drawings of weld defects [55, 62]

Lack of fusion is when a part of the FZ weld metal fails to fuse to the base metal or other portions of the weld (Figure 2.8c). The presence of slag or oxide on the metal surface due to improper pre-weld cleaning as well as insufficient heat input to cause melting of the base metal or dissolution of fluxing or filler are some of the causes of this problem [55].

Figure 2.8e, shows *incomplete penetration,* which means the resulting weld does not penetrate the material thickness. This defect may be seen as the result of low beam power, high speed or improper focusing [55]. In applications subjected to a transverse tensile load at the root of the weld, a full penetration weld is required [55].

Shrinkage voids occur due to high volumetric shrinkage upon solidification; in addition, they naturally occur between dendrites near the center of the weld metal and characterized as irregular outlined porosity [55].

Other surface irregularities are also process related discontinuities.

Figure 2.8c, shows *spatters*, the eruption or flow away of molten metal from the keyhole, which land on top of the alloy surface [69]. Spattering forms small balls of solidified metal on the surface of the alloy being welded. This defect leads to loss of metal and insufficient metal to fill weld pool, which could also result in undercuts or underfills [15, 69].

Slag inclusions are as result of the entrapment of insoluble oxides and non-metallic solids, formed by chemical reaction during welding, in the weld metal or between the weld metal and base metal (Figure 2.8b) [55]. Good cleaning practices and proper surface preparation of joint surfaces can prevent this [55].

Humping (Figures 2.8d and f) is the periodical undulation of the weld bead with a sequence of a hump (hill) and a valley [62]. The top surface of the bead appears uneven with bumps.

2.3.7.2 **Metallurgical Discontinuities**

Metallurgical discontinuities are changes in the weld or base metal properties. The rapid solidification tendency of laser welding might result in porosity [55]. Figure 2.8b shows porosities. They form as a result of gases in air, shielding gases or metal gas being entrapped in rapidly solidifying weld metal that form air pockets of generally spherical or elongated shape [75, 76]. Porosity can also form due to gas plasma that blocks metal vapour from escaping out of the molten pool [61] or due to metal ablation [75].

Cracks or fissures are associated with weld metal (Figure 2.8d) and base metal (Figure 2.8b). These are insidious weld defects that significantly affect the integrity of welds and will be discussed in detail in the next section. Figures 2.8g is an example of defect free weld.

2.4 Weld Cracking

Two types of hot cracks, weld solidification and HAZ liquation, occur in weldments. Unlike cold cracks, hot cracks occur at relatively higher temperatures when chemical composition form low melting constituents [48, 55]. These are typically intergranular cracks.

2.4.1 Weld Solidification Cracking

Solidification cracking that frequently occurs in casting ingots can also be present in fusion welding and take place during solidification. The two main reported theories for solidification cracking are the shrinkage brittleness theory and the strain theory of hot tearing [48]. Borland et al. [48] presented summaries of both theories. They suggest that a wide freezing range increases solidification time, rendering a weld more prone to cracking [48]. During solidification, the interdendritic region has a certain amount of liquid film, which is of much lower freezing temperature than the solidified dendrites metal, such that sufficient shrinkage stress imposed on this region of liquid film produces cracks between dendrites. The liquid film with a low melting point is formed as a result of the segregation of alloying elements (especially S, P) into the solidifying liquid, which depresses the solidification temperature and permits wetting of these regions [48, 77] . Cracks initiate while the weld metal is semi-solid at the terminal solidification stage, which consist of coherent interlocking solidified metal separated by a liquid film (i.e when the fraction of solid f_S is close to 1 during cooling from a temperature either just below the liquidus or solidus) and when the tensile stresses developed across the adjacent grains exceed the strength of the almost completely solidified weld metal [78, 79, 80]. These cracks will exist as dendrite boundaries openings if there is no sufficient liquid metal to flow into initial “incipient cracks” that form and cause “healing” by back filling phenomenon [48, 54]. FZ cracking can be minimized by the addition and choice of filler material [22, 45, 81]. Researchers report insignificant or no FZ cracking during the welding of cast or wrought IN 718 [8, 82].

2.4.2 Heat Affected Zone Liquation Cracking

Not only are nickel-based superalloys sensitive to solidification cracking, they also are prone to HAZ cracking due to intergranular liquation [14]. HAZ liquation cracking is more difficult to prevent as it is generally caused by grain boundary liquation during welding, which occurs as a result of different mechanisms [22, 83].

Cracking is due to the combined effect of [14, 22, 48]:

i. material sensitive to cracking – reduced ductility of an alloy caused by grain boundary liquation, due to weld and base metal composition, presence of impurities or alloy elements which embrittle grain boundaries etc, and

i. weld stress – solidification shrinkage stresses as a result of the heat and cooling cycle (process parameter) and restraint (joint geometry). Other process mechanical stress factors that may intervene include those related to the environment, such as the weld fastening system [14, 81].

2.4.3 Mechanisms of HAZ Liquation Cracking

Grain boundaries can liquate either by super-solidus melting or non-equilibrium sub-solidus melting. Sub-solidus melting is more detrimental because it extends the temperature range over which grain boundary liquid solidifies in welds, hence increasing

susceptibility to cracking [22]. There are two main mechanisms of sub-solidus melting [11, 22] :

i. Elemental segregation of melting point suppressant on grain boundaries during solidification, thermal processing of alloys and pre-weld heat treatments, and/or

ii. Constitutional liquation of secondary phase particles e.g. carbides, Laves and δ phases present on grain boundaries.

2.4.3.1 **Theory of Elemental Segregation**

IN 718 with a high Nb solute content is difficult to melt without segregation [7]. Therefore, to understand the structural response of cast and wrought 718, the knowledge of elemental segregation and the role of Nb segregation on phase reactions is required [31]. Elemental segregation is the enrichment of impurity atoms at interfaces and the extent of segregation is controlled by diffusion [31, 84]. Elemental segregation on grain boundaries prior to welding can be induced during different thermal processes, such as casting, hot forming and pre-weld heat treatment [22]. There are two types of elemental segregation.

Equilibrium Segregation

Equilibrium segregation occurs at interfaces, like grain boundaries and free surfaces, by impurity atoms moving to these loosely packed interface regions and, as a result,

reducing interfacial free energy [85, 86]. Grain boundary segregation is dependent on temperature and impurity atoms, such as S and P, which form a saturated region with a width of a few submonolayers at equilibrium [47, 84]. Equilibrium segregation is a thermodynamic process. It occurs when a material is kept at a certain temperature, but it decreases with increasing holding temperature [87]. Slow heating conditions, which allow the material to be held at a sufficiently high temperature, permit diffusion of impurity atoms from inside the grains matrix to the grain boundary [22, 84]. This kind of segregation is likely to occur during isothermal pre-weld heat treatment.

Non-equilibrium Segregation

Non-equilibrium segregation was first noticed and investigated by Westbrook and Aust et al. [88, 89, 90], and the related theory was further developed by Anthony [91]. Non-equilibrium segregation is a process of kinetics and involves rapid heating rates, such as in a welding process or during the cooling from elevated temperatures [22, 87]. This kind of segregation results in solute accumulation near the grain boundary interface of a width that reaches tens of nanometres [47]. Solute accumulation is possible through the flow of vacancy-solute complexes, i.e. vacancies accompanied by impurity atoms, which are deposited near the grain boundary [85, 87]. Non-equilibrium segregation depends on cooling start temperature and cooling rate [85, 87]. It is also dependent on the binding energy of vacancy-solute atom [85].

2.4.3.2 **Constitutional Liquation**

A study of what occurs in the HAZ of 18-Ni maraging steel welds contributed to the proposition of a mechanism of HAZ cracking called “constitutional liquation” by Pepe and Savage [92, 93]. It was found that the constitutional liquation of titanium sulphide (TiS) phase has a significant effect on HAZ cracking. In equilibrium behaviour, an alloy containing secondary phase particles is heated slowly and, as the temperature increases, the melting of the particles occur by dissociation. With the slow heating time, the resulting solute atoms of the particles easily diffuse and are accommodated by the surrounding matrix. The ease of solute movement means that the secondary particles will be completely dissolved at solvus temperature, $T_{V,}$ and the alloy is then converted to a single phase alloy. Further heating results in grain growth until the solidus temperature, $T_{S,}$ where normal alloy melting initiates [92].

In non - equilibrium conditions, secondary particles form a liquid pool in the alloy before melting temperature, T_S, is reached. This dissolution behaviour is representative of constitutional liquation and promoted by rapid rates of heating. In this case [92, 93]:

a. the rapid heating of the alloy rapidly above its solubility temperature, T_v, does not allows enough time for dissolution by solid state diffusion and the particle remains in the matrix. Dissociation only begins at temperatures close to the eutectic temperature, $T_{E,}$ with diffusion of the solute atoms in the secondary phase to the phase/matrix interface. The solute diffusion creates a solute equilibrium composition at the particle/matrix interface. The higher temperature facilitates

rapid solute diffusion, such that the equilibrium composition is easily reached since the matrix cannot rapidly receive and accommodate the solute atoms, and

b. in heating the alloy to T_E, the phase size continues to decrease and the composition attained at the interface activates a eutectic-type of reaction. The reaction leads to the formation of a single phase liquid that surrounds the particle. Further heating above T_E causes localized melting at temperatures below, T_S.

Similarly, the constitutional liquation of Nb-rich phase, like MC phase [94], δ phase [95], Laves phase [96] and γ' precipitates [97, 98],which cause grain boundary liquation in nickel-based superalloys, has been reported. In most cases these are associated with HAZ cracking. In essence, these phases can react with the matrix to form liquid below T_S. When these particles reside on the grain boundaries, liquation results in the penetration and wetting of boundaries by a solute-rich liquid phase [92].

2.4.4 Effect of Alloying Elements on Liquation Cracking

As highlighted in the role of elements, Nb promotes formation of strengthening phases, but leads to the precipitation of NbC and the Laves phase. MC carbides and Laves phase have been associated with reduced weldability [44, 51]. In cast IN 718, Fe and Si promote the formation of the Laves phase [34, 42, 43]. Nb and Mo are involved in the formation of MC carbides and Laves phase, and the tendency to form Laves phases is reduced by increased Ni and Fe content [1]. Therefore, Nb sensitises IN 718 to intergranular liquation [14, 44, 99].

Considering non-metallic alloying elements, Knorovsky et al. [43] suggested that C increases the amount of MC carbides at the expense of the Laves phase. An increase in C promotes the formation of MC carbides and depresses solidus temperature of IN 718, both of which increase cracking susceptibility [42, 99] . The welding of cast IN 718 with low C content filler is translated as a decreased C/Nb ratio, which leads to insufficient C to tie up Nb [42]. An increase in available Nb results in a marked increase in low melting Laves phase, which is also detrimental to low cycle fatigue (LCF) properties [42, 100]. The presence of S > 0.008 wt %, P > 0.025wt % and B > 0.010 wt% cause solidification problems [1]. Kelly [34] reported that B content as low as 50ppm (0.005%) reduces the weldability of IN 718 using EBW, but the complete removal of B is unfavourable for notch ductility at high temperatures [34].

2.4.5 Effect of Segregation on Liquation Cracking

Solution heat treatment of alloys, which results in a softened condition, is normally done before welding to reduce the risk of cracking [9, 14, 27]. Initially, this heat treatment was suggested by weld simulation testing, through the Gleeble hot ductility test. Thompson and Genculu [51] showed that for heat treatment of IN 718, solution is preferred over age-hardening. Radhakrishnan and Thompson [101] conducted a study on the effect of intergranular liquation on the hot cracking of cast IN 718. After an initial homogenization heat treatment of cast IN 718, an aging temperature of 650^{o}C/1hr showed more cracking than solutioning above that temperature. Evidence showed that, pre-weld heat treatment can alter the extent of hot cracking by affecting the grain boundary liquid distribution

[101]. Thompson et al. [51, 102] reported the possibility that segregation of impurity elements, during pre-weld heat treatment, can modify the grain boundary chemistry, melting temperature of grain boundaries and the distribution of intergranular liquid phases during cooling. Further investigation by hot ductility testing strongly reiterated their results, which means that heat treatment in fact will not change the mechanism of liquation, but can affect the manner of liquid spreading across grain boundaries; that is, -wettability, which is a function of trace elements [44, 99]. There are also suggestions that heat treatment can cause Nb and impurity elements, C and S, to segregate along the grain boundary and cause intergranular liquation [44, 51].

Also, the amount of grain boundary intergranular liquid film has been related to cracking. An equation has been proposed by Chadwick and Miller [103]:

$$\boldsymbol{\sigma = 2\frac{\gamma_L}{h}} \qquad \textbf{(2)}$$

which is related to the tensile stress, σ, required to separate grain boundaries held together by surface tension, $\gamma_{L,}$ of a liquid film with a thickness, h. This equation suggests that a thick boundary liquid requires less tensile stress for grain boundaries separation compared to a thin liquid film. It has been reported that, in simulated welds of IN 718 specimens subjected to different heat treatments, the amount of intergranular liquid formed in the HAZ differed and cracking susceptibility is related to the amount as well as distribution of intergranular liquid film [51].

Segregation of surface-active impurities also occurs during solidification of weld FZ. These surface-active elements in the weld FZ can penetrate the grain boundaries of the base metals and lower the intergranular strength [48]. Savage et al. [77] attributed solidification cracking susceptibility in Inconel 600 to impurity elements, such as S and P, through their influence on wetting behaviour of intergranular liquid.

Therefore, it can be said that segregation of impurity elements reduces the melting temperature along grain boundaries, which can cause local melting and result in both solidification and HAZ liquation cracking during welding [1, 45].

2.4.6 Effect of Grain Size on Liquation Cracking

Generally considered for alloys, large grain size increases susceptibility to cracking [11]. Thompson et al. [104] studied the effect of grain size on cracking of IN 718 and observed that grain size does have an effect on microfissuring. The effect of grain size is postulated to be related to two aspects: the presence of intergranular liquid distribution [49] and stress concentration due to grain boundary sliding as hypothesized by William and Singer [105]. Also, grain boundary orientation is another dominant factor that influences the intergranular behaviour of bulk materials [106]. In the welding of IN 718 it is shown that the orientation of grains affected the probability of elemental intergranular segregation and the tendency of grain boundary to liquate [107].

2.4.7 Effect of Multiple Heat Treatment Cycles on Liquation Cracking

Component repairs can reduce expenses since the cost of replacement is eliminated. In the repair welding of turbine engines, heat treatment is done to restore the properties of the surrounding material; hence, there is an accumulation of large numbers of heat treatment cycles during its lifetime [10]. Hot ductility testing by Hooijmans et al. [10] and Qian et al. [106] using multiple heat treatment on alloys have shown that multiple heat treatment may either be detrimental or not.

2.4.8 Effect of Welding Parameters on Liquation Cracking

Fluid flow and thermal conditions in and near the molten pool affect the size and shape of the keyhole [71]. The span or width of the HAZ is an attribute of heat input [56], which is dependent on welding speed and power [54, 108]. In continuous wave LBW, weld penetration and geometry are affected not only by welding power and speed, but also by the kind of laser of different wavelength, beam diameter, shielding gas type and gas flow rate used [15, 69]. Researchers have indicated that during high density welding, there exists a strong dependence of liquation cracking on welding parameters [4, 5, 6, 109, 110]. These studies show that the resulting shape of penetration and thermal conditions, which are determined by the welding parameters, could alter stresses that develop and the extent of liquation during welding.

2.5 Objectives of Investigation

Points noted from the literature review were used to establish the objective of the research undertaken. Welding is an accepted means of joining alloys to fabricate components of different shapes. Also, the repair of damaged components by welding can be cost effective. One primary focus of this study is the investigation of applying a new welding process, fiber laser welding, to join IN 718 alloy. As previously mentioned, fiber laser welding has recently become attractive for industrial application due to its advantages, such as rapid welding speed, high power, low distortion, compact design, and flexibility. However, after 30 years of studies, effect of laser welding, especially in the deep penetration keyhole mode, is still not well understood [111]. There are limited data and studies on the use of more recent high power fiber lasers to weld alloys, including IN 718. In addition, there have been reports which indicate that other similar laser welding techniques can result in HAZ cracking and other weld defects.

Previous investigators have shown that HAZ cracking and weld defects are due to weld stress which is a function of heat input. Also HAZ cracking susceptibility is primarily influenced by the pre-weld heat treatment, which results in segregation and changes in secondary phase content. Therefore, this research involved the use of fiber laser welding to study:

1. Heat input effect on the HAZ cracking behaviour of IN 718.
2. The effect of pre-weld heat treatment on the HAZ cracking susceptibility of IN 718.

Wrought and conventionally cast IN 718 are used in this investigation.

3 Experimental Procedure

3.1 Materials

3.1.1 Wrought IN 718

The as-received wrought IN 718 material used in this study is in the form of plate with thickness of 7 mm. Table 3.1 provides the chemical composition of alloy IN 718.

3.1.2 Cast IN 718

The as-cast IN 718 material used in this study are produced at the University of Manitoba by casting IN 718 blocks with approximate dimensions of 120 mm length with 30 mm x 30 mm cross-section.

3.2 Preparation of Welding Test Coupons and Pre-weld Heat Treatment

A numerically controlled electrodischarge machine (EDM), which is a wire-cutting machine, was used to cut all weld test coupons from the as-received wrought plate and as-cast block. A typical weld test coupon is shown in Figure 3.1. The machined coupons were subjected to a pre-weld heat treatment performed in a tube furnace. To prevent severe oxidation, the test coupons were wrapped with stainless steel foil before placement in the furnace for heat treatment. After heat treatment, the surface oxides on the test coupons were removed by surface grinding.

Table 3.1: Nominal composition of alloy IN 718

Element	wt%
Ni	54.4
Cr	17.9
Fe	17.6
Nb	5.4
Mo	2.9
Ti	0.9
Al	0.5
Si	0.05
Mn	0.05
B	0.04
C	0.026
P	0.007
Mg	0.0014
S	< 0.007

Wrought IN 718 welding test coupons that are 65 mm in length and with a cross-section of 15 mm x 7 mm were machined from the bulk as-received plates. To study the effect of pre-weld heat treatment, heat treatments were carried out for 1 hour at a single temperature and, in some cases, a combination of two temperatures. Table 3.2 shows the heat treatment schedule, which included air-cooling (AC) and water-cooling (WC).

Another set of welding test coupons for cast 718 were cut from the as-cast blocks of IN 718 to produce specimens that are 55 mm in length with a cross-section 15 mm x 4 mm. Table 3.3 provides information on the pre-weld heat treatment done on cast 718. Four temperatures were used for a period of 1 hour.

3.3 Fiber Laser Welding

Bead-on-plate autogenous welding, one welding pass of the laser, was carried out on pre-weld heat-treated test coupons by using a fiber laser welding machine at Standard Aero Ltd. in Winnipeg. The laser welding machine used was the IPG YLR 6000 and its capabilities are given in Table 3.4. A typical bead-on-plate weld produced for this study is shown in Figure 3.2. To check the effect of heat input, welding was done at various welding parameters, speeds and powers, as shown in the Table 3.5. Spot size and incidence angle of laser were kept at 0.5mm and 90^{o} respectively. Focal point, shielding and welding gas flow rate were also kept constant.

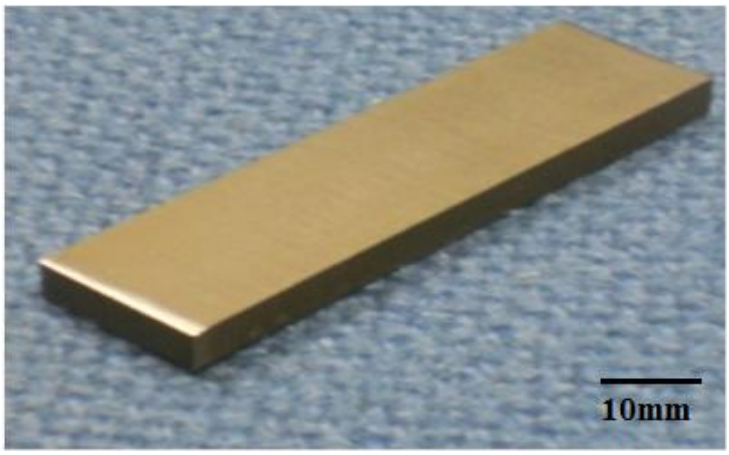

Figure 3.1: Typical weld test coupon

Table 3.2: Pre-weld heat treatments used for wrought IN 718

900^{o}C/1hr/AC
950^{o}C/1hr/AC
950^{o}C/1hr/WC
1050^{o}C/1hr/AC
1050^{o}C/1hr/WC
1150^{o}C/1hr/AC
1150^{o}C/1hr/WC
1050^{o}C/1hr/WC + 950^{o}C/1hr AC
1150^{o}C/1hr/WC + 950^{o}C/1hr AC

Table 3.3: Pre-weld heat treatments used for Cast IN 718

1050^{o}C/1hr/AC
1100^{o}C/1hr/AC
1125^{o}C/1hr/AC
1175^{o}C/1hr/AC

Table 3.4: Maximum specifications of the fiber laser welding equipment

Power	Speed	Focal length	Shielding gas flow rate (He)	Welding gas flow rate (Ar)
6kW	90m/min	200mm	60 Litres/min	80 Litres/min

Figure 3.2: Bead-on-plate fiber laser weld of IN 718

Table 3.5: Welding parameters

	Power(kW)	Welding speed (m/min)	Focal Point (mm)	Welding Gas (Helium litre/min)	Shielding Gas flow rate (Argon litre/min)
1	2.5	0.5	-2.0	20	20
2	2.5	0.7	-2.0	20	20
3	2.5	0.1	-2.0	20	20
4	2.5	1.5	-2.0	20	20
5	2.5	2.0	-2.0	20	20
6	2.5	2.5	-2.0	20	20
7	3.0	2.0	-2.0	20	20
8	3.0	2.5	-2.0	20	20
9	3.0	3.0	-2.0	20	20
10	4.0	2.0	-2.0	20	20
11	4.0	2.5	-2.0	20	20
12	4.0	3.0	-2.0	20	20
13	6.0	2.0	-2.0	20	20
14	6.0	3.0	-2.0	20	20
15	6.0	3.5	-2.0	20	20
16	6.0	4.0	-2.0	20	20
17	6.0	4.5	-2.0	20	20
18	6.0	5.0	-2.0	20	20
19	6.0	5.5	-2.0	20	20
20	6.0	6.0	-2.0	20	20
21	6.0	6.5	-2.0	20	20
22	6.0	7.0	-2.0	20	20

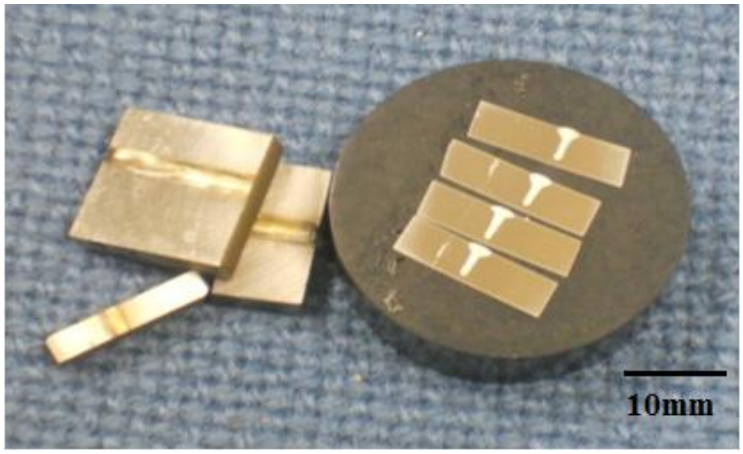

Figure 3.3: Metallographically prepared specimens sectioned from a welded coupon

3.4 Metallography Specimen Preparation

As-received and as-cast material, heat-treated material and welded coupons were prepared for microstructural studies. A total of 106 coupons were welded and out of those 53 coupons were examined for cracking.

After welding, specimens used for evaluation for weldability were sectioned perpendicular to the weld direction at an interval of 3 mm. The EDM machine was used for the sectioning to produce 10 weld cross-sections, which had a 3 mm thickness, from each test coupon. The 10 sections were mounted in bakelite by using a Buehler mounting press. The mounted sections were ground and polished to a 1µm finish after which they were eletrolytically etched in aqueous 10% Oxalic acid by using 5 Volts DC in 3 - 4 Seconds for the microstructural study.

In some cases, etching with modified Kallings and Kallings No.2 regent was used for macrostructural studies because these etchants enhance contrast of grains and hence revealed detailed grain structures in the HAZ and FZ. Micrographs, in this work, where these specific etchants were used are stated. A typical example of mounted and metallographically prepared weld specimens is shown in Figure 3.3.

3.5 Microstructural Examination

A scanning electron and two optical microscopes were used to examine etched specimens of the materials, heat-treated material before welding and welded coupons.

A preliminary microstructural study of the metallographically prepared specimens was performed by using a ZEISS Axiovert 25 inverted-reflected light (optical) microscope equipped with CLEMEX Vision 3.0 image analysis software. Mean grain size measurements were carried out by a grain boundary intercept method using 2 diagonal lines and 4 parallel lines per screen on the images from the ZEISS optical microscope. This measurement was carried out for twenty micrographs in each condition and the standard deviations were calculated.

A Nikon EPIPHOT-TME inverted optical microscope was used for the overall viewing of the weld cross-sections and for the measurement of weld depth and width.

A more detailed microstructural study by semi-quantitative and spectroscopy analyses was performed by using a JEOL 5900 scanning electron microscope (SEM) equipped with an Oxford (Oxford Instruments, Oxford, United Kingdom) ultra-thin window energy dispersive spectrometer (EDS). The SEM was used in both secondary emission (SE) and backscatter emission (BSE) mode to identify microstructural change and compositional contrast, respectively. Weld crack measurement was performed using the SEM as well. The measurements were taken from 10 sections of each welding coupon to obtain the total crack length (TCL), and standard deviation for three measurements was determined per coupon in some cases.

4 Results and Discussion

4.1 Wrought IN 718

The microstructure of as-received wrought IN 718 was examined prior to heat treatment to identify the phases that exist in the finished forged plates. In addition, the microstructure of the pre-weld heat-treated material was studied before welding. After welding, the effect of the process on the microstructure and extent of cracking were investigated. The extent of HAZ cracking was compared for different welding parameters and pre-weld heat treatments to determine the effect of these factors on weldability.

4.1.1 Microstructural Examination of As-received Wrought IN 718

As shown in the SEM micrograph in Figure 4.1, the microstructure of the as-received wrought IN 718 has blocky Nb and Ti-rich carbides distributed inter- and intragranularly in the matrix. These phases are generally referred to as MC carbides [28]. The SEM/EDS spectra of the Nb and Ti-rich particles are shown in Figures 4.2a and 4.2b, respectively. The Nb-rich carbides are predominantly larger in size. There are no Laves phase particles observed in the wrought material. In addition, a mean grain size of 26 ± 5μm was measured at this material condition.

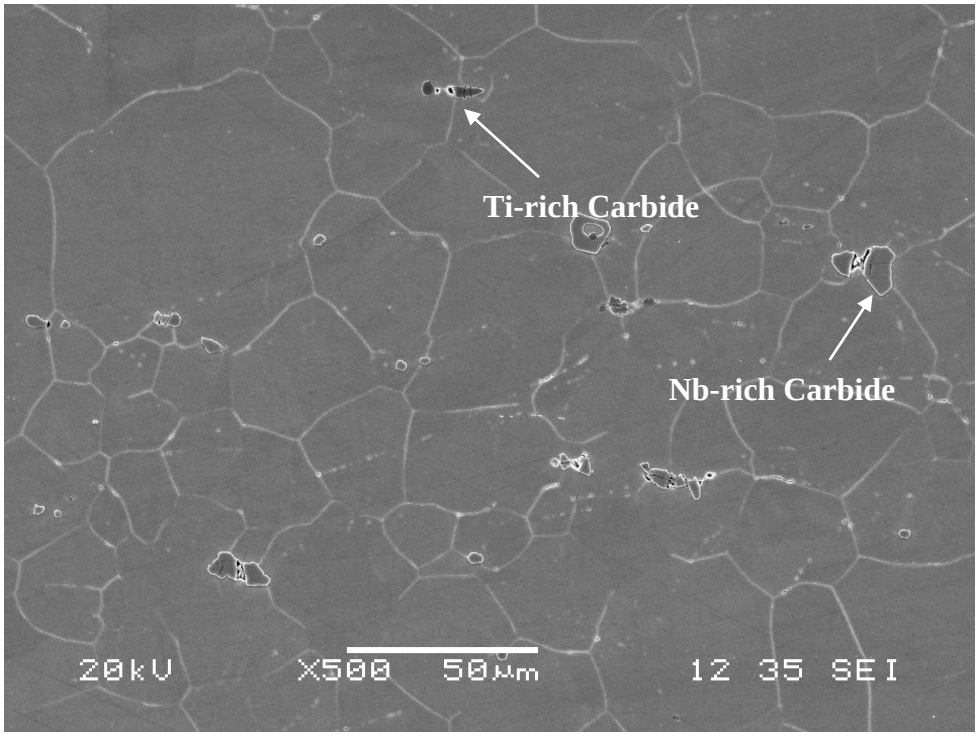

Figure 4.1: SEM micrograph of as-received wrought IN 718

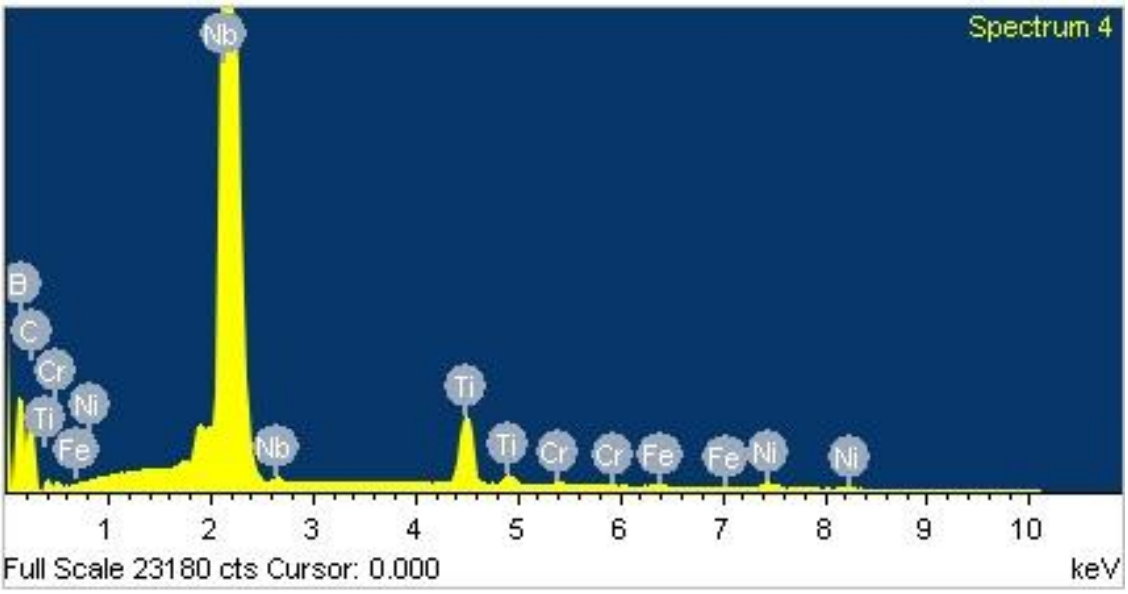

(a)

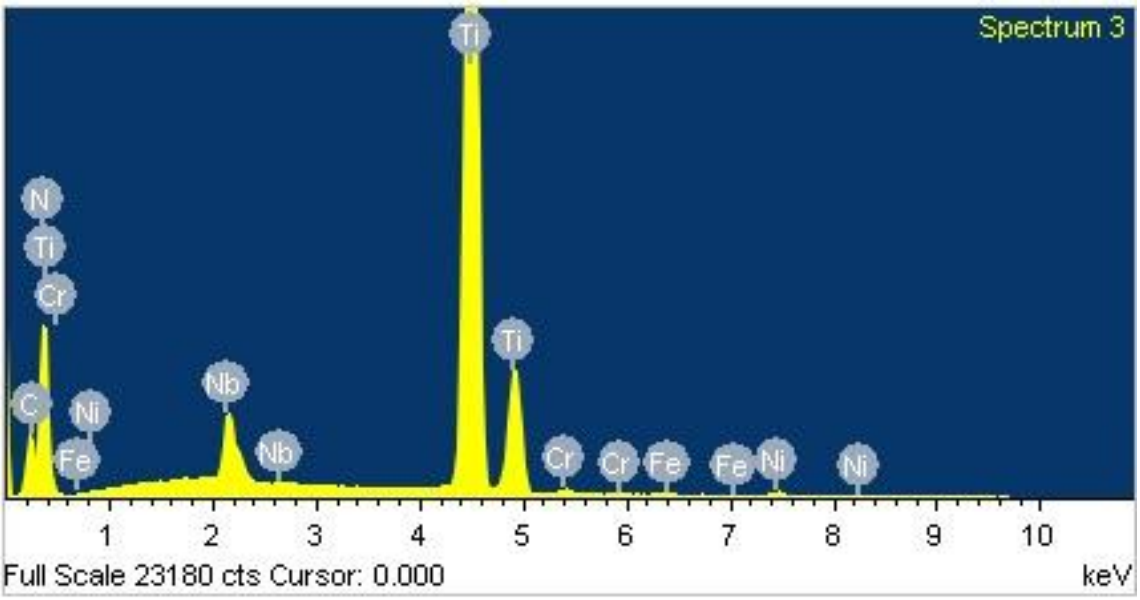

(b)

Figure 4.2: SEM/EDS spectra of (a) Nb-rich carbide (b) Ti-rich carbide in as-received wrought IN 718

4.1.2 Microstructure of Wrought IN 718 Subjected to Pre-weld Heat Treatment

Prior to welding, superalloys are normally subjected to a solution heat treatment, which is done to reduce hardness. This heat treatment lowers susceptibility to cracking [9]. In the present work, wrought IN 718 test coupons are subjected to a pre-weld heat treatment at 1050^{o}C for 1 hr followed by air-cooling. This pre-weld heat treatment condition was used in the welding experiment to study the influence of heat input on cracking in the alloy.

Figure 4.3 shows a typical SEM micrograph of wrought IN 718 after it was given heat treatment at 1050^{o}C for 1 hr and subsequently air-cooled (1050^{o}C/1hr/AC). Blocky Nb and Ti-rich carbides can be observed to be distributed in the matrix at the grain boundaries and within grains. These carbides have similar morphologies as those in the as-received material, which suggest that no dissolution took place during the pre-weld heat treatment. The presence of carbides is expected since the heat treatment temperature is well below the MC carbide dissolution temperature range, which is reported as 1200^{o}C - 1260^{o}C for alloys with high Nb [1, 28]. In the heat treatment at 1050^{o}C/1hr, a mean grain size of 100±30μm was measured. Therefore, mean grain size increased approximately by a factor of 4X in comparison to the as-received material.

4.1.3 Microstructural Examination of Welded Wrought IN 718

The macrostructure of the fiber laser welds consist of BM, (HAZ) and (FZ). The top width of the cross section of the welds is wider than midsection width and that forms a curved neck zone in between both regions, as shown in Figure 4.4.

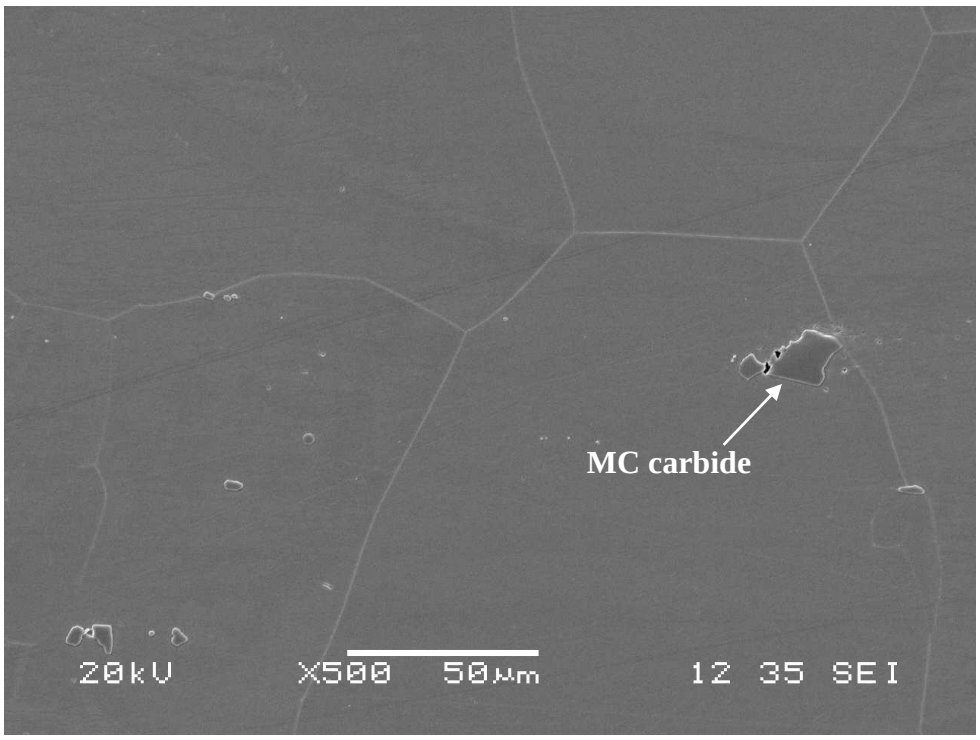

Figure 4.3: SEM micrograph of wrought IN 718 pre-weld heat-treated at 1050°C/1hr/AC

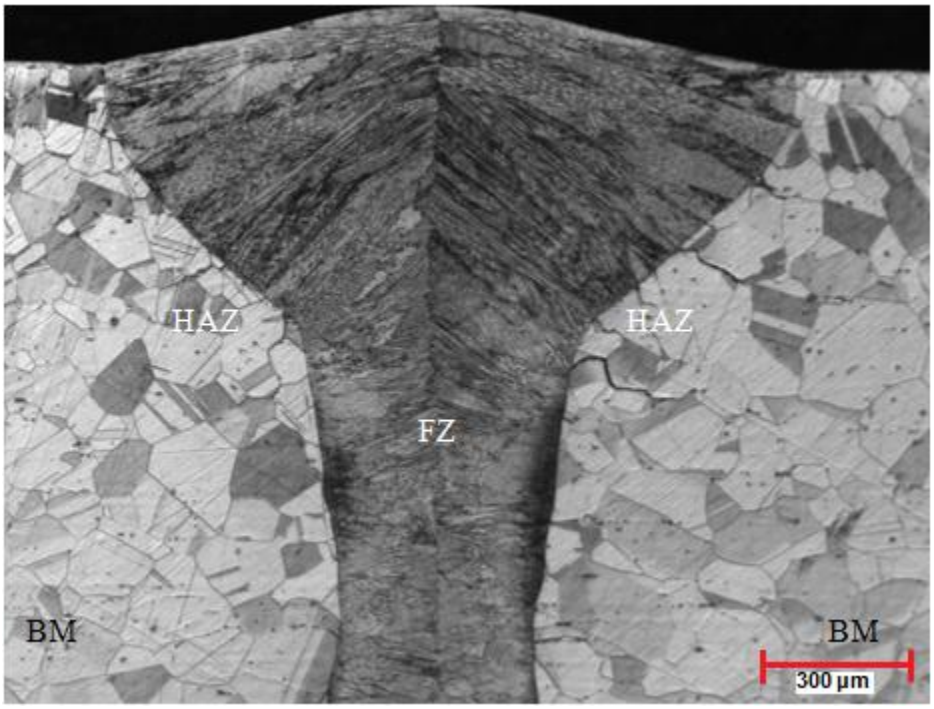

Figure 4.4: Optical micrograph of weld macrostructure of wrought IN 718

This optical micrograph was taken after etching with modified Kallings. The SEM micrograph of the FZ microstructure is shown in Figure 4.5 a and b, where the right-hand side of the micrograph is adjacent to the FZ/HAZ interface region at the top and mid section of the weld, respectively. The microstructure becomes dendritic towards the FZ center in Figure 4.5 b. Generally, the FZ microstructure is mostly dendritic and the scale of the dendritic microstructure varies. The epitaxial growth of columnar dendrites normally occurs towards the weld centreline.

To explain the microstructure of the FZ, the solidification parameters, which include the thermal gradient (G) and solidification growth rate (R) at the solid/liquid interface, become pertinent [71, 112]. Heat transfer is considered to be in the horizontal plane (from the FZ centerline toward the HAZ) because G in this plane is large in comparison to that of the vertical plane [58]. Therefore, epitaxial solidification growth often starts from the weld interface and continues towards the center by following the direction of maximum G [74]. In solidification, section 2.3.5, microsegregation promotes dendrites formation. Therefore, the dendrites grow towards the center. G changes from a maximum value at the FZ/HAZ interface to a minimum at the weld center and vice versa for R [74]. The cooling rate, defined by (G·R), significantly influences the scale of the solid/liquid interface morphology [71]i.e. scale of the microstructure that forms during solidification. A higher (G·R) results in reduced dendritic microstructure [53, 112, 113]. Therefore, it is expected that at the FZ centerline, where G is lowest and R is much higher, there should be a fine dendrite microstructure compared to that at the FZ/HAZ [54].

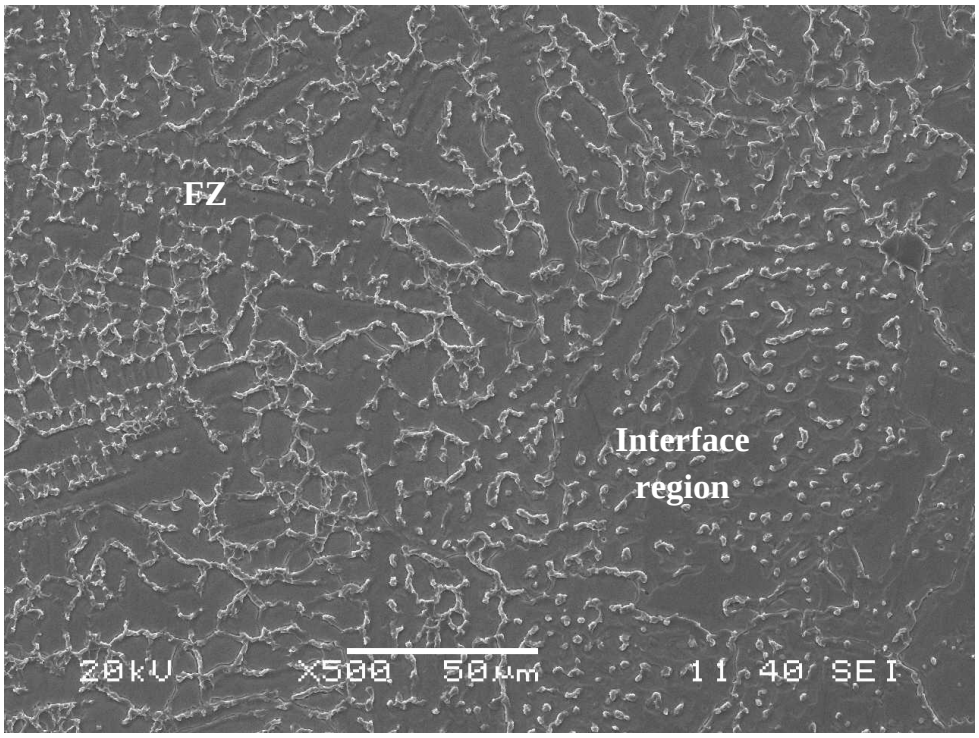

(a)

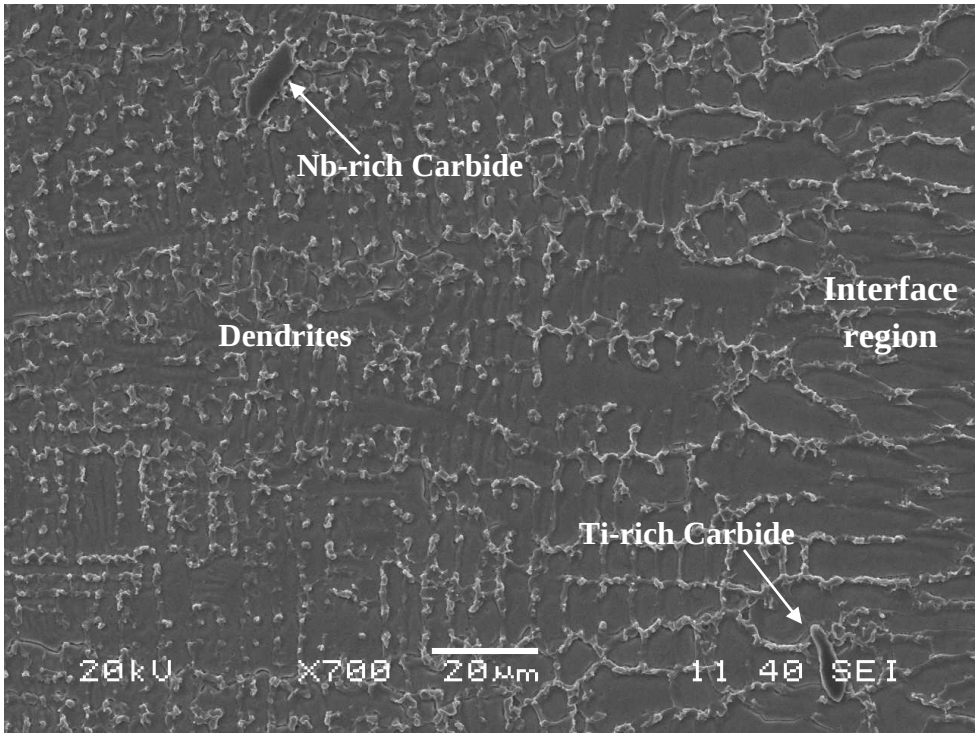

(b)

Figure 4.5: SEM micrograph of FZ microstructure at (a) weld - interface at top of weld (b) weld center - interface at mid section of weld

Large MC carbides are observed in the FZ. The SEM/EDS spectra of the carbides are shown in Figure 4.6, and are similar to those in the as-received material (Figure 4.2). In addition, bright second phase particles, sized less than 1μm, are observed in the interdendritic region of the FZ. In the FZ, non-equilibrium solidification forms phases [71], such as the Laves phase in IN 718 [114]. Krenz et al. [82] used transmission electron microscopy (TEM) to identify the fine particles that formed in the FZ of laser welds of IN 718. They confirmed that the bright particles are mainly FCC MC type carbides and HCP Nb-rich Laves phase. Therefore, the larger MC carbides are most likely prior MC carbides that survived during the melting of welding.

4.1.3.1 **Microstructural Examination of Heat Affected Zone**

The SEM examination showed signs of liquation in the HAZ of weld coupons subjected to pre-weld heat treatment at 1050^{o}C for 1 hr. A grain boundary feature with a eutectic morphology is found in the HAZ of the weld. This re-solidifed product, shown in Figure 4.7, is depleted in Cr and Fe and has much higher concentrations of Nb and Mo compared to the matrix.

Cracks are observed in the HAZ as shown in Figures 4.8a and 4.8b. The cracks have a zig-zag nature along the grain boundary and are closely associated with intergranular Nb eutectic re-solidified product, which suggest that cracking was due to grain boundary liquation. It can be noticed, as well, that the cracks were often connected to the FZ by a thick strip of this Nb rich re-solidified product.

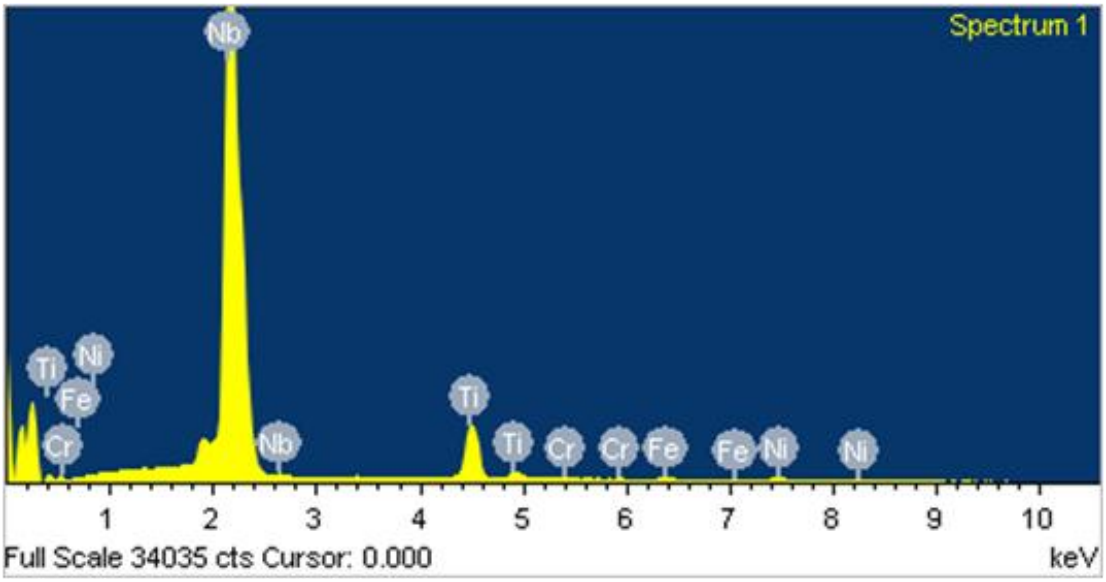

(a)

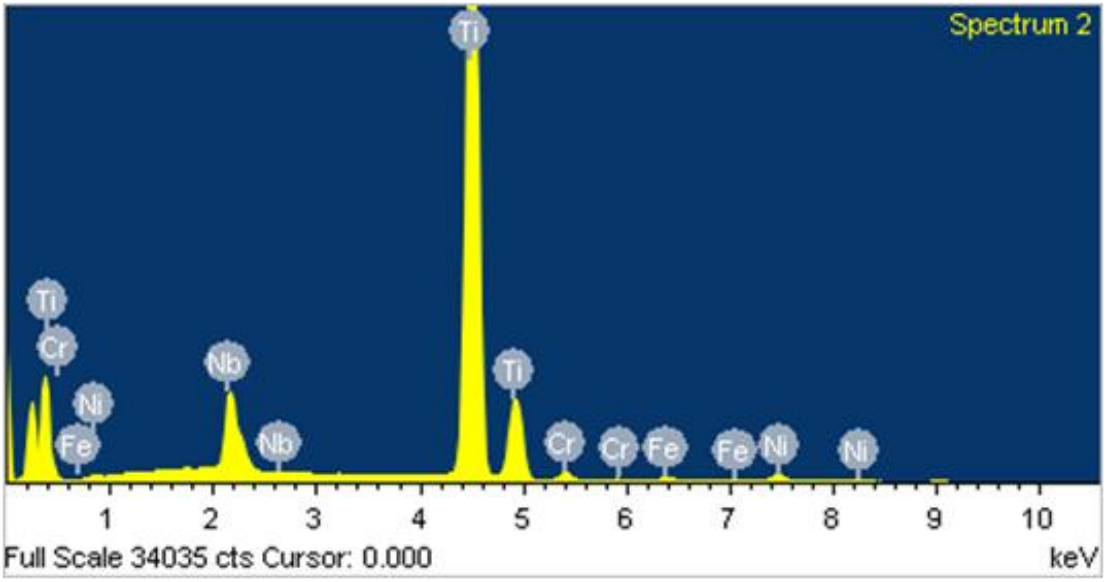

(b)

Figure 4.6: SEM/EDS spectra of (a) Nb-rich carbide and (b) Ti-rich carbide in FZ

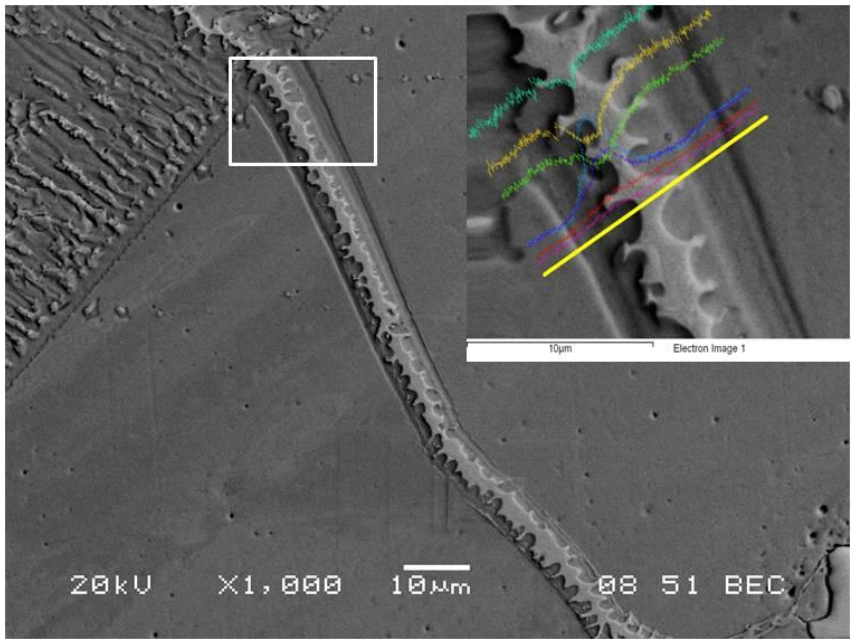

(a)

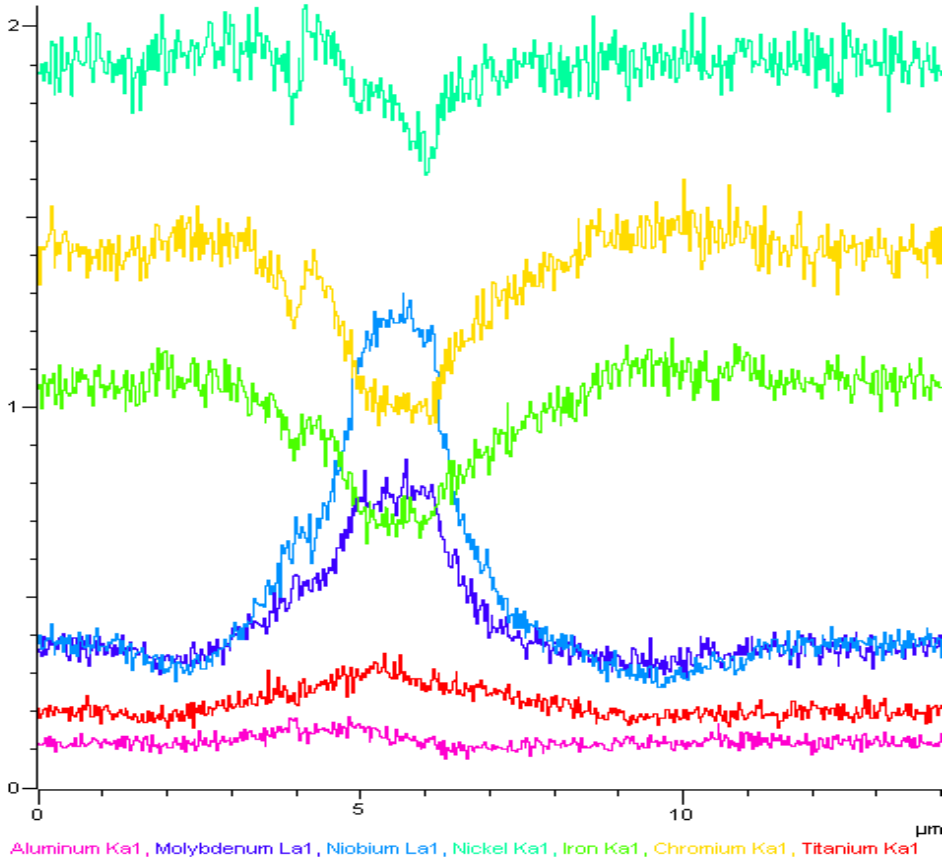

(b)

Figure 4.7 : (a) SEM micrograph and (b) SEM/EDS line scan of Nb-rich re-solidified product on grain boundary in HAZ

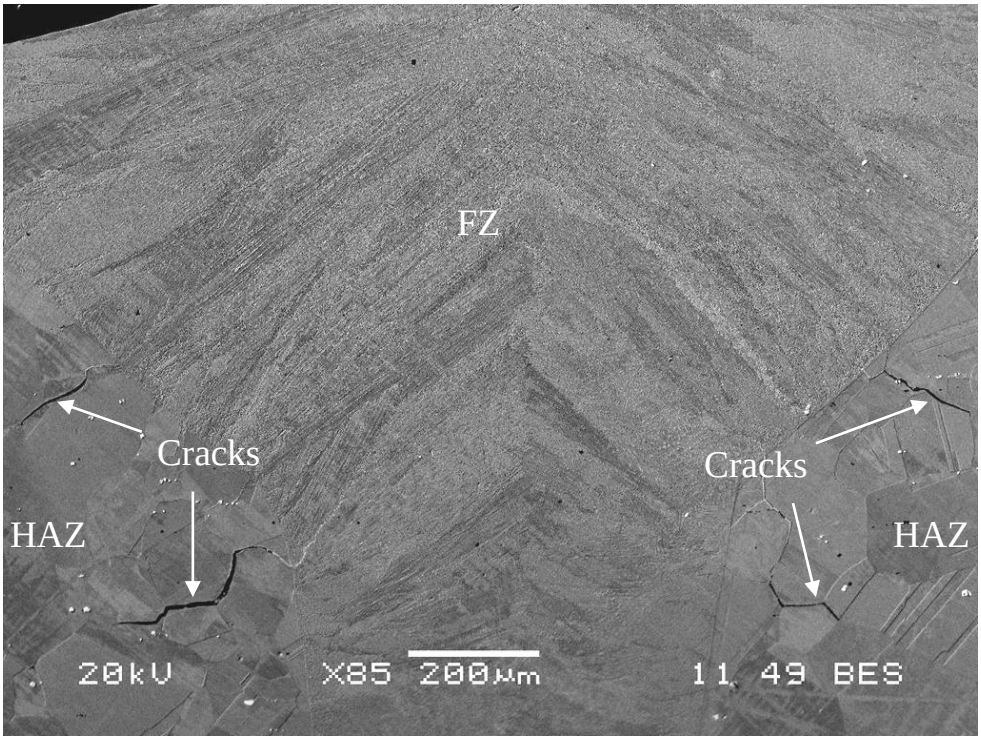

(a)

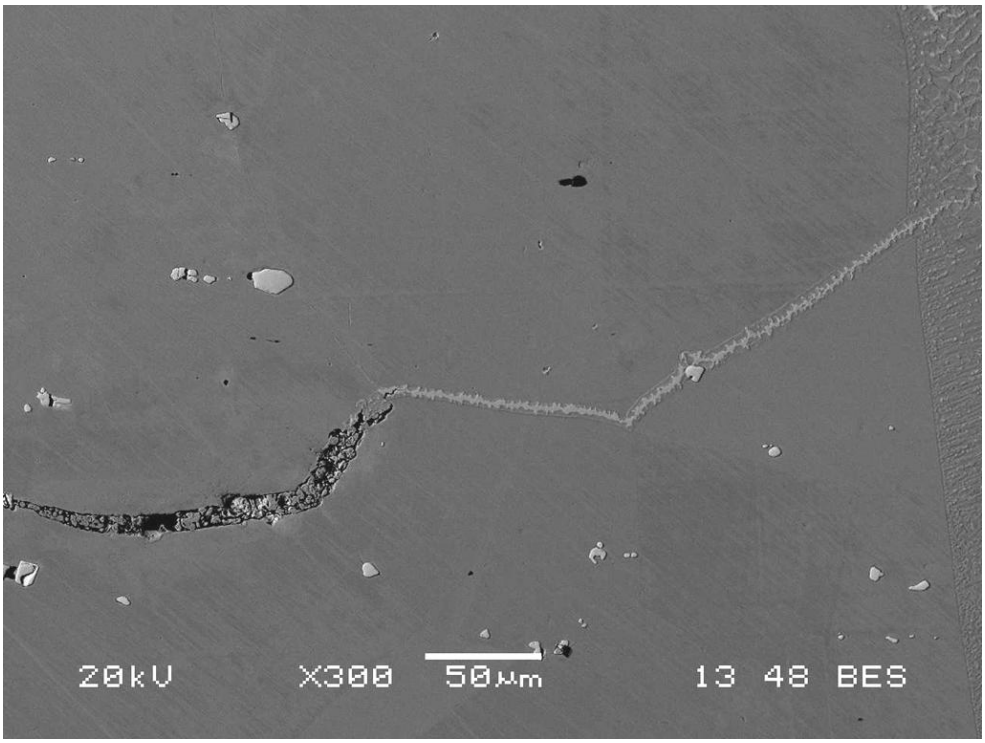

(b)

Figure 4.8: SEM micrograph of HAZ cracks in IN 718 coupons pre-weld heat-treated at 1050^{o}C/1hr/AC (a) weld top view (b) higher magnification

HAZ cracking, in other nickel-base superalloys, has been attributed to constitutional liquation of secondary phase precipitates, such as Nb-rich carbides and Laves phase particles [44, 115]. Under equilibrium heating conditions, Nb from Nb-rich carbides diffuses into the γ matrix [22] without the occurence of liquation. However, under non-equilibrium conditions, like welding, the liquation of Nb-rich carbides occurs by a Nbc-γ eutectic type reaction forming a liquid that wet the grain boundaries [51]. If strain builds up while the intergranular liquid is present, then cracking may occur [44]. The liquid solidifies to produce a Nb-rich Laves eutectic product similar to that observed along the HAZ crack paths in the present work. Vincent [23] has cited the possibility that HAZ cracks may be also healed by backfilling from the FZ. In such a case, the Nb-rich FZ liquid that backfills the crack solidifies to form a similar Laves phase product across the FZ to the HAZ.

4.1.4 The Effects of Welding Parameters

Variation of heat input, by changing laser power and welding speed, is used in this study to determine the effect of parameters on weld penetration achieved and the extent of HAZ cracking that occurred.

4.1.4.1 **Effect of Heat Input on Weld Depth**

Weld depth limits the allowable thickness of alloys that can be joined by a particular welding process. The effect of welding speed and laser power on weld penetration is shown in Figures 4.9a and 4.9b. Weld penetration decreases with speed and increases with power.

Heat input per unit length of a weld is related to the welding power and speed by the following expression [54, 108]:

$$\mathbf{Q} = \eta \frac{\boldsymbol{Power(P)}}{\mathbf{Speed(S)}} \qquad \textbf{(3)}$$

where, η = efficiency of the heat source. Accordingly, a decreased speed or an increased power increases the amount of heat released into the material, which can increase the amount of base metal melting. Consequently, the increased amount of heat produces a deeper weld as observed in the present work. Hence, it can be said that welding at slow speed or high power is advantageous in terms of penetration.

4.1.4.2 **Effect of Heat Input on HAZ Cracking**

Low heat input keyhole welding is generally preferred. The narrow HAZ and FZ of welds that are produced, which suggests that there is less heat conducted to the alloy during welding, indicate that metallurgical properties of the alloy are less affected.

To study the effect of heat input on HAZ cracking, the TCLs in test coupons that were welded with various laser powers and welding speeds were measured.

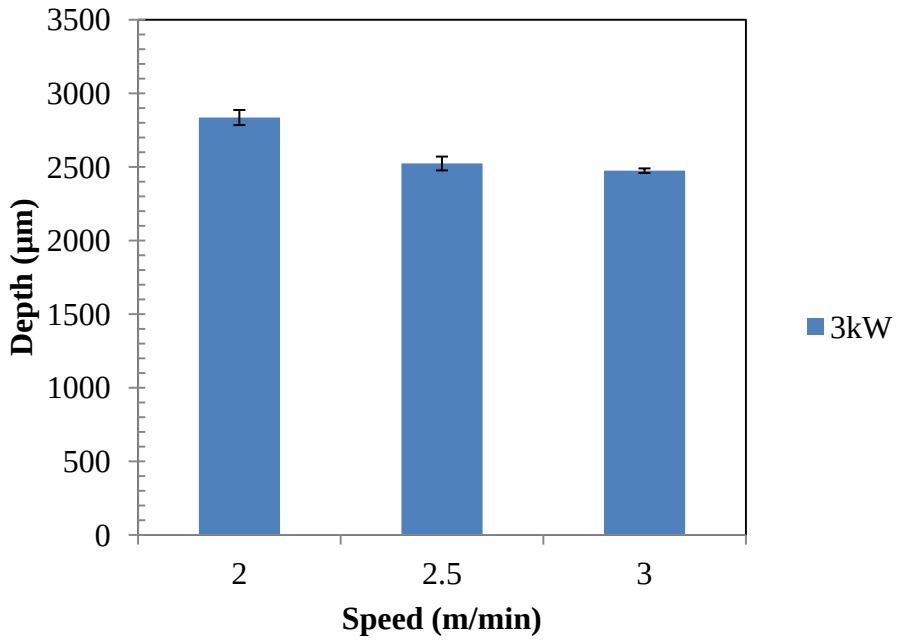

(a)

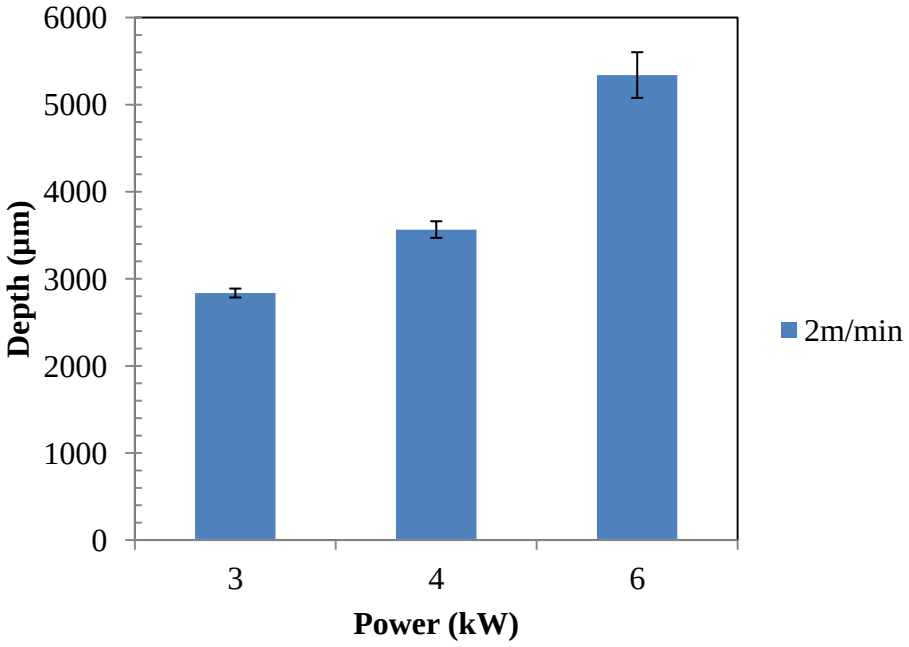

(b)

Figure 4.9: Variation of weld depth with (a) welding speed (b) laser power

In this study the laser welding power was initially kept constant at 2.5 kW and the welding speed was varied to produce a range of heat input values (Table 4.1). A typical cross-section of weld is shown in Figure 4.10. The effect of various speeds on the TCLs is shown in Figure 4.11. An increase in speed increases the TCL. This result is in agreement with reports by other researchers, which show that increase in welding speed increases HAZ cracking for high power density welding [4, 6, 13, 109, 110].

It is known that HAZ liquation cracking is due to a combination of thermal stress and crack susceptible material condition. Welding parameters influence thermal stresses. Thermal stresses increase with cooling rate. An analysis of heat flow in welds by Adams et al. [116, 117] showed that the cooling rate is inversely proportional to the heat input. This relationship is logical because it implies that the weld cools slowly when there is a high amount of heat input in the metal. Therefore, relating this analysis to Equation (4) suggests that cooling rate decreases with reduction in welding speed or increase in power. Corroboratively, Choi et al. [118] illustrated that reduced welding speed not only lowers cooling rate, but also reduces thermal stresses generated. At slow welding speeds, higher heat input, melting along the welding direction occurs slowly. In effect, the laser beam is within a particular position for a longer time causing gradual temperature change, low thermal gradient, in the different weld regions and slowing down the cooling rate behind the molten keyhole.

Table 4.1: Welding parameters and associated heat input for 2.5 kW laser power

High range	Power(kW)	Speed (m/min)	Heat Input J/mm	Depth
	2.5	1	150	
	2.5	0.7	214.3	
	2.5	0.5	300	3.3 - 4.1mm

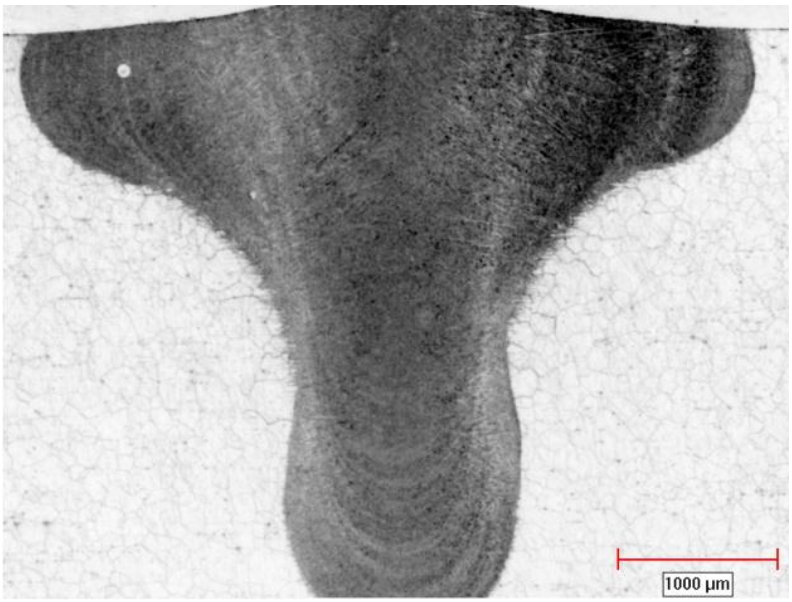

Figure 4.10: Optical micrograph showing cross-section of weld produced using a 2.5kW laser power and a welding speed of 0.5 m/min

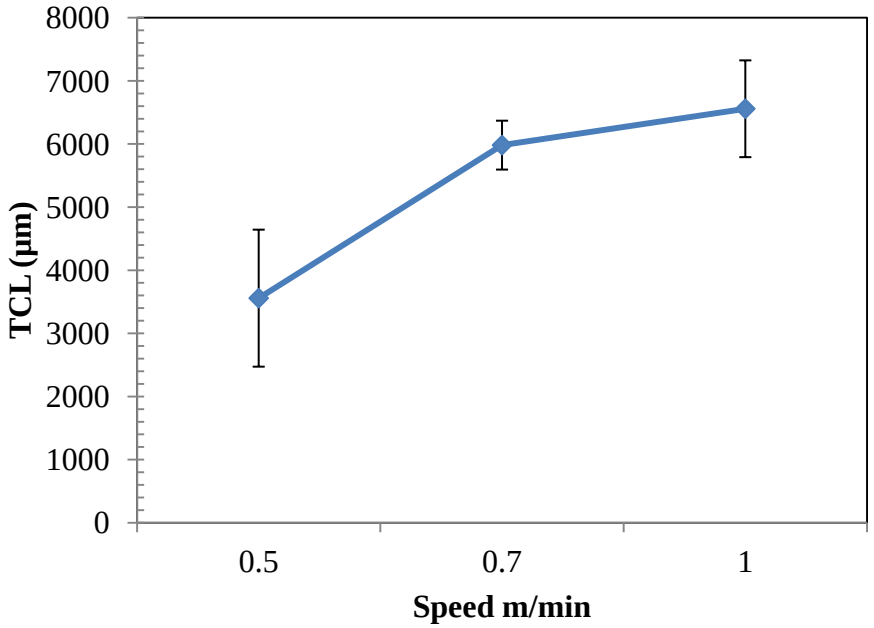

Figure 4.11: Variation of total crack length with speed for 2.5 kW laser power welds

The weld cooling gradually could reduce the magnitude of the contraction and expansion experienced in the joint, which lowers the thermally generated welding stresses. Therefore, the reduction of HAZ cracking with an increase in heat input caused by a decrease in welding speed can also be related to slow cooling rate and the resultant lower thermal stresses that drive cracking. This behaviour is consistent with the theoretical models in the literature, which show that an increase in welding heat input would reduce the welding stresses that drive HAZ cracking [82, 119, 120]. Hence, a slow welding speed is attractive not only for the increased weld penetration, but also for reduced susceptibility to HAZ cracking.

This observed effect in which an increase in heat input minimizes HAZ cracking, however, was not seen in all of the welding parameters used in this study. Welds were produced by using higher values of laser powers at 3 kW, 4 kW, 6 kW and the heat input range is shown in Table 4.2. The Figure 4.12a shows a variation of HAZ cracking (TCL) with welding speed of the coupons welded using a power of 3 kW and 4 kW. As can been seen from the figure, when heat input is increased by reducing speed, TCL rather increases, which is contrary to the previous results in this study. This behaviour seen at these high power levels also goes against the prediction by the theoretical models discussed in the literature, which consider that welding stresses decrease with increase in heat input and normally should cause the HAZ cracking to reduce. A similar anomalous dependence of HAZ cracking on heat input is seen in this study when the heat input is increased by increasing laser power. As shown in Figure 4.12b, when the laser power is increased, while the welding speed is held constant at 2.0m/min, TCL increases.

Table 4.2: Welding parameters and associated heat input for higher power values

	Power (kW)	Speed (m/min)	Heat Input (J/mm)	Depth(mm)
Low range				
	3	3	60	
	3	2.5	72	
	3	2	90	2.5 - 2.8
	4	3	80	
	4	2.5	96	
	4	2	120	3.1 - 3.6
	6	2	180	5.1

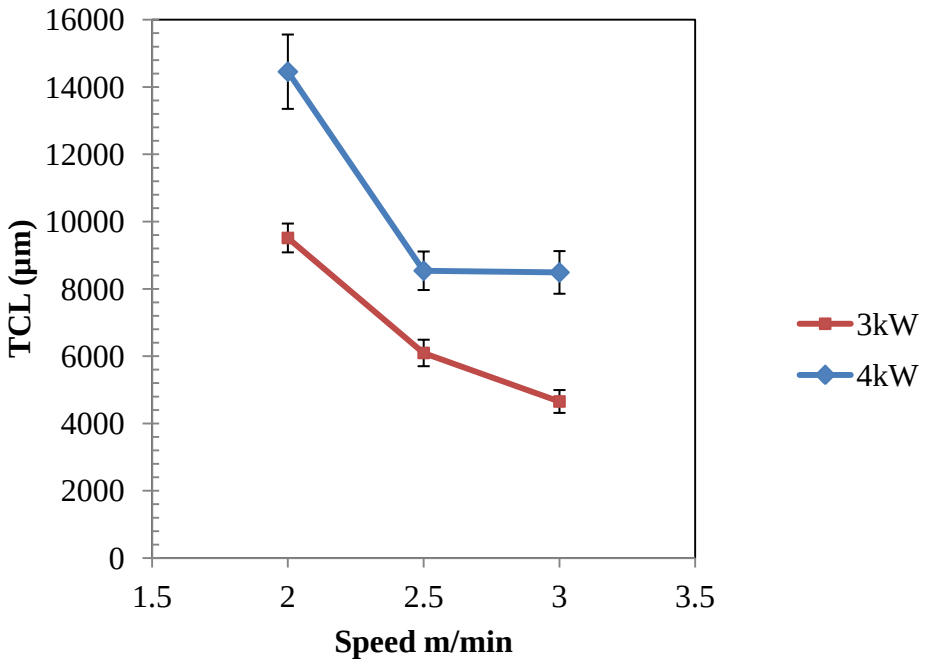

(a)

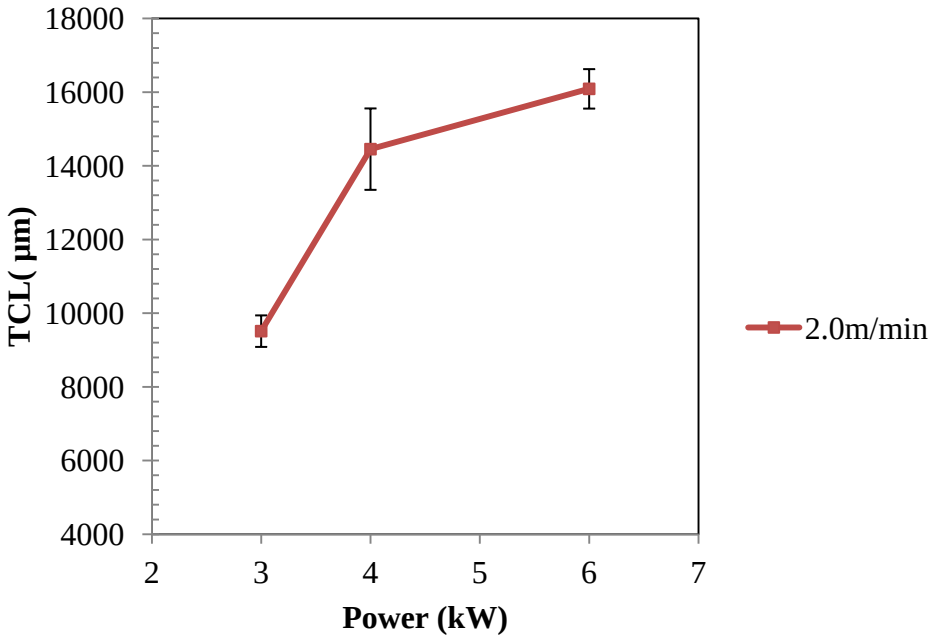

(b)

Figure 4.12: Variation of total crack length with (a) speed and (b) power

Due to the fact that this trend could not be explained by most existing models in the literature, effort has been made in this work to investigate the possible cause of this anomalous behaviour and will be discussed in the two next sub-sections.

4.1.4.3 **Cause of Anomalous Dependence of Cracking on Heat Input**

A closer macro examination of all the weld beads was done. All welds produced at 2.5kW, which exhibit a heat input effect on HAZ cracking that is consistent with theoretical model predictions in the literature, showed no surface irregularities. In addition, the weld cross-section and bead are generally continuous (Figures 4.10 and 4.13a-c) and no FZ cracks can be observed in these welds.

Conversely, in the welds that exhibit an anomalous effect of heat input on HAZ cracking, it was observed that several surface irregularities, including discontinuous weld beads (humping), spatters, undercuts, overlaps as well as excessive porosity occur in the weld cross-section (Figures 4.14a-f). The extent of humping and spattering is observed to increase with heat input as seen in Figure 4.14f. IN 718 is generally known to be resistant to FZ cracking [8, 82]. However, cracking is observed in the weld FZ (Figure 4.15), which are only seen in some of the higher power weld coupons. FZ cracking with a total length of about 0.5 - 1 mm per weld coupon was measured. The FZ solidification cracks are transverse fusion cracks since they are connected to the FZ and HAZ. In this study, these cracks are mostly at the mid section of the weld, associated with porosities.

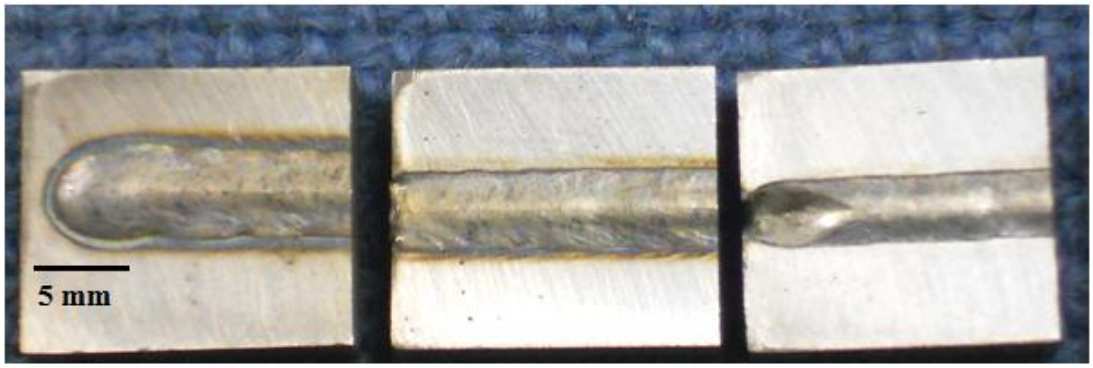

Figure 4.13: Surface of weld beads produced using 2.5 kW laser power with speeds (a) 0.5 m/min (b) 0.7 m/min (c) 1 m/min

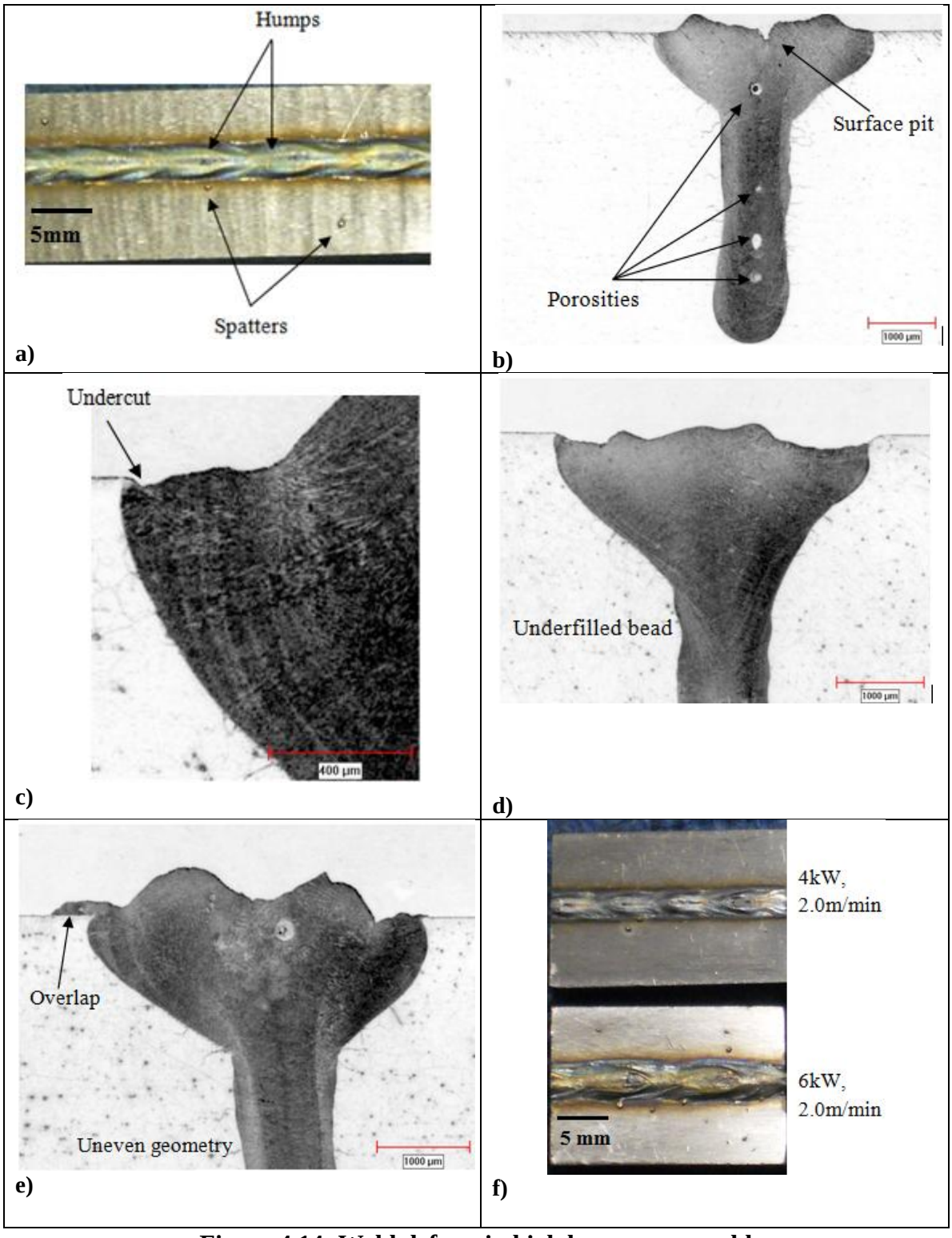

Figure 4.14: Weld defects in high laser power weld

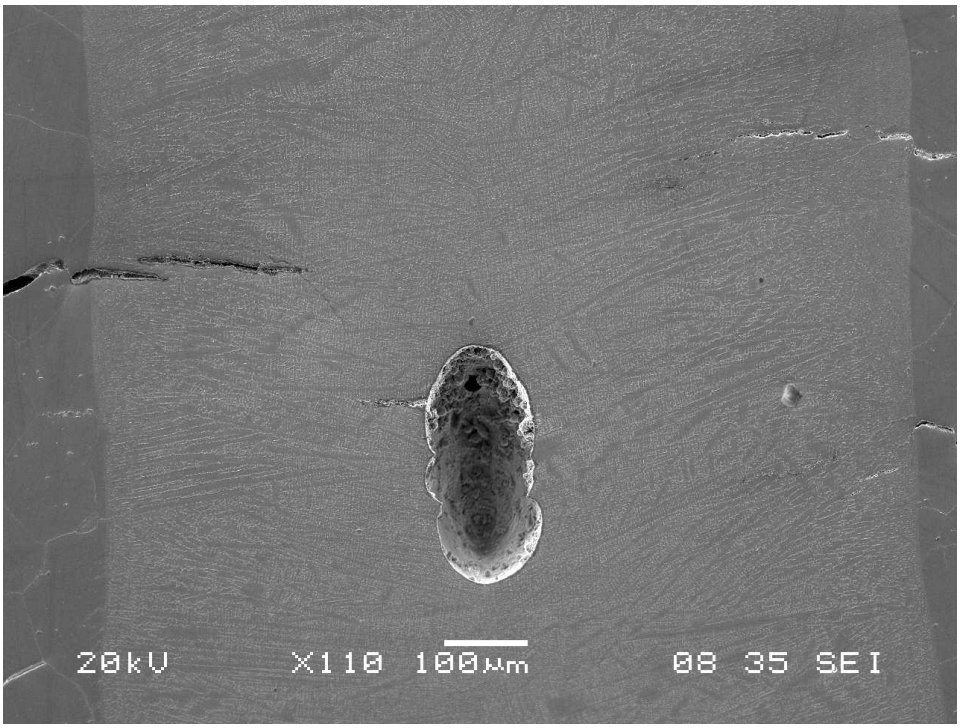

(a)

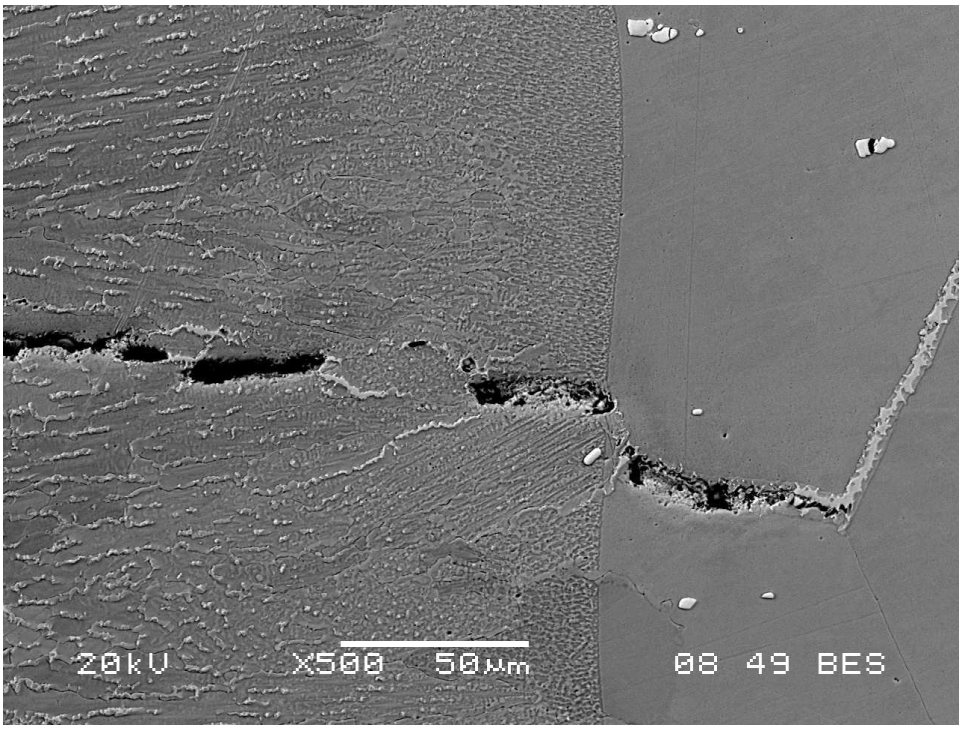

(b)

Figure 4.15: SEM micrographs showing (a) porosity and cracks (b) crack in fusion zone of high power welds

The formation of surface irregularities that are observed in this work, such as discontinuous beads [81], undercuts, excessive porosity etc. [18, 69, 70, 81, 111, 121, 122], have been related to a phenomenon generally referred to as Instability of the laser welding process in the literature.

After several studies of other laser welding process, viewing with high-speed camera and x-ray methods, there is, however, no consensus theory on the detailed mechanisms of how exactly process instability occurs.

Researchers have reported that, depending on the parameters used, the laser welding process can become unstable, which leads to the formation of weld defects [62, 69, 122]. A weld pool keyhole is stable when it is kept open by the vapour pressure of the molten metal, surface tension and fluid flow that draw hot liquid away from the center of the keyhole [59]. Stability is possible when there is heat energy to keep the keyhole open or prevent collapse of the molten metal into the keyhole [59] .

For the most part, process instability has been attributed to the loss of laser energy to laser induced plasma plumes and the resultant unstable molten metal flow due to friction associated with the ejection of plumes from the keyhole [15, 69, 111, 123].

It has been observed that the interaction of the laser, plasma plumes and molten keyhole is dependent on the keyhole front shape, which is dependent on welding parameters [69, 111]. Cicala et al. [81] reported that in the laser welding of Al, the process stability can be affected by welding speed. For instance, if welding is done at a speed that forms a large melt ahead of the keyhole [69, 111]. The laser irradiating continuously on the front

wall of the keyhole results in vaporization of the molten metal and/or gas in a cyclic manner [15, 121, 122]. The ejected plasma plume partially blocks the incident laser beam and absorbs a portion of energy for the welding process [15]. Accordingly, although laser supply power is continuous, the keyhole will vigorously fluctuate [121] since the cyclic emission of plasma intermittently blocks the beam. As welding progresses, the weld depth fluctuates because, in the cycle of plasma formation, instances of small sized plasma that blocks the laser results in lower energy loss, which promotes deeper penetration [18, 59]. Deflection of the beam by plasma causes chaotic flow in and around the keyhole and molten metal may fall in (collapse) or is pushed out of keyhole, which leads to the occurrence of the suggested humping, porosity or spattering [15, 20, 62, 66, 111, 121] i.e welds of poor quality.

The plasma plume is much greater in the welding of low melting temperature alloys, like aluminum [15]. The low melting temperature of Al makes it easy to be vaporized. It is not surprising that reports of instability during welding Al with both low power CO_2 (with a characteristic high wavelength that can easily ionize metal and gas) and YAG (low wavelength) are documented in the literature [15, 59, 121, 122]. There are also reports of process instability in alloys with high melting temperature. The instability phenomenon has also been observed in the CO_2 and YAG welding of steel [15, 18, 111, 121]. These reports have focused on the surface irregularities caused by instability. However, cracks can be generated by process instability [15, 81]. Instability causes variation in the temperature of the molten pool and the non-uniformity of welds [81]. The

partial absorption of incoming laser beam energy by the plasma disrupts the uniformity of the weld by intermittently reducing the amount of based metal melted, which can significantly change the temperature distribution within the FZ and HAZ. The change can set up a substantial variation in the thermal gradient of the FZ and HAZ that may result in considerable weld stresses that cause cracking.

It has been observed that the process instability during laser welding increases with a decrease in welding speed or increase in power [69, 121, 122] implying that process instability increases with heat input. It can be rationalized by the fact that an increase in heat input would increase the amount of plasma produced during welding, which may result in a greater loss of laser energy and enhance process instability. This effect of heat input is in agreement with some of the report in the literature where laser welding at slower speeds (higher heat input) increases cracking and welding defects [16, 123].

Therefore, it is suggested in this study that an anomalous increase in HAZ cracking with an increase in heat input is likely due to process instability which also causes significant weld defects during the fiber laser welding process.

4.1.4.4 **Weld Cross-sectional Shape and HAZ Cracking**

The weld cross-sectional shape is considered as an indication of thermal conditions in the weld pool. As a result, HAZ cracking has been associated with the weld shape, which is influenced by heat input [6, 124]. Welds that have a greater width at the top than bottom cause more solidification shrinkage and thermal contraction at the top of the weld [54].

More shrinkage and contraction could result in higher risk for cracking. Examples of weld cross-sections with varying widths are shown in Figure 4.16. The nail head shaped bead has an obvious neck zone.

Generally, in welding, an increase in heat input causes an increase in weld width [24]. Boucher et al. [124] related HAZ cracking during welding to the shape of the weld cross-section. They reported that high heat input welding produces a wide weld with cross-sectional shape where the difference between the width at the top and bottom is relatively smaller (similar to left of Figure 4.16) compared to the low heat input weld. The weld cross-section produced by high heat input results in a shallower thermal gradient and, thus, lowers the stresses and HAZ cracking [124]. Similar occurrence is reported for a weld parameter range where the weld cross-section has varying widths within a neck zone. Shinonzaki et al. [125] and Woo et al. [6] showed that increased heat input causes weld cross-section to transition from a slim "nail head" shape to a wide "wine cup" shape and that reduces HAZ cracking. The wide wine cup has a gentle curved neck zone while the nail head has a sharp curved neck zone. Furthermore, through analytical model analysis Luo et al. [5] predicted that weld shape with a sharply curved neck zone would experience higher welding stresses and strains during cooling, which then increase HAZ cracking. Recently Gao et al. [126] used numerical model simulation to study the effect of welding heat input on weld cross-sections and thermal stresses that influences HAZ cracking. Their result showed that thermally generated strain rates starts at the weld neck region and decreases with increase in heat input.

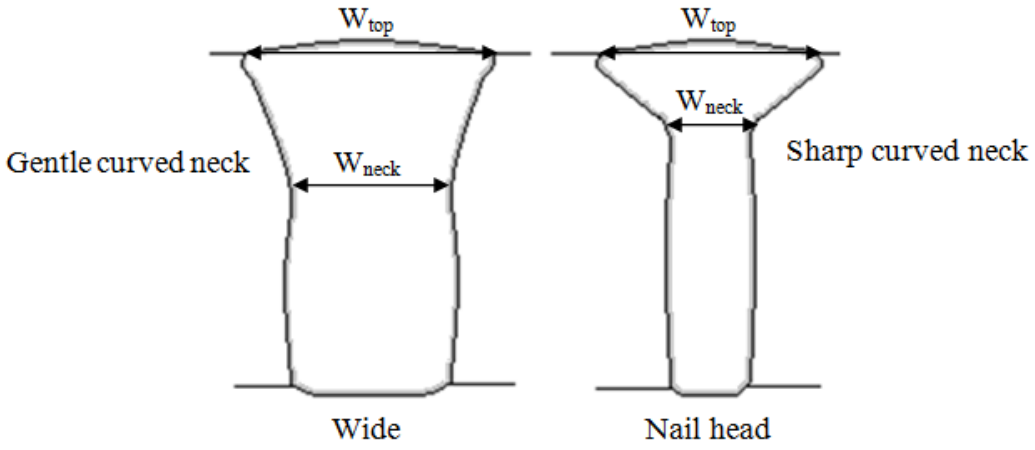

Figure 4.16: Schematic drawing of weld cross-sections showing Wtop and Wneck

These reports indicate that an increase in heat input will not only widen weld cross-section, but also increase weld width uniformity from the top surface to the bottom, which could reduce the strain at the neck region and thus, lower HAZ cracking.

By taking these findings into consideration, the ratio of the width at the top surface (W_{top}) compared to the width at neck zone (W_{neck}), hence forth referred to as width ratio (WR) was suggested and computed to assess the relationship of weld shape with HAZ cracking in the present work. A high WR should signify a sharp reduction of the top width that produces a slimmer mid section width and an associated sharp neck zone that experiences high strains, which cause increased HAZ cracking.

The cross-section and experimental results of the WR measurements of the coupons welded at laser power of 2.5 kW are presented in Figures 4.17 and 4.18, respectively. The results of the coupons that were welded at a laser power of 2.5kW and higher correlate well with the expected trend of variation in HAZ cracking with WR. As can be seen by comparing Figures 4.11 and 4.18, Figures 4.12a and 4.19 and also Figures 4.12b and 4.20, an increase in WR causes an increase in HAZ cracking. In literature, the numerical simulation results by Gao et al. [126] shows weld cross-section shapes and an increase in WR does correspond to increase in the reported thermally generated strain rates in the neck region, which could increase the extent of the HAZ cracking. However, the important difference is in the dependence of WR on heat input for welds produced at 2.5 kW power and those of higher power in this study.

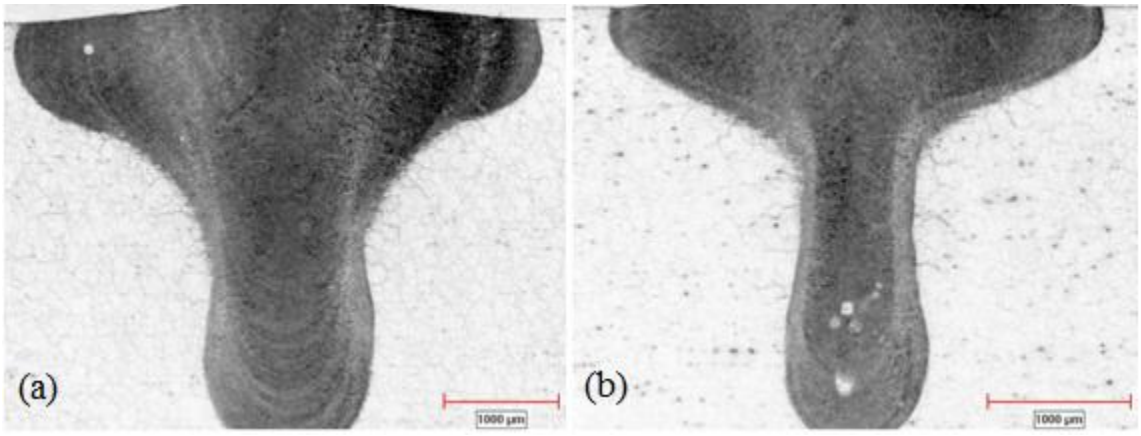

Figure 4.17: Optical micrograph of weld cross-section (a) 2.5kW, 0.5 m /min (b) 2.5kW, 1 m/min

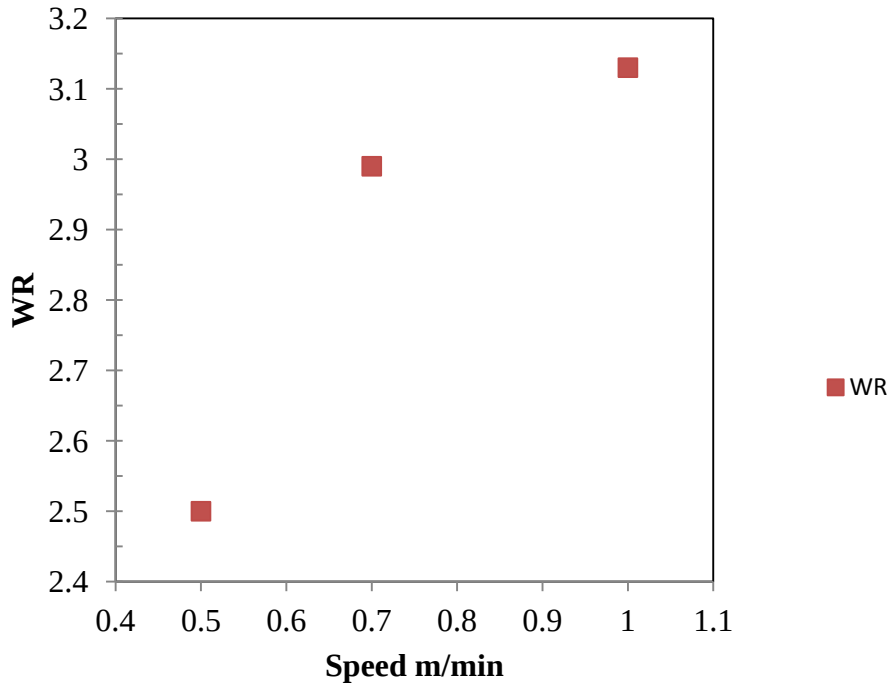

Figure 4.18: Variation of width ratio with speed for 2.5 kW welds

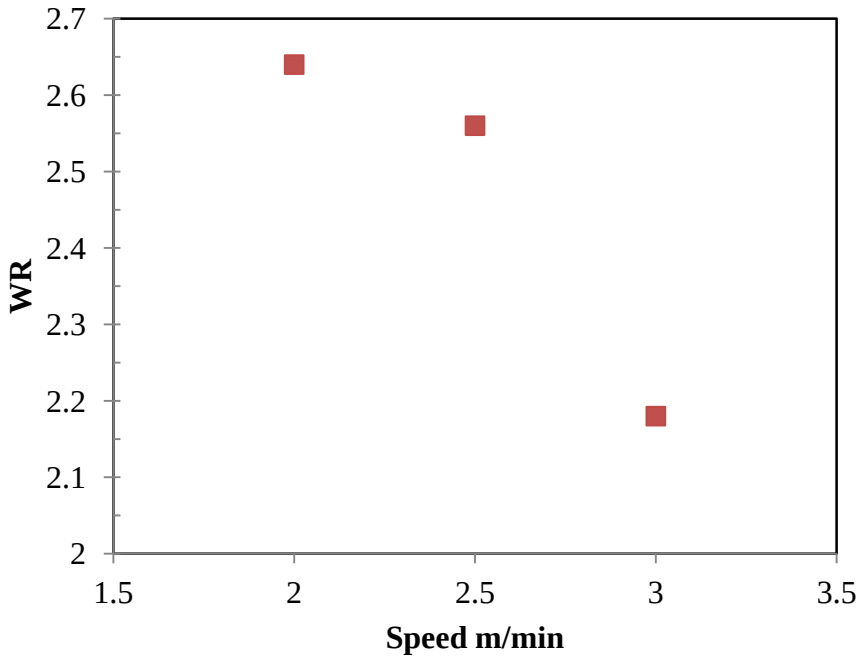

a)

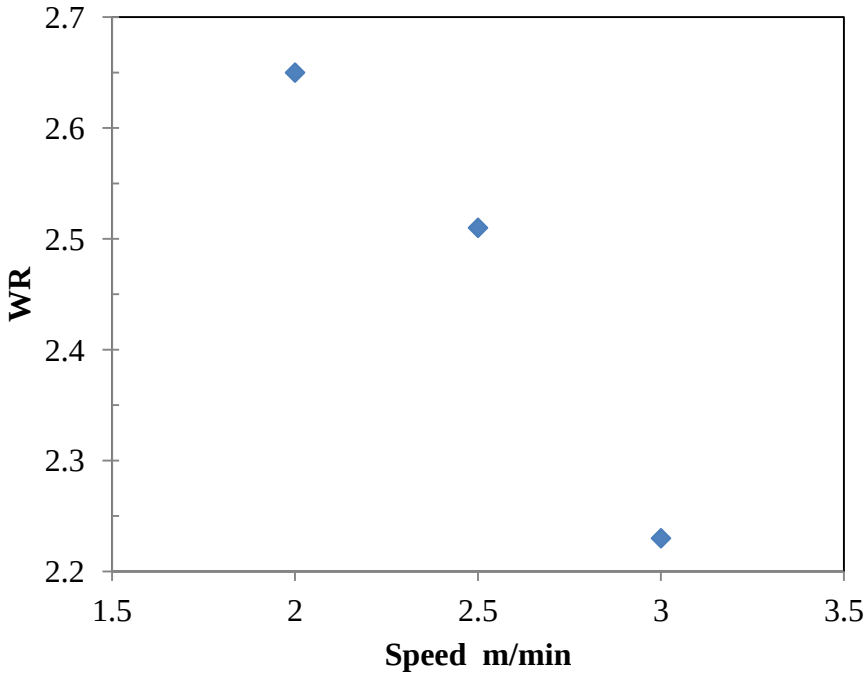

b)

Figure 4.19: Variation of width ratio with speed for (a) 3 kW (b) 4 kW welds

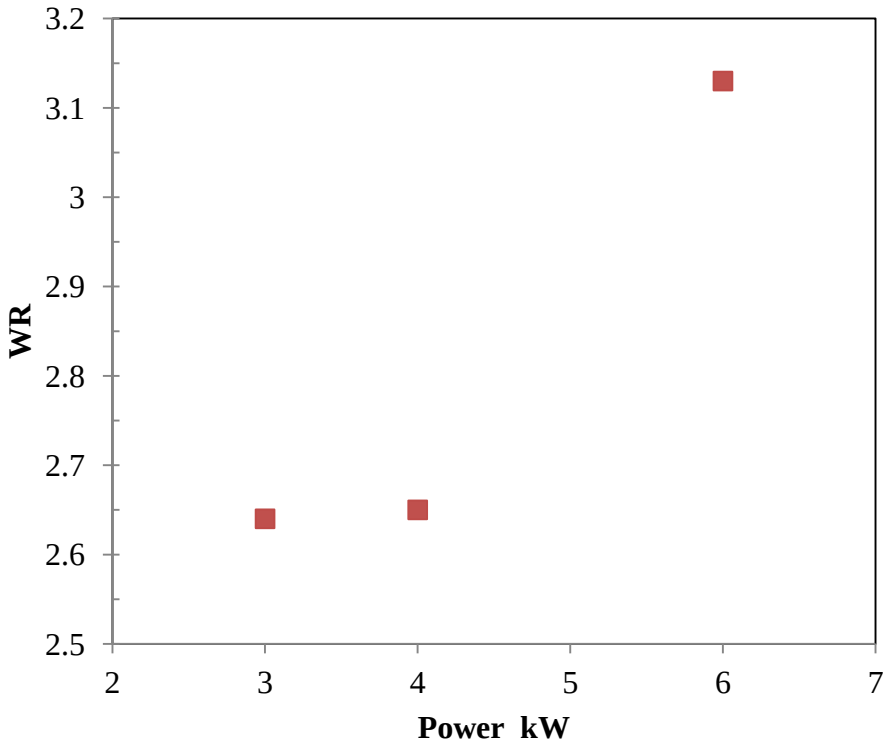

Figure 4.20: Variation of width ratio with power at a welding speed of 2.0 m/min

An increase in the heat input would usually cause a smaller variation in weld cross-sectional width, in agreement with reported results in the literature [6, 124, 125, 126]. Therefore, an increase in heat input is expected to reduce WR, which is the behaviour that is observed in welds produced at 2.5kW laser power Figure 4.18. In contrast, in the weld produced at high power levels, increase in heat input, rather, increases the WR. This abnormal trend can be observed by increasing the heat input by reducing the welding speed (Figure 4.19) and by increasing the laser power (Figure 4.20).

Notably, the set of welds that exhibit an anomalous trend of variation of WR with heat input are the same specimens that show microstructural features and weld defects of laser welding process instability as discussed in section 4.1.4.3.

Process instability, as previously discussed, is caused by loss of laser energy due to blocking of the laser beam by plasma. The loss of energy increases with heat input. It is conceivable that the loss of energy will result in a reduction in the melting of the material within the work-piece, which could translate to decrease in the weld width at the neck region (W_{neck}). A reduction in the W_{neck} with an increase in heat input can, thus, cause the WR to increase rather than the expected decrease.

In the study of welding parameters, hence, the anomalous effect of high heat input increasing HAZ cracking, in IN 718, is due to process instability, which results in welds of poor quality and wide variation in cross-sectional width.

4.1.5 Effect of Pre-weld Heat Treatment on HAZ Cracking in Wrought IN 718

Apart from the heat and cooling cycle caused by welding parameters, it is well known that material metallurgical factors can affect weldability. Therefore, the effect of pre-weld heat treatments on HAZ cracking in fiber laser welds is studied. The TCLs in the coupons, which were given 1hr pre-weld heat treatment at 900^{o}C, 950^{o}C and 1050^{o}C for 1 hr and Air-cooled, was determined.

SEM was used to study the specimen microstructures treated at 900^{o}C for 1 hr and 950^{o}C for 1hr before welding and the micrographs are shown in Figure 4.21. In addition to carbides, these microstructures have intergranular and intragranular needle-like phase particles. The diameter of the needle-like phase particles are less than 1μm in size, and therefore, composition quantification by SEM point analysis is unreliable. The result of the SEM/EDS line scan of the needle-like phase is shown in Figure 4.22. The particles are enriched in Nb and depleted in Cr, Fe compared to the matrix and their morphologies suggest that they are δ phase particles as reported in the literature [95].

The rapid formation and precipitation of the Nb-rich δ phase in nickel-alloys occur in the temperature range of 840^{o}C - 950^{o}C [26] with a peak rate at 900^{o}C [41]. Promoted δ nucleation effectively controls grain size [1, 26] i.e. the particles will mitigate the usual grain growth process. The result of mean grain size measurements (Table 4.3) shows that coupons which are heat-treated at 900^{o}C/1hr and 950^{o}C/1hr have a similar mean grain size as the as-received material of 26 ± 5μm.

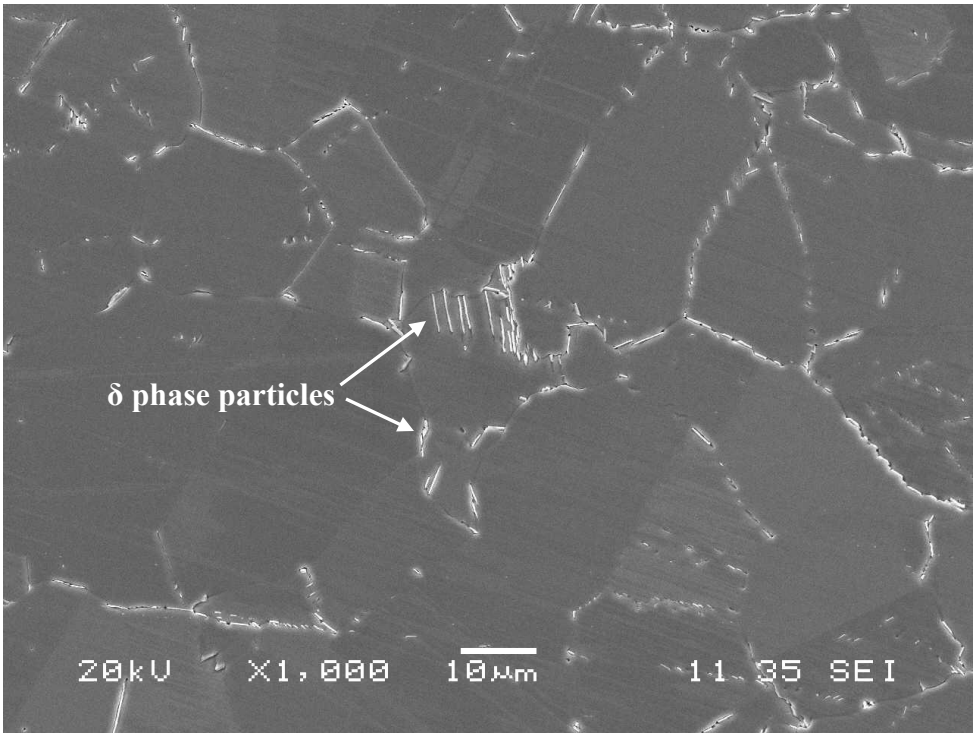

a)

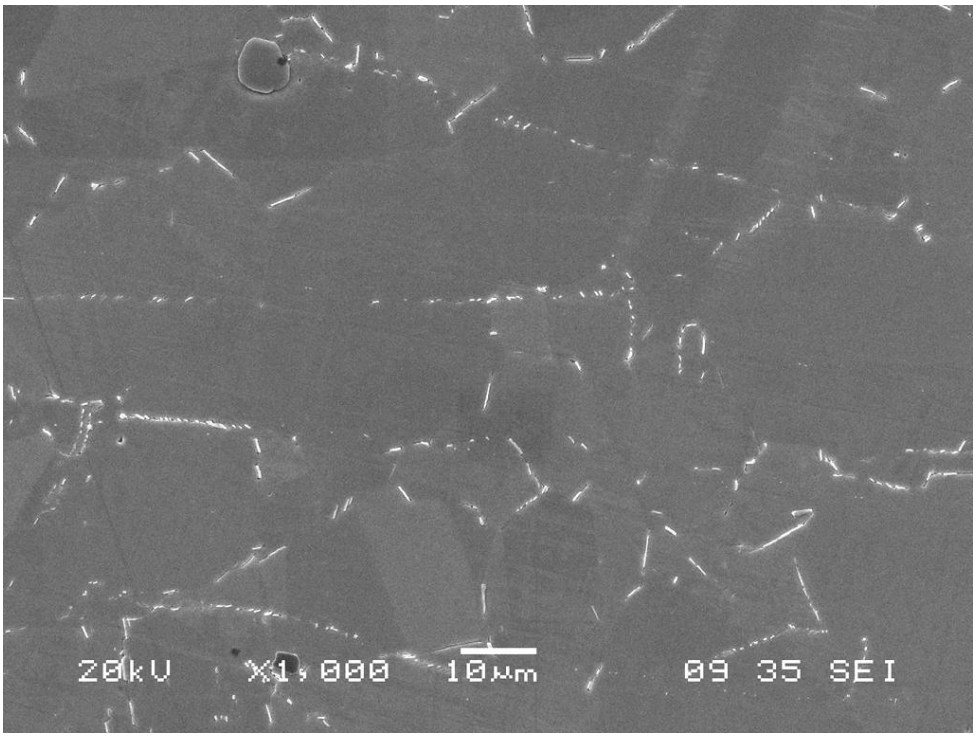

b)

Figure 4.21: SEM micrograph of pre-weld microstructure of IN 718 heat-treated at (a) 900°C/1hr/AC (b) 950°C/1hr/AC

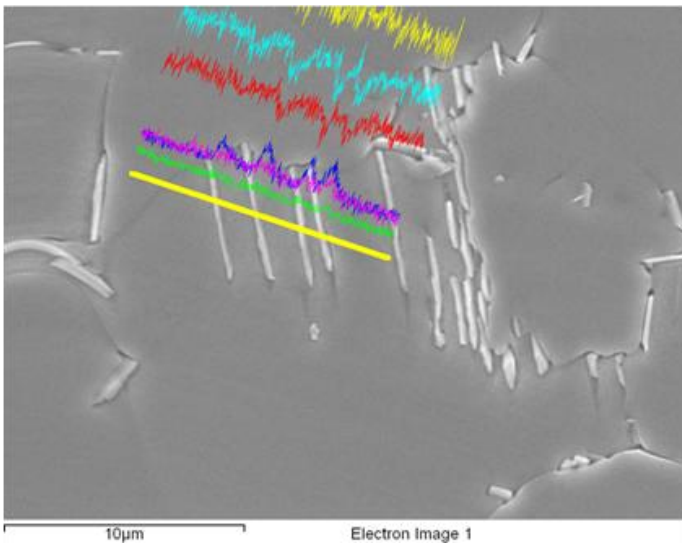

a)

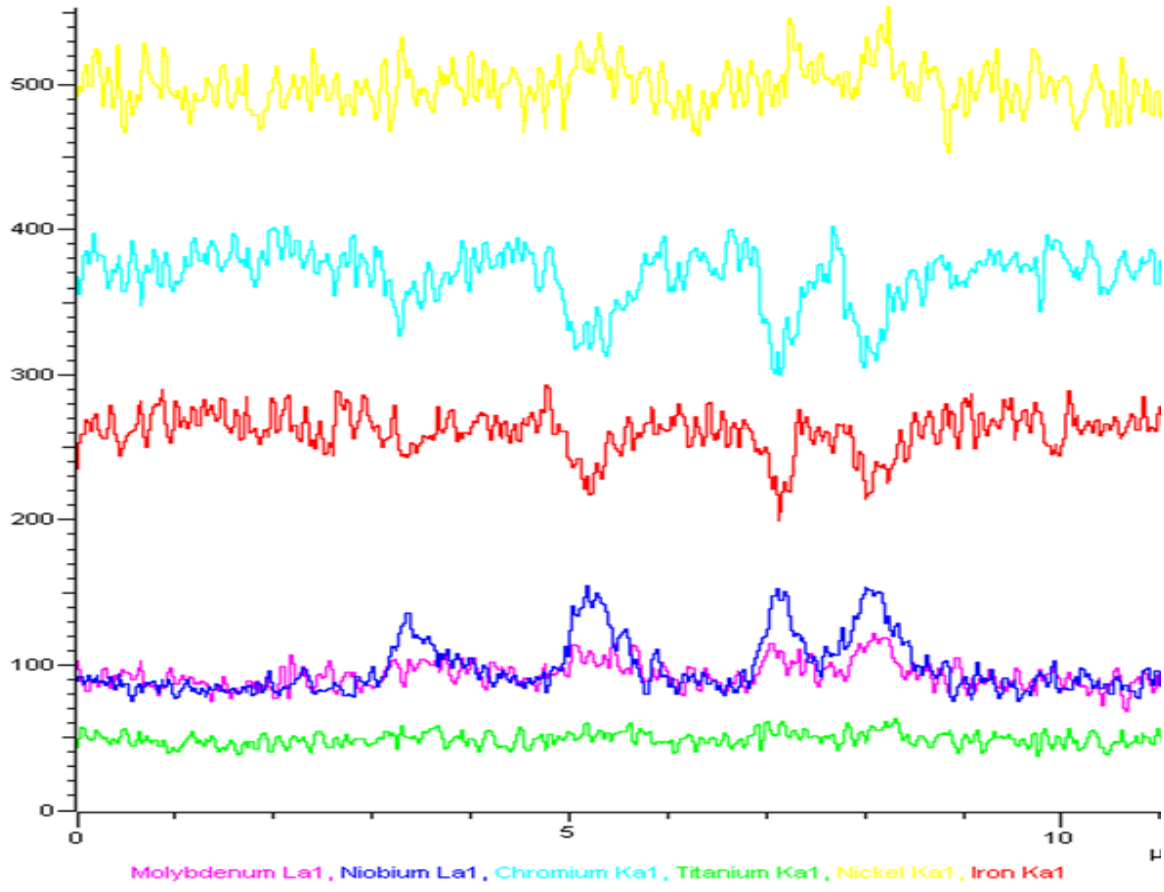

b)

Figure 4.22: SEM/EDS Line scan of δ phase precipitates in IN 718 heat-treated at 900°C/1hr/AC

Table 4.3: Mean grain size of pre-weld heat treated coupons

Grain size Measurement for Pre-weld Heat treatment	
900^{o}C/1hr/AC	29±6µm
950^{o}C/1hr/AC	29±6µm

It is possible that existing δ phase particles restricted grain growth by pinning down the grain boundaries.

A SEM examination was performed on the HAZ of all pre-weld heat-treated coupons after welding. SEM micrographs were taken in the weld neck region, which shows the greatest extent of HAZ liquated grain boundaries in all treatments. The HAZs of the 900^{o}C and 950^{o}C, as shown Figure 4.23, show extensive grain boundary liquation (dissolved Nb- rich δ phase) compared to the HAZ of 1050^{o}C (Figure 4.24).

The TCLs in the HAZ of welded coupons subjected to the different pre-weld heat treatments are shown in Figures 4.25 a and b. The results show that heat treatment at low temperatures of 900^{o}C and 950^{o}C produce better resistance to HAZ cracking than treatment at 1050^{o}C, for all welding parameters used.

Generally, pre-weld heat treatment affects the susceptibility of material to HAZ cracking by altering grain boundary liquation through elemental intergranular segregation and changing grain size.

In polycrystalline material, it is important to consider grain boundary sliding and intergranular liquid film thickness in relation to cracking susceptibility [127]. Significant grain boundary sliding, which causes stress concentration, together with intergranular liquid distribution can cause crack initiation and propagation from grain boundary triple points [104].

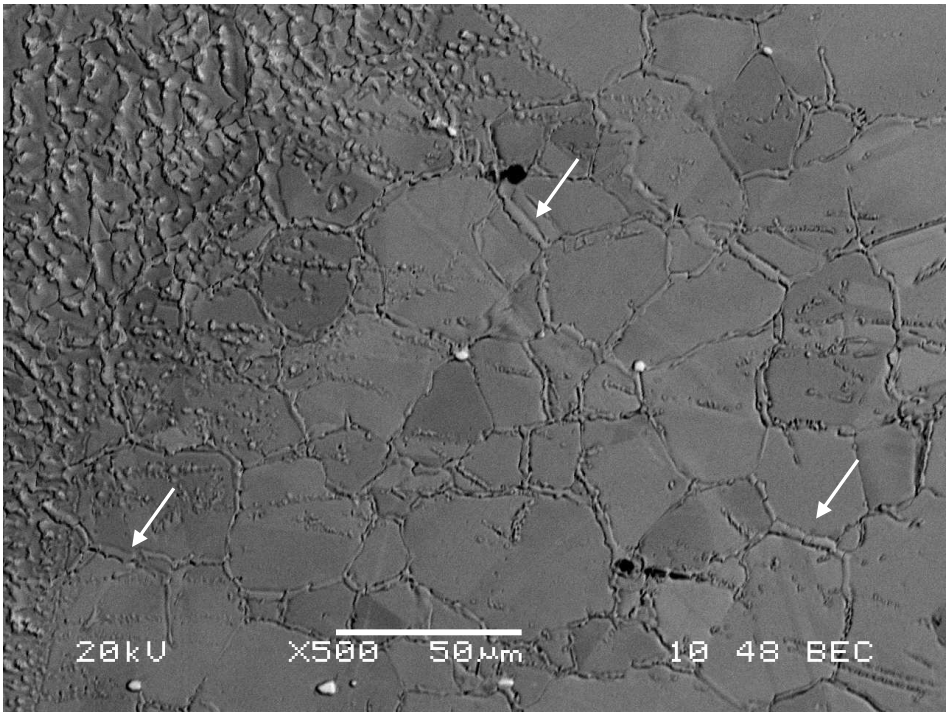

a)

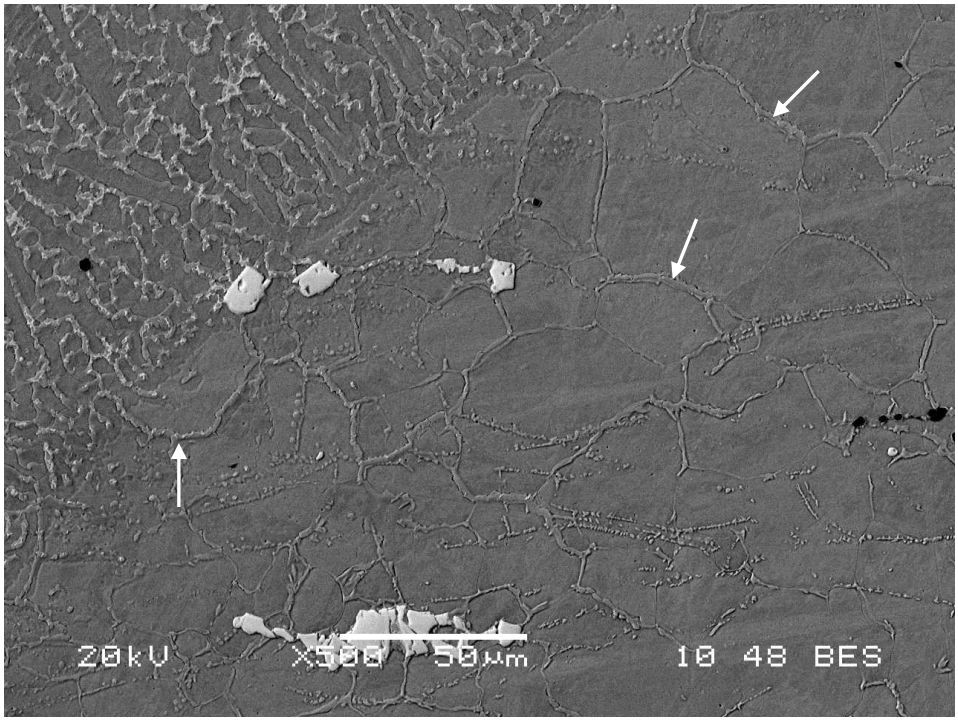

b)

Figure 4.23: SEM micrograph of HAZ in the weld-neck region of coupons pre-weld heat-treated at (a) 900°C/1hr/AC (b) 950°C/1hr/AC. Arrows point at some liquated grain boundaries

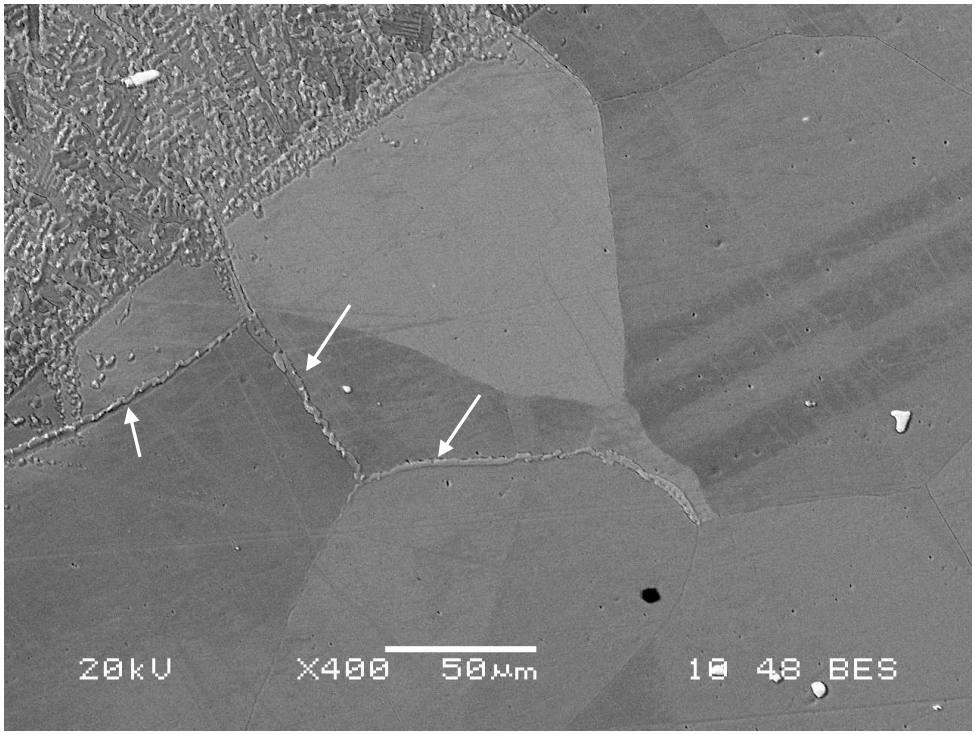

Figure 4.24: SEM micrograph of HAZ in the weld-neck region of coupon pre-weld heat–treated at 1050°C/1hr/AC. Arrows point at some liquated grain boundaries

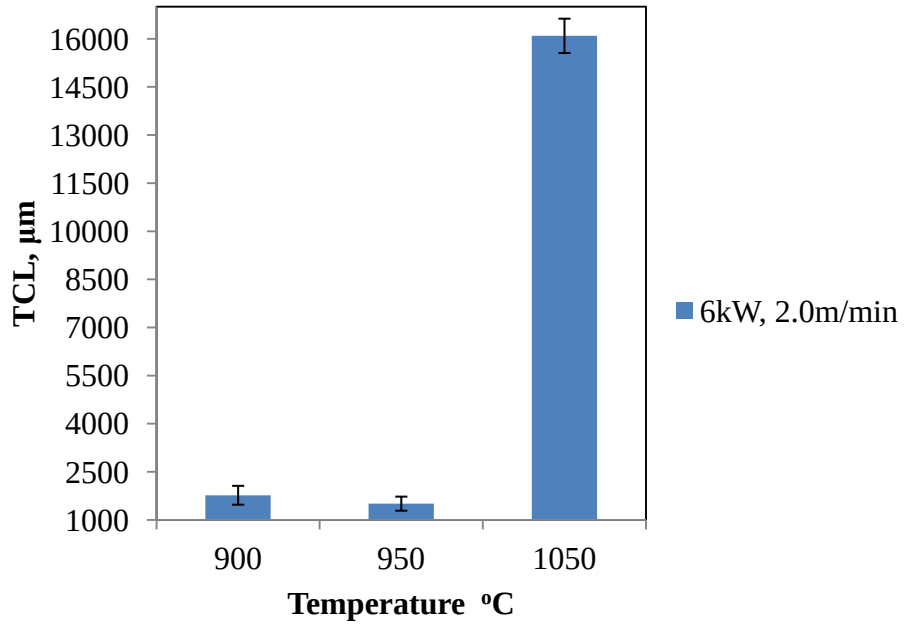

a)

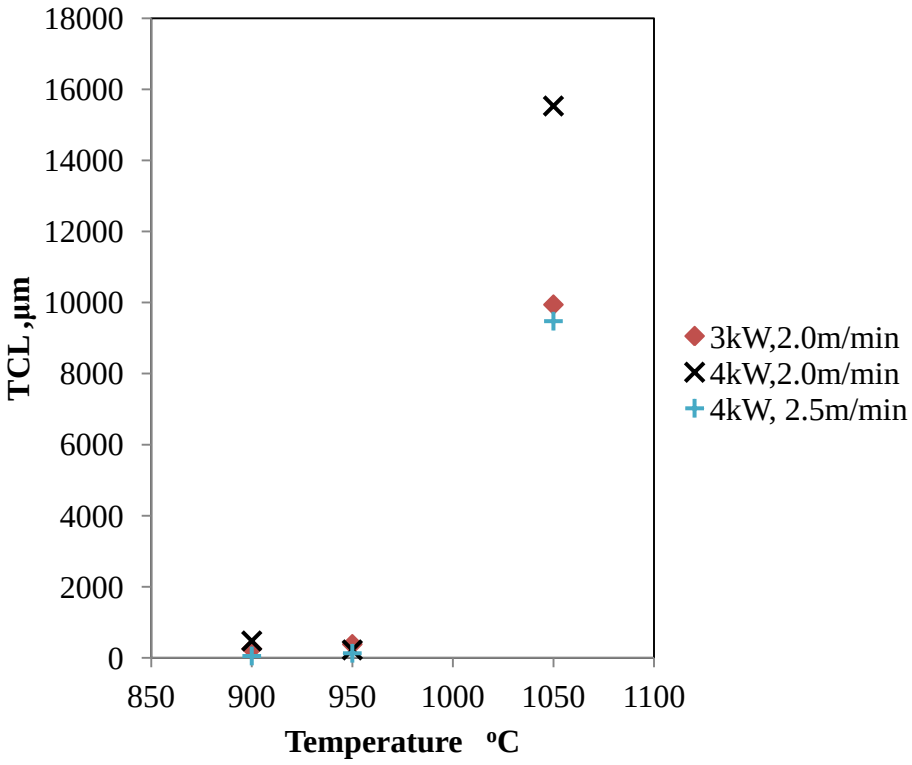

b)

Figure 4.25: Variation of total crack length in coupons pre-weld heat treated at different temperatures and welded with different parameters

In addition, according to the Equation (3) developed by Chadwick and Miller [103]:

$$\sigma = 2\frac{\gamma_L}{h}$$

a large, h, i.e. thick grain boundary liquid, would require less tensile stress ,σ, for grain boundaries to separate. In addition, liquation of Nb-rich particles have been associated with HAZ cracking [44, 51].However, in the current study, heat treatments at 900^{o}C and 950^{o}C, which show significant grain boundary liquation in the HAZ due to the dissolution of δ phase, resulted in higher resistance to cracking. Pellini [128] suggested that hot cracking can be prevented in the case of thick interdendritic films, i.e. "mushy or pasty zone", due to uniform distribution of weld stresses/strains as opposed to a situation with a very thin film. The semi-rigid mass can freely move to accommodate stresses and, even if cracks occur, the copious liquid can fill spaces between grain boundaries. However, the amount of grain boundary liquid is not the only necessary factor that can be used to explain the cracking susceptibility of IN 718 welds.

Materials become more susceptible to HAZ intergranular cracking by constitutional liquation and/or elemental segregation of melting point depressant along grain boundaries during pre-weld heat treatment [11, 22]. Thompson et al [51, 101, 102] suggested that pre-weld heat treatment, which alters grain boundary chemistry, has a strong influence on cracking susceptibility of IN 718 superalloy. It is also suggested that grain boundary chemistry could also be altered by constitutional liquation of MC carbides and Laves phase during welding, but the grain boundary is mostly affected by surface-active

impurity segregation caused by heat treatment [101]. Heat treatment, in essence, does not change the mechanism of constitutional liquation, but can affect the manner by which the liquid spreads along grain boundaries – wettability, which is a function of the intergranular segregation of impurity elements [44]. Vincent [23] and Kelly [34] indicated B as the most significant depressant of the melting point of grain boundaries in comparison to S and P. Therefore, B has a more detrimental effect on the weldability of IN 718. Reduction in the melting temperature of grain boundaries by segregated B atoms causes a longer lasting intergranular liquid to exist during the cooling of the weld. It can be said that the extent of cracking depends not only on the amount of liquid but also on the time that grain boundary liquid exists [48, 129]. A low melting liquid film (long life film), which causes lasting wetting [104], provides a situation for concentration of weld strains to be imposed on the intergranular film and leads to cracking [48, 129]. In considering these reports, it can be suggested that lower melting intergranular liquid makes a material more susceptible to cracking because it may allow time for strains to develop across weakened liquated grain boundaries, which can eventually cause cracking. Karlsson et al. [84, 130] reported that non-equilibrium grain boundary B segregation, in austenitic stainless steel, is sensitive to heat treatment temperature and cooling rate.

Therefore, in the present work, test coupons were pre-weld heat treated at 950^{o}C, 1050^{o}C and 1150^{o}C for 1 hr and subsequently cooled at different rates, since the cooling rate affects the extent of elemental intergranular segregation. The AC (lower cooling rate) coupons were compared to water-cooled (WC, faster cooling rate) coupons. For the same temperature, grain size was constant while cooling rates, cooling from the temperature,

were differed to initiate different extent of intergranular segregation. The mean grain size of WC specimens showed no significant increase in comparison to AC specimens as shown in Table 4.4. Subsequently, theses coupons were welded by using a laser power of 2.5kW and a speed of 1m/min and good quality welds were produced.

The TCL for each condition is shown in Figure 4.26. From these results, it is important to note that for the parameters used, HAZ cracking does not occur in welds given a pre-weld heat treatment of 950^{o}C for the two cooling rates used. On the other hand, 1 hr of pre-weld heat treatment at 1050^{o}C and 1150^{o}C results in HAZ cracking. The cracking increases with temperature, and the highest TCL is recorded at 1150^{o}C condition. Also, HAZ cracking decreases with increasing cooling rates in coupons heat-treated at 1050^{o}C and 1150^{o}C before welding. Hence, a faster cooling rate WC results in lower TCLs than AC conditions. It is evident that TCL, in this study, is also sensitive to pre-weld temperature and cooling rate, which suggest cracking is affected by intergranular segregation.

A material maintained at a high temperature consists of an equilibrium concentration of vacancy-solute complexes and vacancies [85, 87]. Vacancy-solute complexes form based on the positive binding energy (attraction) that exists between vacancy and solute atoms [131]. Upon rapid cooling to a lower temperature, vacancy concentration becomes supersaturated. To attain equilibrium vacancy concentrations of lower temperatures, loss of vacancies occur at interfaces, such as grain boundaries and free surfaces, which act as sinks for vacancy annihilation.

Table 4.4: Grain sizes of pre-weld heat-treated IN 718 coupons for different temperatures and cooling rates

950^{o}C/1hr/AC	29±6μm
950^{o}C/1hr/WC	28±6μm
1050^{o}C/1hr/AC	100±30μm
1050^{o}C/1hr/WC	100± 23μm
1150^{o}C/1hr/AC	274± 75μm
1150^{o}C/1hr/WC	253± 61μm

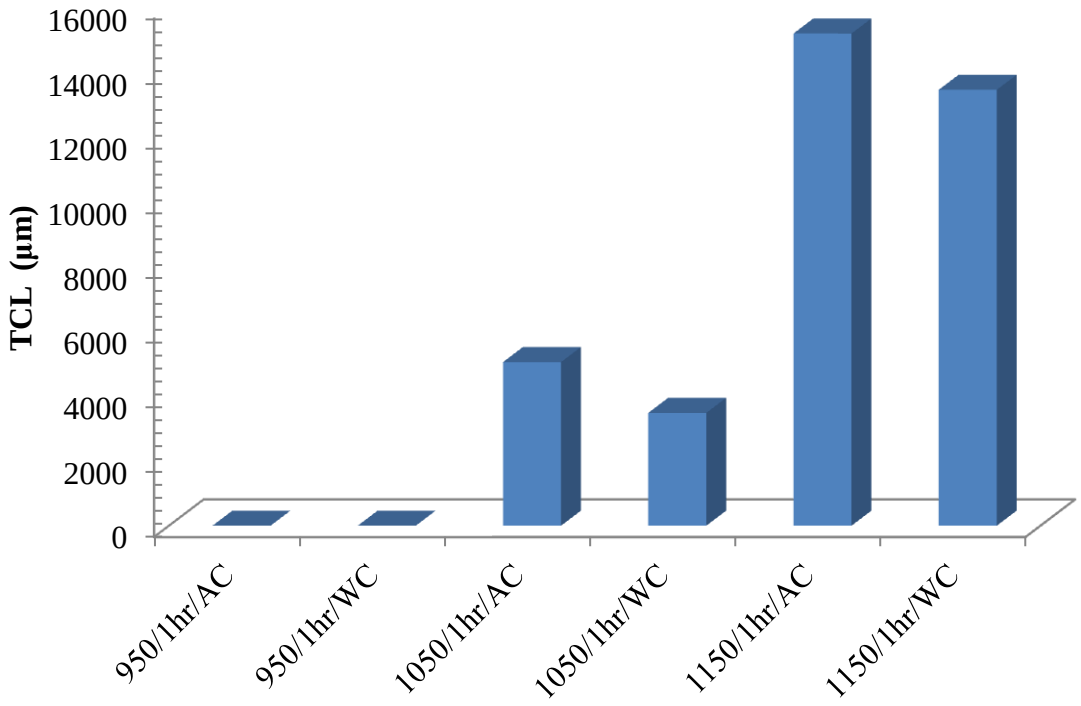

Figure 4.26 : Variation of HAZ total crack length with pre-weld heat treatment temperature and cooling rate

The loss results in a decrease in the concentration of vacancies near the vacancy sinks. Generally, there remains a supersaturated concentration in the grain interior. Therefore, between the grain boundary and further into the intragranular regions, a concentration gradient of vacancies will exist. The concentration gradient drives the diffusion of vacancies, which are associated with solute atoms [89] (due to positive binding energy), from the remote intragranular regions to be deposited at the grain boundary sinks. The diffusion of complexes is supported by the fact that the diffusion coefficient of the solute-vacancy complex exceeds that of vacancy alone [131]. Also, this diffusion of solute-vacancy to the grain boundary is driven by a reduction in free energy, which is associated with the annihilation of excess vacancies at sinks (grain boundaries) [90] and, hence, there is formation of a solute-rich boundary layer. This explains how non-equilibrium grain boundary segregation occurs during the cooling of alloys from elevated temperatures. Considering the temperatures above which diffusion becomes significant [85], high cooling rates are quick enough to preclude the diffusion of elements almost completely during cooling [87]

Detailed experimental studies that used secondary ion mass spectrometry **(**SIMS) in analysis, such as those by Huang et al. [131] and Idowu et al. [132], have revealed that nickel-based alloys, like IN 718, undergo non-equilibrium B segregation to grain boundaries and the segregation increases with heat treatment temperature and reduced cooling rate after heat treatment. Therefore, previous findings on segregation are used to analyse the findings in this study.

It can be expected that grain boundary B segregation should be the highest for coupons subjected to treatment at 1150^{o}C for 1 hr, which is the highest cooling start temperature used in this study. In addition, it is suggested that a slower cooling rate allows time for vacany-B complexes to diffuse from within the grains to deposit B (solute atom) at grain boundaries, such that, AC coupons can have a higher degree of B segregation than WC coupons. As a result, the possible increase of B segregation to grain boundaries can be the reason for the higher TCL in the treatments at 1150^{o}C for 1 hr and AC coupons in comparison to the lower heat treatment temperatures and WC coupons, respectively.

Another factor that can affect crack behaviour is grain size when considering fine grained wrought material. Heat treatment of IN 718 above the solvus temperature of the δ phase (approximately 1000^{o}C) will dissolve δ phase, which pins grain boundaries [114]. If there is no pinning of grains in fine grained material, grain growth will occur. To further investigate the effect of grain size on HAZ cracking, pre-weld heat treatments that involve a combination of treatment were used and are given as follows:

1. 1050^{o}C for 1hr with WC plus a final treatment at 950^{o}C for 1hr with AC , and
2. 1150^{o}C for 1hr with WC plus a final treatment at 950^{o}C for 1hr with AC.

Initial heat treatment increased grain size. The specimens of heat treatment 1 and 2 had mean grain sizes of 102±22μm and 257±60μm, respectively. The final heat treatment, before welding, is likely to produce similar segregation behaviour of 950^{o}C/1hr/AC, but with a different grain size. The mean grain size of the above two heat treatments, 1 and 2,

in comparison to 950^{o}C for 1 hr (Table 4.4) increased by magnitude of approximately 4X and 8.5X, respectively.

The results in Figure 4.27 show that even though all conditions had similar final heat treatment at 950^{o}C for 1 hr before welding, with likely similar segregation behaviour, increased grain size causes an increase in the TCL. This result shows that larger grain size adversely affects resistance to the cracking of IN 718.

The following points could be explanations for the effect of grain size on HAZ cracking of IN 718 fiber laser welds. Large grains decrease the grain boundary surface area available for grain boundary segregation of surface-active elements, like B, which reduces the melting temperature of the intergranular regions [85, 132]. The decreased grain boundary area means that, for the same heat treatment condition, there would be more B solute segregates per grain boundary area for large grained materials. Also, a smaller grain size provides more grain triple junctions, hence, more grain boundary area to hinder crack propagation [106]. Therefore, large grain size materials that have less grain boundary triple points can also be a detrimental factor.

In the present work, there is more indication that possible reduced non-equilibrium segregation of B at a lower temperature mitigates HAZ cracking. This is evident by the decrease in TCL for coupons heat treated at 1150^{o}C/1hr/WC and given a final heat treatment at lower temperature of 950^{o}C/1hr/AC in comparison to a heat treatment at 1150^{o}C/1hr/AC and 1150^{o}C/1hr/WC (Figures 4.26 and 4.27). The three heat treatments have similar grain sizes (Table 4.4. and Figures 4.27).

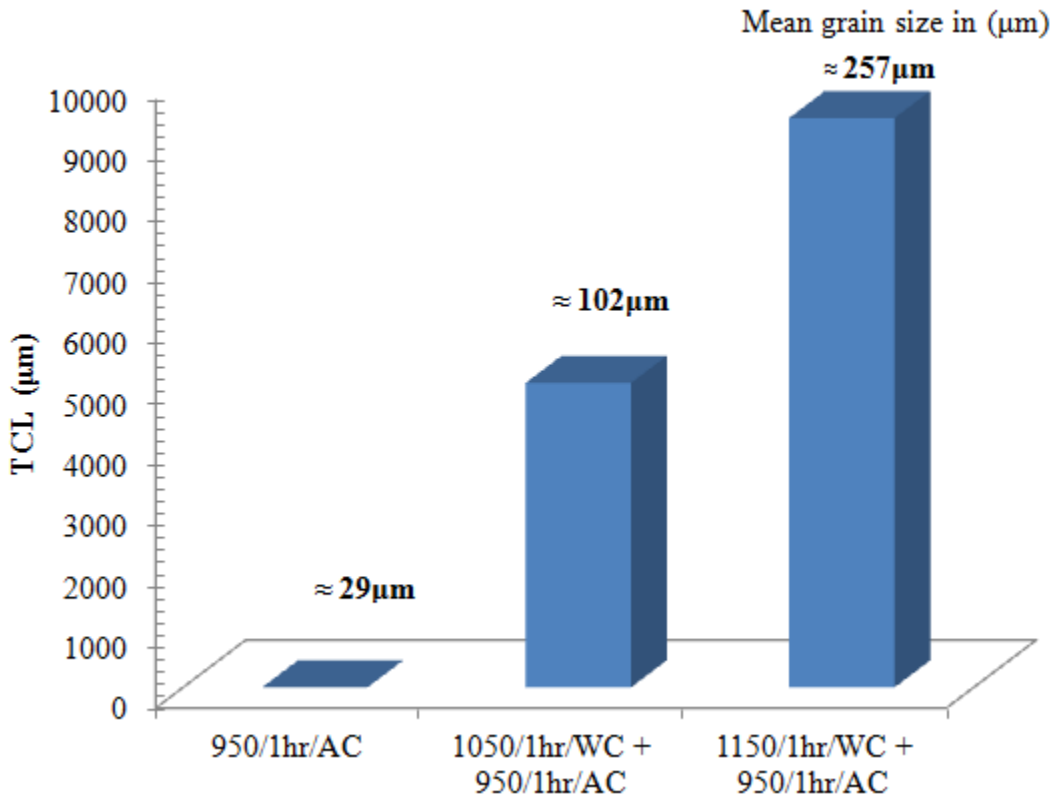

Figure 4.27 : Variation of total crack length with pre-weld heat treatment that produced different grain sizes

The pre-weld heat treatments carried out at 900^{o}C for 1hr and 950^{o}C for 1hr are more resistant to cracking for both stable and unstable welding conditions than higher temperatures, that is, at 1050^{o}C for 1hr and 1150^{o}C for 1hr. Therefore, based on observations in this study and correlation to previous studies, the following are suggestions about the possible influence of pre-weld heat treatment on the HAZ cracking of the fiber laser welded wrought IN 718. Although extensive dissolution of Nb-rich δ phase occurred at the HAZ grain boundaries of the 900^{o}C and 950^{o}C coupons, the amount of liquid at grain boundaries formed a semi-rigid mass that could have acted as a stress reliever or filled cracks if they occurred. Also, more grain boundary triple points of smaller grained material could have mitigated crack propagation. In addition, the possible lower intergranular B segregation, due to lower cooling start temperature and more grain boundary area, could have shortened the life of the grain boundary liquid film. Accordingly, the intergranular liquid possibly solidified before significant stresses, which could have caused the severe cracking, developed. Therefore, the amount of liquid at the grain boundary, smaller grain sizes and short life of intergranular liquid due to lesser extent of B segregation had positive effects on the weldability of IN 718 in treatment of 900^{o}C for 1hr and 950^{o}C for 1hr. In contrast, the detrimental effect of large grain size as well as the longer life of the liquid formed at grain boundaries caused by more intergranular B segregation likely resulted in reduced resistance to HAZ cracking of coupons that were heat treated at higher temperatures of 1050^{o}C for 1 hr and 1150^{o}C for 1 hr.

4.1.6 Effect of Multiple Heat Treatment on HAZ cracking in Wrought IN 718

To save on the costs of replacement and prolong the life of service-damaged alloy components, repair welding can be implemented. As stated earlier, pre-weld solution heat treatment is carried out to prepare the material in a condition where it is more weldable. However, heat treatment is also done to dissolve deleterious phases that precipitate during service. It is possible that during the life time of a component, it will undergo several cycles of heat treatment. A pre-weld heat treatment at 950^{o}C for 1hr has good resistance to HAZ cracking. Therefore, to investigate the effect of the multiple use of heat treatment at 950^{o}C/1hr for the repair welding of IN 718, a heat treatment at 950^{o}C was carried for 100 hours/AC and the coupons were subsequently welded.

Specimens from pre-weld coupons treated at 950^{o}C for 100hrs have a microstructure with an average grains size of 30±6μm, which is comparable to that of 950 for 1hr (Table 4.4). Also, there is extensive precipitation of the Nb-rich δ phase within the grains and grain boundaries as shown in Figure 4.28. The presence and size of the δ phase particles had significantly increased in comparison to the 1hr heat treatment (Figure 4.21b) and their presence could have helped maintain mean grain sizes similar to 950^{o}C for 1hr.

The HAZ of the welded coupons given the pre-weld heat treatment at 950^{o}C for 100hrs exhibited a more extensive liquation around the weld than those subjected to 950^{o}C for 1hr. (Figures 4.29 and 4.23 b). HAZ cracks occurred and are associated with liquated Nb-rich carbides and δ phase precipitates (Figure 4.30).

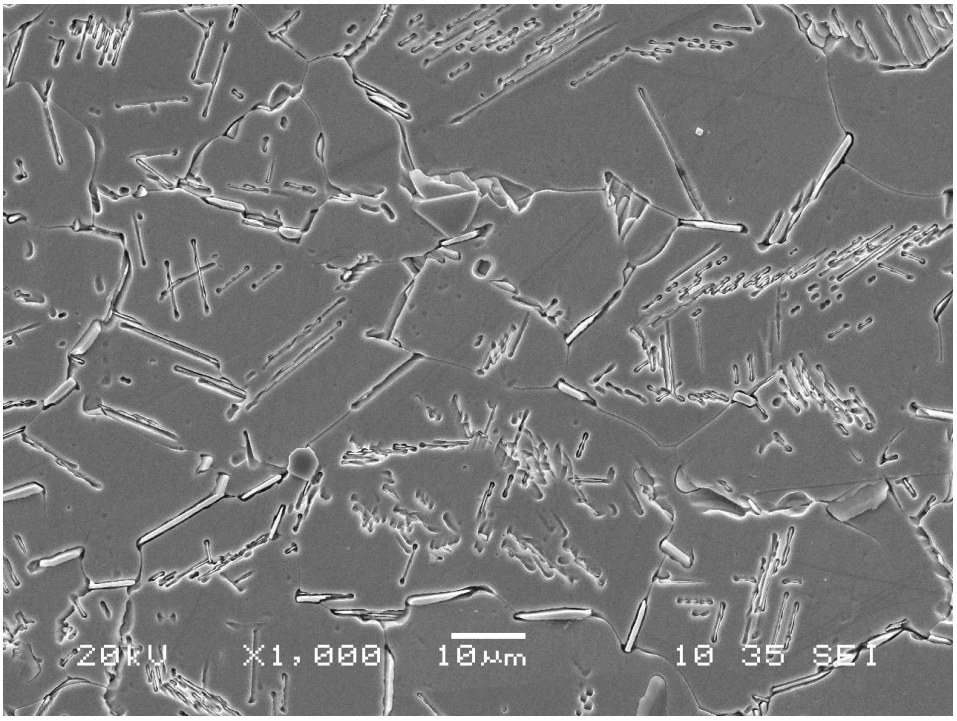

Figure 4.28: SEM micrograph of IN 718 pre-weld heat-treated at 950^{o}C/100hr/AC

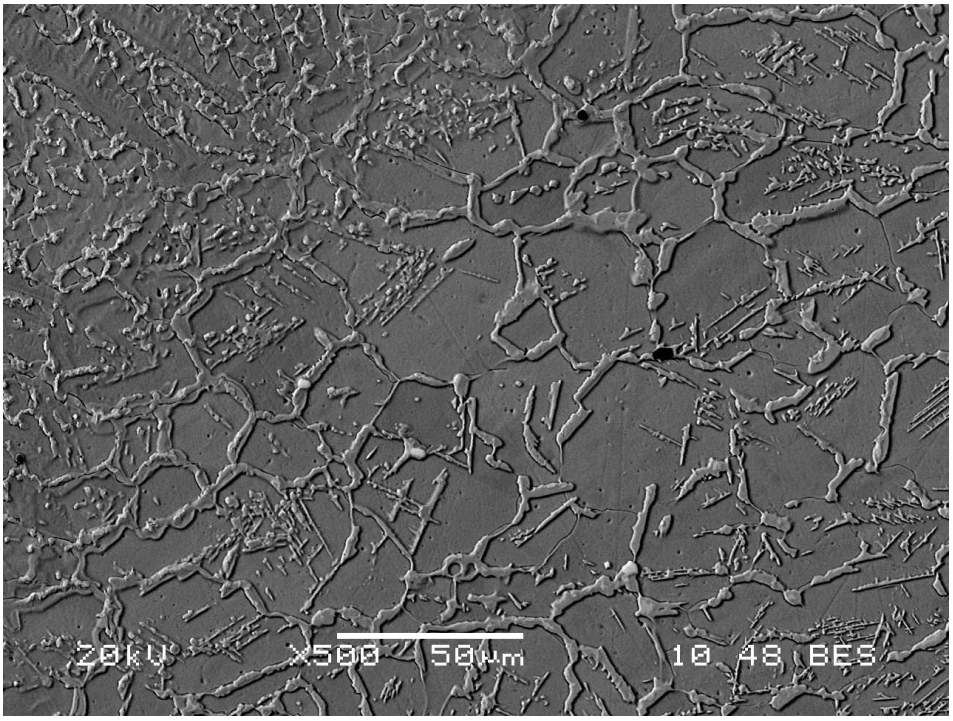

Figure 4.29: SEM micrograph of HAZ in the weld-neck region of coupon pre-weld heat-treatment at 950^{o}C/100hr/AC

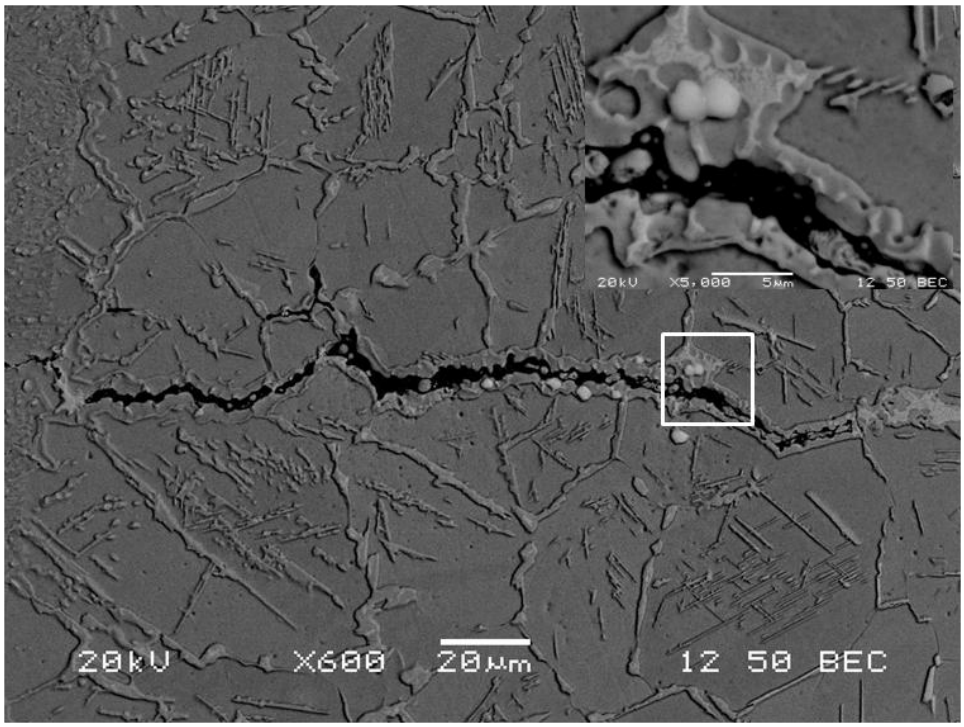

Figure 4.30: SEM micrograph showing liquated microconstituent along HAZ crack in coupons pre-weld heat treatment at 950^{o}C/100hr/AC.

A comparison of TCLs in coupons given pre-weld treatment at 950^{o}C for 100hrs and 950^{o}C for 1hr (Figure 4.31) shows that the TCL in both heat treatments are comparable.

Hooijmans et al. [10] and Qian et al. [133] reported that prolonged heat treatment in the temperature precipitation range of δ phase causes a progressive increase in δ phase increase along grain boundaries. Also, during welding, the dissolution of the extensively precipitated δ phase can increase the concentration of melting point depressing solute, Nb, along grain boundaries, which can cause enhance intergranular liquation and increase cracking susceptibility [10, 133].

In this study, the use of a heat treatment temperature of 950^{o}C for prolonged period of time produces more extensive grain boundary liquation. Nonetheless, this liquation did not drastically decrease IN 718 resistance to HAZ cracking. It is interesting to note that prolonged heat treatment at 950^{o}C for 100hrs shows better resistance to HAZ cracking than 1050^{o}C for 1hr (Figure 4.31) for the same welding parameter (higher power). This observation further highlights that an increase in the amount of grain boundary liquid film is not always an indication of liquation cracking susceptibility. The life of the liquid film (how long the film lasts) as determined by segregation of melting point depressant, B, is an important factor.

Therefore, the use of 950^{o}C as the pre-weld heat treatment temperature may not only be useful for the fabrication welding of new IN 718 components, but also is promising for multiple pre-weld heat treatments necessary for repair welding of service-damaged parts.

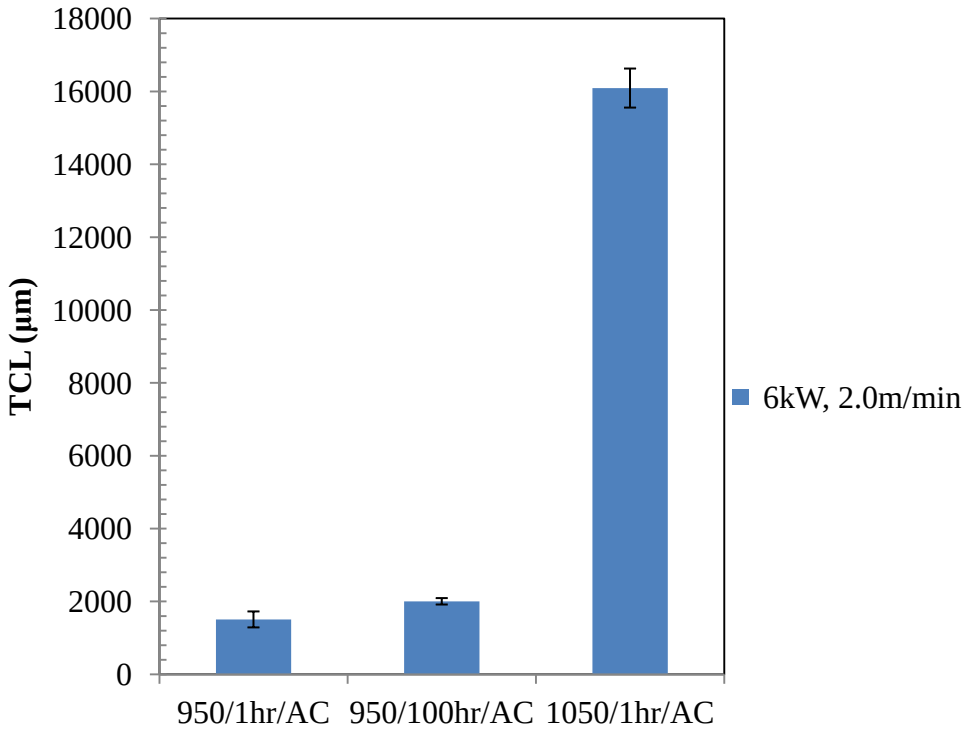

Figure 4.31: Variation of HAZ total crack length with 1 hour and 100 hour pre-weld heat treatments in coupons welded using a laser power of 6kW.

4.2 Cast IN 718

Generally, cast IN 718 is more difficult to weld due to microstructure inhomogeneity but this manufacturing process could be cheaper and faster to produce parts. Engines that contain cast component parts still exist and may require repair by welding throughout their life. The microstructure of the as-cast IN 718 was examined prior to heat treatment to identify the phases that formed during casting solidification. Select temperatures were used to perform heat treatments on the cast weld coupons and the resultant microstructures were examined before welding. After welding, the effect of the process on microstructure and extent of HAZ cracking was investigated for each pre-weld heat treatment condition.

4.2.1 Microstructural Examination of As-cast IN 718

Specimens were cut from as-cast block of IN 718 produced at the University of Manitoba to examine the microstructure. Under an optical microscope, cast IN 718 appeared to have a microstructure which is heavily dendritic and consists of a mixture of columnar and equiaxed coarse grains. This observed microstructure is in contrast to those produced by the more recent micro-cast process, which are made of fine equiaxed grains. An optical micrograph of as-cast IN 718 is shown in Figure 4.32. The interdendritic region contains secondary phases which appear as dark regions under the optical microscope.

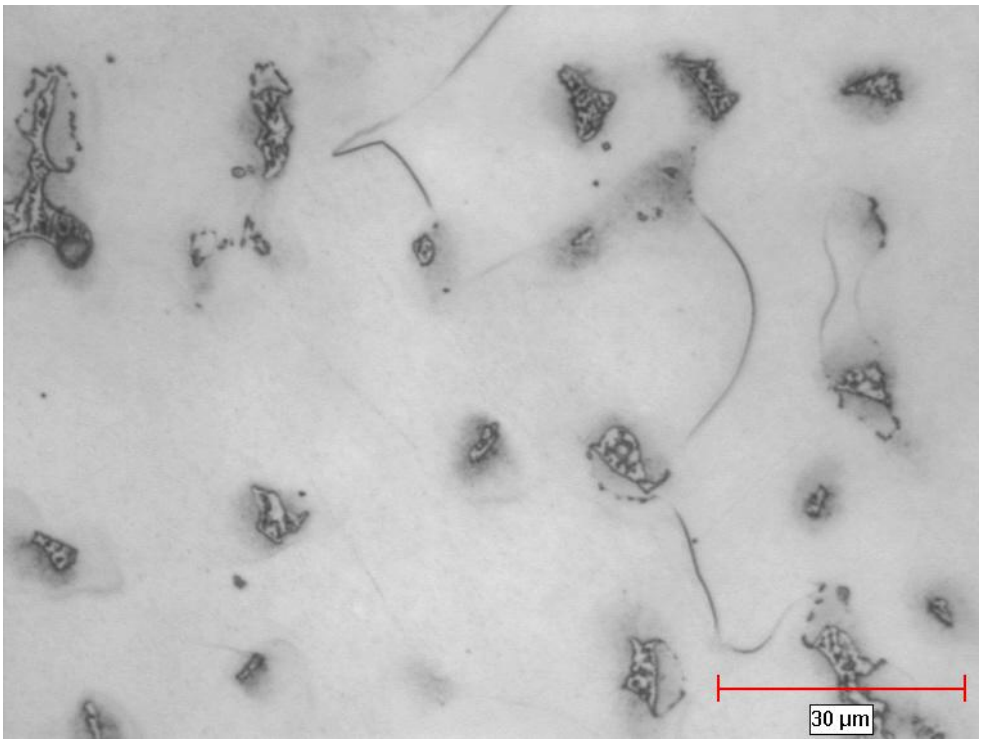

Figure 4.32: Optical micrograph of as-cast IN718 microstructure

Under SEM backscatter electron emission imaging mode (BSE), the interdendritic area appears to be lighter than the dendrite region as shown in Figure 4.33a. Regions that consist of more Nb and other heavy metals, appears bright when examined in the backscatter electron mode of the SEM [31]. The results of the SEM/EDS line scan analysis are shown in Figure 4.33b and confirm the light areas are depleted of Cr and Fe and had higher levels of Nb and Mo than in the matrix.

Figure 4.34 shows a SEM micrograph of the as-cast IN 718 at a high magnification. The phases present in the as-cast material include lamellar Laves phase with needle-like δ phase and MC carbides. Surrounding the Laves phase particles are fine precipitates that are likely γ" and γ' phase particles. The δ, γ" and γ' phases appeared to be less than 1μm and, hence, could not be compositionally analyzed reliably by SEM/EDS. However, in SEM (BSE) mode, these particles appear to be brighter than the matrix that suggests their enrichment in heavy metals, presumably Nb (Figure 4.34 insert). The presence of theses phases correlates with Radavich's study [35] where γ" and γ' were resolved at 10,000 X or higher magnification and appeared to be bright in SEM (BSE) mode. In addition, δ, γ" and γ' phases had the characteristic morphology reported in literature. The SEM/EDS spectrum of the Laves phase (Figure. 4.35) shows it is Nb-rich.

4.2.2 Microstructural Examination of Heat-treated Cast IN 718

The constitutional liquation of low melting Nb-rich Laves phase particles is reported to cause HAZ cracking during the welding of cast IN 718 [134]. The Laves phase is expected to dissolve with increase in time and temperature during heat treatment above

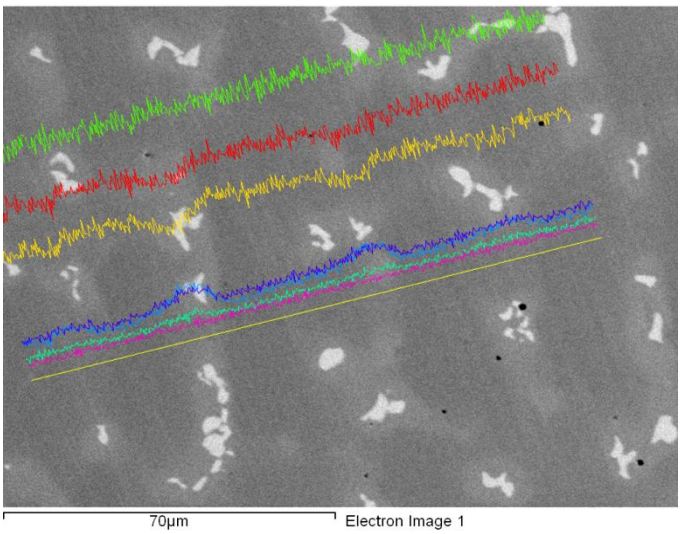

a)

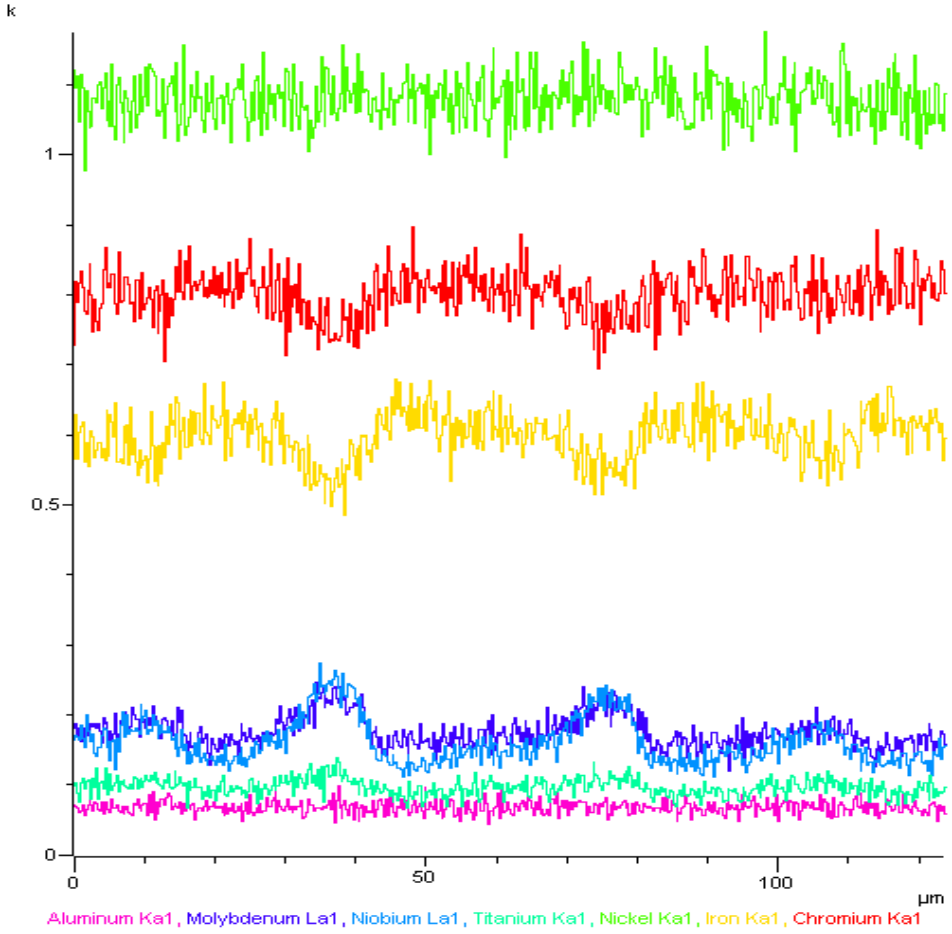

b)

Figure 4.33: SEM/EDS line scan of as-cast IN 718

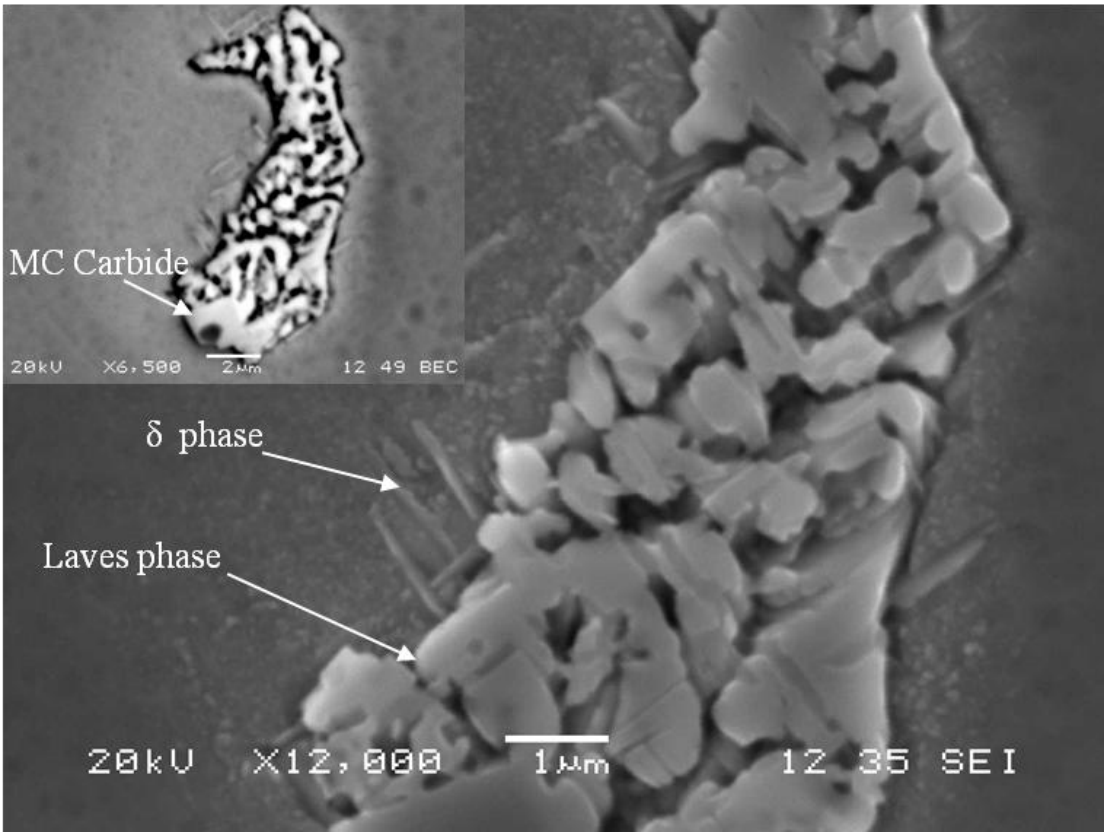

Figure 4.34: SEM micrograph of as-cast IN 718 showing secondary phases. The insert is a SEM back-scatter electron micrograph

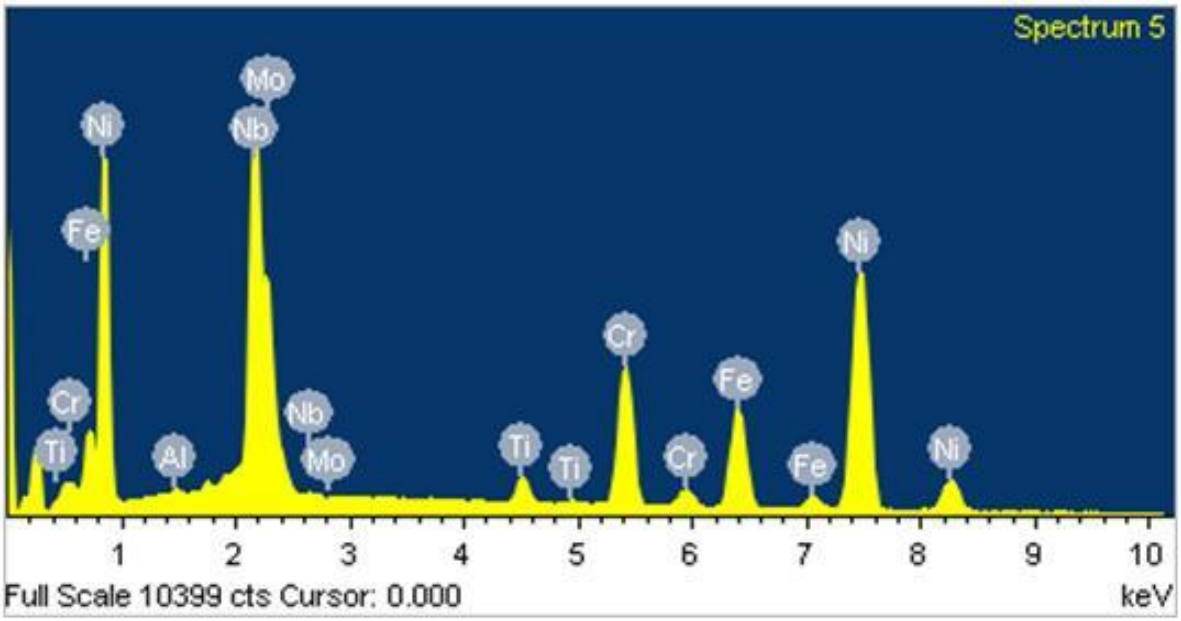

Figure 4.35: SEM/EDS spectra of Laves phase in as-cast IN 718

the Laves phase solvus temperature [9].

In this investigation, heat treatments for 1 hour at 1050^{o}C, 1100^{o}C, 1125^{o}C, and 1175^{o}C are carried out to study the effect of the dissolution of the Laves phase on HAZ cracking. After heat treatment, optical micrographs of the different microstructure were taken and shown in Figure 4. 36 a-d. In the 1050^{o}C and 1100^{o}C specimens, only MC carbides, Laves and needle-like δ phases are present, while γ" and γ' phases are not observed. Eiselstein [30] reported the same finding for cast IN 718, where the γ" and γ' phases are not found at temperature at 870^{o}C. In the specimens that were heat treated at 1125^{o}C for 1hr heat treatment, it was observed that the δ phase precipitates had dissolved and Laves precipitates are sparsely distributed.

The normal solvus temperature at which the Laves phase particles dissolve is 1162^{o}C and heat treatment above this temperature would result in a microstructure of only MC carbides [31]. Huang et al. [127] reported that a heat treatment at 1163^{o}C for 1hr produces a microstructure of MC carbides, nitrides and free of Laves phase particles. However, due to dendritic segregation during the solidification of cast IN 718, there are Laves particles of different compositions and, hence, Laves phases with different solvus temperatures form [9, 31]. Therefore, segregation could be an explanation for the areas with little or no Laves phase particles in heat treatment at 1125^{o}C for 1hr, which is below the normal solvus temperature of Laves phase in IN 718 superalloy. In the pre-weld heat treatment at 1175^{o}C for 1hr, both the Laves and δ phases are not evident and only MC carbides are observed.

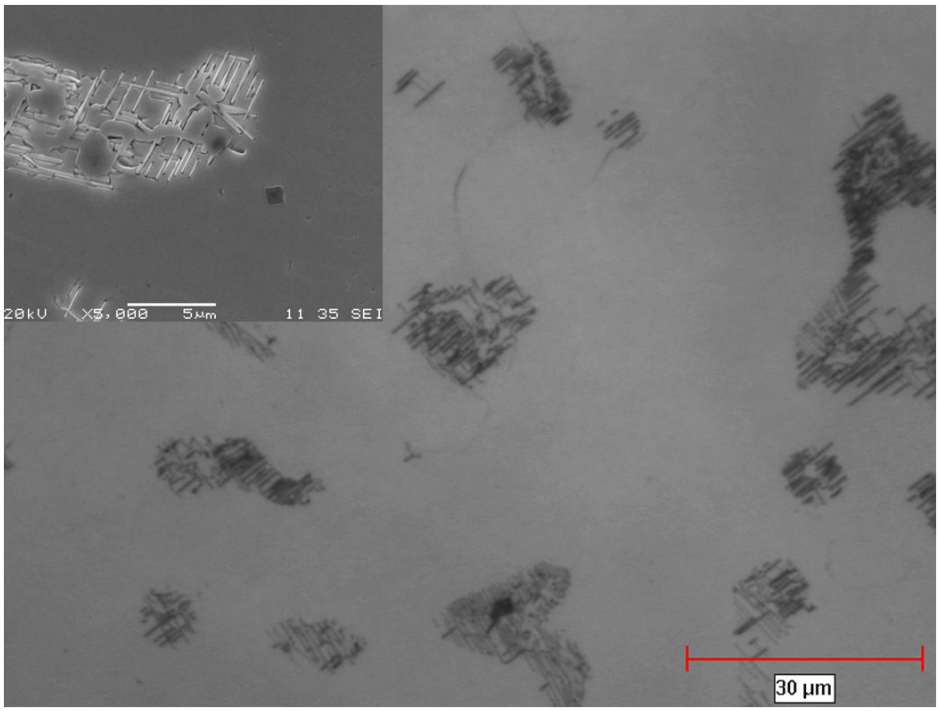

a)

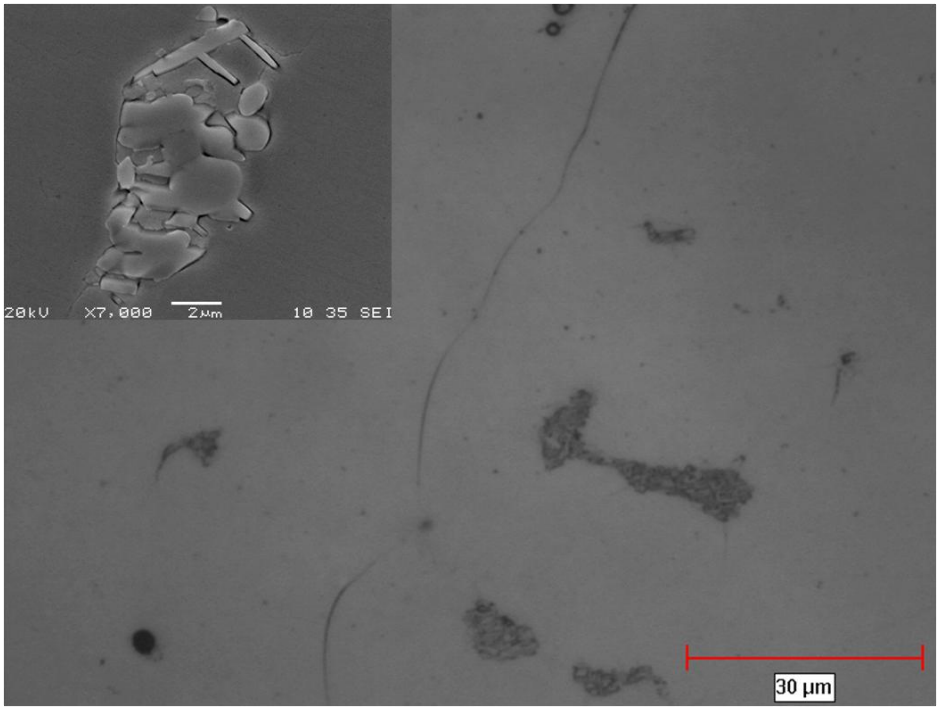

b)

Figure 4.36: Optical micrograph of cast IN 718 heat-treated at (a) 1050^{o}C/1hr/AC (b) 1100^{o}C/1hr/AC Insets show SEM higher magnification micrographs

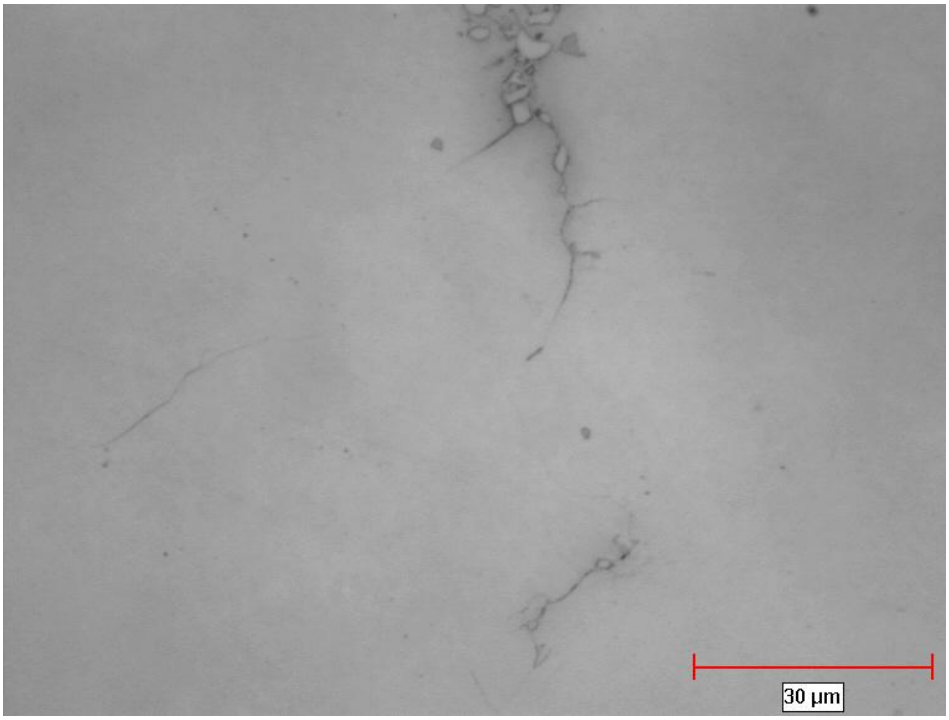

c)

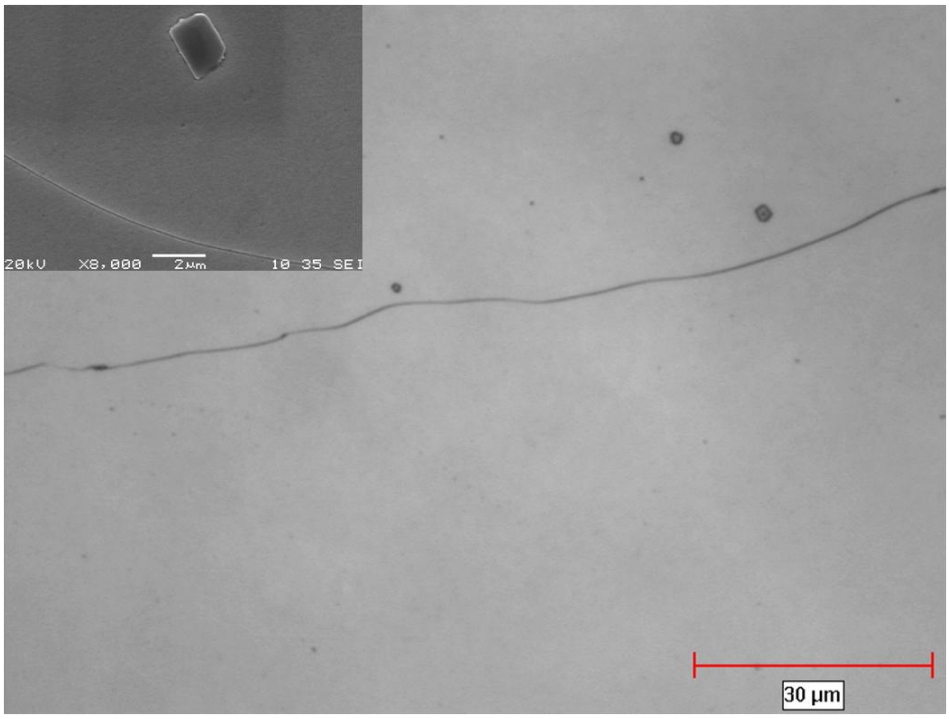

d)

Figure 4.36: Optical micrograph of cast IN 718 heat-treated at (c) 1125^{o}C/1hr/AC (d) 1175^{o}C/1hr/AC. Inset show SEM higher magnification micrograph

The absence of these phases is expected because a treatment temperature of 1175^{o}C is above the solvus temperature of the Laves and δ phase.

4.2.3 Microstructural Examination of Welded Cast IN 718

All heat-treated cast IN 718 coupons were welded using a laser power of 4kW and welding speed of 3.0 m/min. The microstructure of the welded cast material etched with Kallings No.2 reagent is shown in Figure 4.37. The FZ consists of a fine dendritic microstructure similar to that of wrought IN 718 welds. In the HAZ of laser welded cast IN 718, Nb-rich re-solidified product was observed on some of the grain boundaries in the pre-weld heat treated coupons. Liquated Laves and δ phase particles were interconnected with Nb-rich re-solidified products in coupons given a pre-weld heat treated at 1050^{o}C and 1100^{o}C (Figure 4.38) of lower temperature. Cracking occurred in the HAZ of cast IN 718 welds. The cracks are associated with liquated Nb-rich Laves and δ phases and/or eutectic type Nb-rich re-solidified product similar to those in the wrought welds, as shown in Figure 4.39.

4.2.4 Effect of Heat Treatment on HAZ Cracking in Cast IN 718

The results of the TCL measurements in different pre-weld heat-treated coupons are shown in Figure 4.40. The results show that the TCL increases with increased temperatures of pre-weld heat treatment. The results suggest that at lower temperature with liquated Laves phase particles showed less susceptibility to cracking in HAZ.

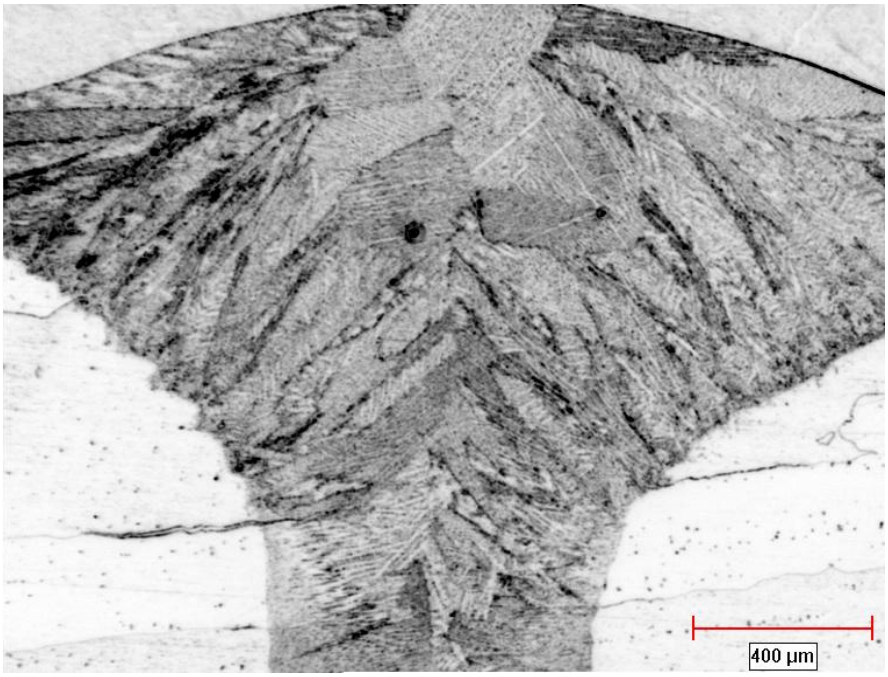

Figure 4.37: Optical micrograph of cast IN 718 weld macrostructure

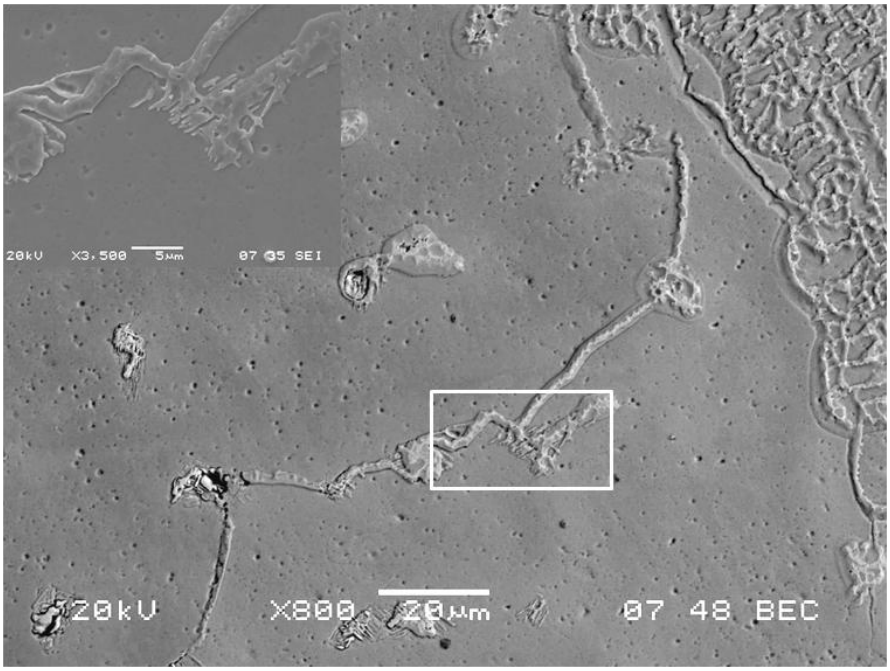

Figure 4.38: SEM micrograph of HAZ liquation in cast IN 718 pre-weld heat-treated at 1050^{o}C/1hr/AC

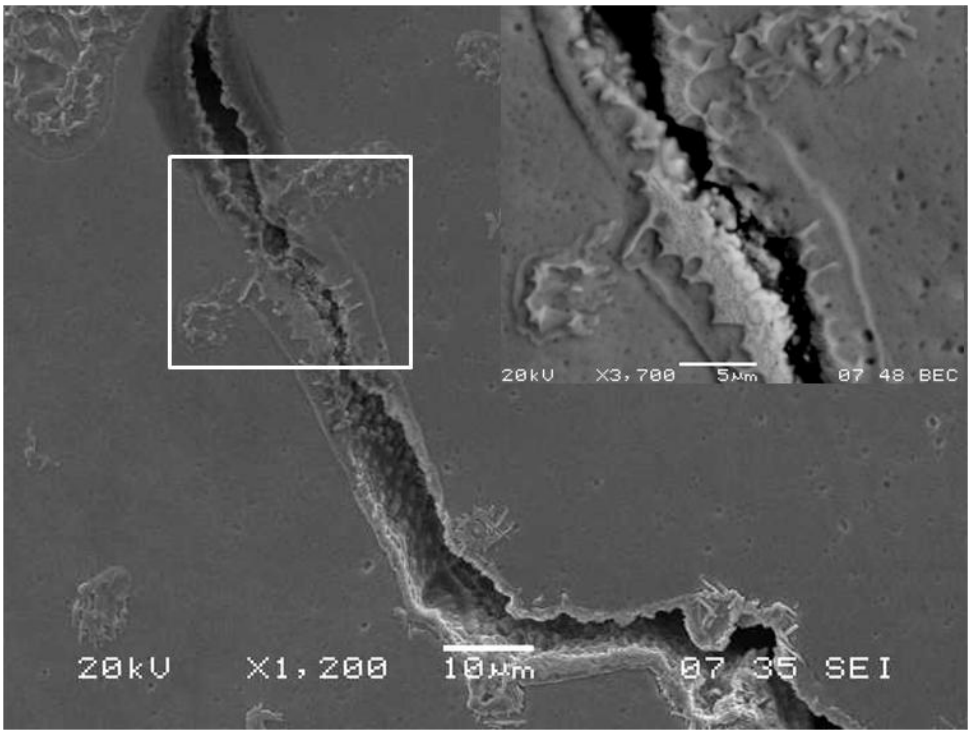

(a)

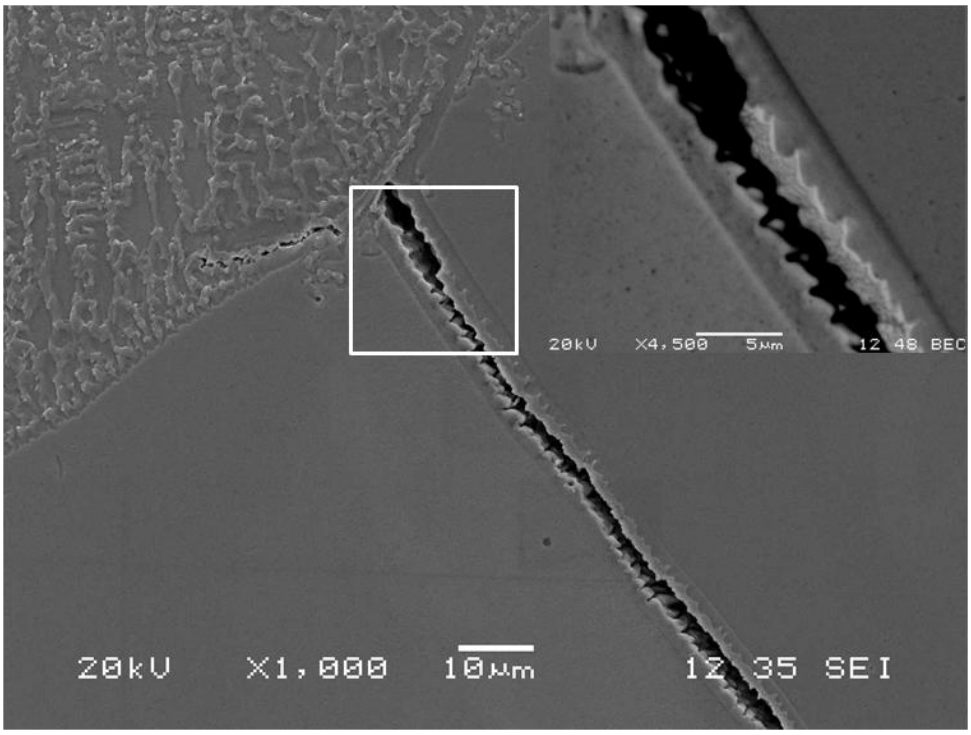

(b)

Figure 4.39: SEM micrograph of HAZ liquation cracking in coupons pre-weld heat-treated at (a) 1050^{o}C/1hr/AC (b) 1175^{o}C/1hr/AC

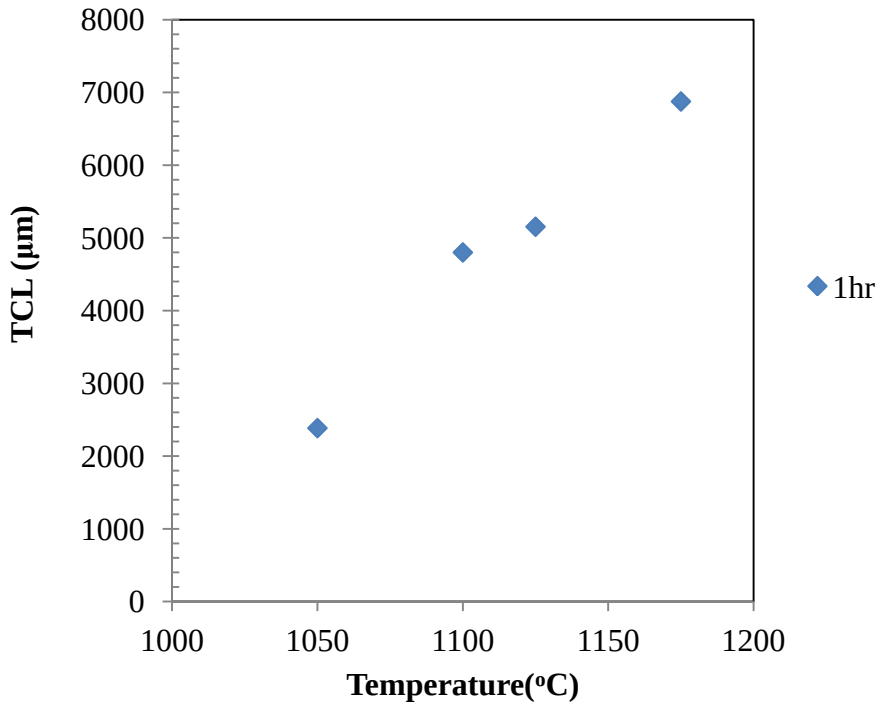

Figure 4.40: Variation of HAZ total crack length with pre-weld heat treatment temperature in cast IN 718.

In coupons that were pre-weld heat treated at low temperatures, there is significant liquated Nb-rich Laves phase particles in the HAZ and they appear associated with HAZ cracks. However, the occurrence of significant liquation of Laves phase particles at low temperatures does not increase the cracking susceptibility of the cast IN 718 compared to pre-weld microstructures produced at higher heat treatment temperature, which are free of Laves phase particles.

It has been reported that Nb-rich intergranular liquid, which can form by constitutional liquation of Nb-rich phases, such as Nb-rich carbide, solidifies to produce a eutectic product similar to Laves phase on HAZ cracks [44]. Similar to the discussion on wrought alloy IN 718, an increase in non-equilibrium intergranular segregation of B with an increase in heat treatment temperature [131, 132] may also be responsible for the increase in HAZ cracking with pre-weld heat treatment temperature, observed in the fiber laser welds of cast IN 718. This is consistent with reported results of the previous research by Huang et al [131] on electron beam welding of cast IN 718 superalloy.

Therefore, based on the results in this study and correlation to previous findings, possible increased non-equilibrium intergranular elemental segregation with heat treatment temperature could be the explanation for the increased HAZ cracking susceptibility in both wrought and cast IN 718 fiber laser welds.

5 Conclusions

The study of welding parameters on the HAZ cracking of wrought IN 718 shows that fiber laser welding exhibits a dual effect of heat input on cracking. An increase in heat input causes a reduction in HAZ cracking and produces good quality welds, when a laser power of 2.5kW is used. In contrast, an increase in heat input causes increases in HAZ cracking when the weld is performed at higher laser powers, which can be attributed to process instability. The process instability is evident by the appearance of several weld defects, severe cracking not only in the HAZ, but also in the weld fusion zone (FZ) in the alloy that is normally resistant to FZ cracking and unevenness of weld cross-sectional profiles.

The following are the conclusions from the study on the effect of pre-weld heat treatment on wedability of wrought IN 718. Pre-weld heat treatments that are carried out at 900^{o}C and 950^{o}C for 1hr respectively show good resistance to cracking. No cracking is observed in coupons that have been pre-weld heat-treated at 950^{o}C for 1 hour and welded with a laser power of 2.5 kW. HAZ cracking increases with an increase in the pre-weld heat treatment temperature from 1050^{o}C to 1150^{o}C, and cracking varied with the cooling rate used after heat treatment. HAZ cracking increases with decreases in the cooling rate after heat treatment. The most susceptible conditions to HAZ cracking are found with air-cooling condition and least with water-cooling condition. This behaviour can be explained by non-equilibrium intergranular segregation of boron reported in earlier studies. A reduction in grain boundary segregation and fine grain size are found to be

favourable for reducing cracking susceptibility at lower pre-weld heat treatment temperatures used in this study. The results of the research also indicate that the use of a pre-weld heat treatment temperature of 950^{o}C can be used for multiple of times without significant degradation in the HAZ cracking resistance of wrought IN 718 which is promising for repair welding.

An analysis of the effect of pre-weld heat treatment on HAZ cracking susceptibility in cast IN 718 shows that, similar to the case of wrought IN 718 material, increase in the HAZ cracking susceptibility is also attributable to the influence of non-equilibrium intergranular elemental segregation at high heat treatment temperatures.

6 Suggestions for future work

Welding trials should be performed, using a systematic combination of several welding parameters, to gain further understanding on the phenomenon of process instability and the influence of other parameters on process instability and how it can be mitigated during fiber laser welding. Also, it is suggested that several post-weld heat treatments should be studied to determine the post-welding cracking behaviour of IN 718 fiber laser welds that are found to be crack free after welding. In addition, evaluation of the mechanical properties of the crack-free welds should be carried out to determine high temperature performance of the joints.

7 Bibliography

[1] A. Lingenfelter, *Superalloy 718-Metallurgy and Applications,* pp. 673-683, 1989.

[2] M. H. McCay, T. McCay, C. Sharp and N. B. Dahotre, *Superalloy 718,625 and Various derivatives,* pp. 719-734, 1991.

[3] J. F. Radavich and T. Carneiro, *6th International Symposium on Superalloys 718, 625, 706 and Derivatives,* pp. 329-340, 2005.

[4] K. Shonozaki, H. Kuroki, X. Luo, H. Ariyoshi and M. Shirai, *Welding International,* vol. XIII, no. 12, pp. 945-951, 1999.

[5] X. Luo, K. Shonozaki, H. Kuroki, S. Yoshihara, Y. Okumoto and M. Shirai, *Welding International,* vol. XVI, no. 5, pp. 385-392, 2002.

[6] I. Woo, C. Kang and K. Nishimoto, *Metals and Materials International,* vol. VII, no. 4, pp. 349-357, 2001.

[7] D. F. Paulonis and J. J. Schirra, *Superalloys 718,625,706 and Various Derivatives,* pp. 13-23, 2001.

[8] K. Nishimoto, I. Woo and M. Shirai, *ISIJ International,* vol. 40, pp. S39-S43, 2000.

[9] J. Andersson, G. Sjöberg and J. Larsson, *Proceeding of The 7th International Symposium on Superalloy 718 and Derivatives,* pp. 439-454, 2010.

[10] J. W. Hooijmans, J. C. Lippold and W. Lin, *Superalloys 718, 625, 706 and Various Derivatives,* pp. 721-730, 15-18 June 1997.

[11] M. T. Rush, P. A. Colegrove, Z. Zhang and B. Courtot, *Advanced Materials Research,* Vols. 89-91, pp. 467-472, 2010.

[12] A. Salminen, H. Piili and T. Purtonen, *Proceedings of the Institution of Mechanical Engineers, Part C (Journal of Mechanical Engineering Science),* vol. 224, no. C5, pp. 1019-1029, 2010.

[13] S. Gobbi, L. Zhang, J. Norris, K. Richter and J. Loreau, *Journal of Materials*

Processing Technology, vol. 56, no. 1-4, pp. 333-345, 1996.

[14] D. Cornu, D. Gouhier, I. Richard, V. Bobin, C. Boudot, J.-P. Gaudin, H. Andrzejewski, D. Grevey and J. Portrat, *Welding International (UK)*, vol. 9, no. 10, pp. 802-811, 1995.

[15] J. Xie, *Proceedings of the Laser Materials Processing Conference. ICALEO'99.*, pp. 11-20, 2000.

[16] J. Hong, J. Park, N. Park, I. Eom, M. Kim and C. Kang, *Journal of Materials Processing Technology*, vol. 201, no. 1-3, pp. 515-520, 2008.

[17] R. Miranda, A. Costa, L. Quintino, D. Yapp and D. Iordachescu, *Materials & Design*, vol. 30, no. 7, pp. 2701 - 2707, 2009.

[18] N. Seto, S. Katayama and A. Matsunawa, *Journal of Laser Applications*, vol. 12, no. 6, pp. 245-250, 2000.

[19] L. Quintino, A. Costa, R. Miranda, D. Yapp, V. Kumar and C. Kong, *Materials and Design*, vol. 28, no. 4, pp. 1231-1237, 2007.

[20] Y. Kawahito, M. Mizutani and S. Katayama, *Science and Technology of Welding and Joining*, vol. 14, no. 4, pp. 588-594, 2009.

[21] S. Ream, in *International Congress on Applications of Lasers and Electro-Optics, Congress Proceedings*, 2004.

[22] M. Chaturvedi, *Materials Science Forum (Switzerland)*, Vols. 546-549, pp. 1163-1170, 2007.

[23] R. Vincent, *Acta Metallurgica*, vol. 33, no. 7, pp. 1205-1215, 1985.

[24] A. Odabasi, N. Unlü, G. Göller and M. N. Eruslu, *Metallurgical and Materials Transactions A: Physical Metallurgy and Materials Science*, vol. 41, no. 9, pp. 2357-2365, 2010.

[25] G. E. Dieter and D. Bacon, Mechanical Metallurgy. SI Metric Edition, McGraw-Hill Book Company, UK, 1988, pp. 203, 211.

[26] C. T. Sims, N. S. Stoloff and W. C. Hagel, Superalloys II- High-Temperature Materials for Aerospace and industrial Power, John Wiley & Sons,Inc, 1987, pp. 3, 97, 99, 101-102, 104, 112, 115-116, 120, 126, 146, 148, 154, 168-172, 180-183.

[27] M. B. Henderson, D. Arrell, R. Larsson, M. Heobel and G. Marchant, *Science & Technology of Welding & Joining,* vol. 9, no. 1, pp. 13-21, 2004.

[28] M. Donachie and S. Donachie, Superallloys : a technical guide, 2nd ed., OH: ASM international, 2002, pp. 15, 18, 35-37, 41, 104, 161.

[29] J. N. DuPont, J. C. Lippold and S. D. Kiser, Welding Metallurgy and Weldability of Nickel-Base Alloys, Portland,United States: John Wiley & Sons, 2009, pp. 15, 17, 35, 157.

[30] H. Eiselstein, *American Society for Testing and Materials -- Special Technical Publications,* no. 369, pp. 62-79, 1965.

[31] J. F. Radavich, *Superalloy 718--Metallurgy and Applications,* pp. 229-240, 1989.

[32] D. F. Paulonis, J. M. Oblak and D. S. Duvall, *ASM Transactions Quartely,* vol. 62, no. 3, pp. 611-622, 1969.

[33] H. J. Wagner and A. M. Hall, *Battelle Memorial Institute-- DMIC Reports,* no. 217, p. 24, 1965.

[34] T. Kelly, *Advances in Welding Science and Technology - TWR '86: Proceedings of an International Conference on Trends in Welding Research.,* pp. 623-627, 1986.

[35] J. F. Radavich, *Journal of Metals,* vol. 40, no. 7, pp. 42-43, 1988.

[36] X. Huang, "A microstructural study of heat affected zone microfissuring of electron beam welds in cast alloy 718," University of Manitoba, Winnipeg, 1994.

[37] J. Oblak, D. Paulonis and D. Duvall, *Metallurgical Transactions A (Physical Metallurgy and Materials Science),* vol. 5, no. 1, pp. 143-53, 1974.

[38] P. Sundararaman, P. Mukhopadhyay and S. Banerjee, *Acta Metallurgica,* vol. 4, pp. 847-64, 1988.

[39] W. C. Hagel and H. J. Beattie, "Iron and Steel Institute Special report," 1964.

[40] M. Sundararaman, P. Mukhopadhyay and S. Banerjee, *Metallurgical transactions. A, Physical metallurgy and materials science,* vol. 19 A, no. 3, p. 453, 1988.

[41] S. Azadian, L.-Y. Wei and R. Warren, *Materials Characterization,* vol. 53, no. 1, pp. 7-16, 2004.

[42] T. Kelly, W. Cremisio and W. Simon, *Welding Journal (Miami, Fla),* vol. 68, no. 1, pp. 14s-18s, 1989.

[43] G. Knorovsky, M. Cieslak, T. Headley, A. Romig and W. Hammetter, *Metallurgical transactions. A, Physical metallurgy and materials science,* vol. 20A, no. 10, pp. 1249-2157, 1989.

[44] R. Thompson, *Advanced High Pressure O2/H2 Technology.,* pp. 164-179, 1985.

[45] J. C. Lippold and D. J. Kotecki, Welding Metallurgy and Weldability of Stainless Steels, John Wiley & Sons, Inc, 2005, pp. 19, 20-23, 166, 189.

[46] W. Dahl, C. Duren and H. Musch, *Stahl und Eisen,* vol. 93, no. 18, pp. 813-822, 1973.

[47] M. P. Seah and E. D. Hondros, *Proceedings of the Royal Society of London, Series A (Mathematical and Physical Sciences),* vol. 335, no. 1601, pp. 191-212, 1973.

[48] J. C. Borland and R. N. Younger, *British Welding Journal,* vol. 7, no. 1, pp. 22-59, 1960.

[49] T. Morrison, C. .. Shira and L. Weisenberg, *PAPER FROM EFFECTS OF MINOR ELEMENTS ON THE WELDABILITY OF HIGH-NICKEL ALLOYS, WELDING RESEARCH COUNCIL,* pp. 47-67, 1969.

[50] R. G. Carlson and J. F. Radavich, *Superalloy 718: Metallurgy and Applications,* pp. 79-95, 1989.

[51] R. Thompson and S. Genculu, *Welding Journal (Miami, Fla),* vol. 62, no. 12, pp. 337-345, 1983.

[52] M. Xiao, C. Poon, P. Wanjara, M. Jahazi, Z. Fawaz and P. Krimbalis, *Materials Science Forum,* Vols. 546-549, pp. 1305-8, 2007.

[53] D. Ellis and R. Squires, *Metal construction,* vol. 15, no. 7, pp. 388-393, 1983.

[54] S. Kou, Welding Metallurgy, John Wiley & Sons Inc., 2003, pp. 11, 13-19, 22-24, 29-33, 37, 122-124, 128, 145, 155, 199-203, 263,303-319.

[55] R. L. O'Brien, Ed., Welding Handbook, vol. 2, Miami: American Welding Society, 1991, pp. 69-70, 507, 509-510, 707-709, 714, 717, 719, 725-727.

[56] L. P.Connor, Ed., Welding Hanbook, vol. 1, Miami, FL: American Welding Society, 1987, pp. 22, 103-104, 136-137, 218-224, 353-354, 359.

[57] G. Moraitis and G. Labeas, *Journal of Materials Processing Technology,* vol. 198, pp. 260-269, 2008.

[58] R. Rai, T. A. Palmer, J. W. Elmer and T. Debroy, *Welding Journal (Miami, Fla),* vol. 88, no. 3, pp. 54s-61s, 2009.

[59] T. Forsman, J. Powell and C. Magnusson, *Journal of Laser Applications,* vol. 13, no. 5, 2001.

[60] Y. M. Yaman and M. C. Kushan, *Journal of Materials Science Letters,* vol. 17, no. 14, pp. 1231-1234, 1998.

[61] Z. Sun, A. S. Salminen and T. J. I. Moisio, *Journal of Materials Science Letters,* vol. 12, no. 14, pp. 1131-3, 1993.

[62] T. C. Nguyen, D. C. Weckman, D. A. Johnson and H. W. Kerr, *Science and Technology of Welding & Joining,* vol. 10, no. 4, pp. 447-459, 2005.

[63] T.-Y. Kuo and Y.-D. Lin, *Materials Transaction,* vol. 48, no. 2, pp. 219-226, 2007.

[64] T.-Y. Kuo and Y.-T. Lin, *Materials Transactions,* vol. 47, no. 5, pp. 1365-1373, 2006.

[65] Y. Kawahito, T. Terajima, H. Kimura, T. Kuroda, K. Nakata, S. Katayama and A. Inoue, *Materials Science and Engineering B: Solid-State Materials for Advanced*

Technology, vol. 148, no. 1-3, pp. 105-109, 2008.

[66] Y. Kawahito, M. Mizutani and S. Katayama, *Journal of Physics D: Applied Physics*, vol. 40, no. 19, pp. 5854-5859, 2007.

[67] U. Reisgen, M. Schleser, O. Mokrov and E. Ahmed, *Applied Surface Science*, vol. 257, no. 5, pp. 1401-1406, 2010.

[68] A. Heß and F. Dausinger, *Proceedings of the international Conference on Stuttgarter lasertage,Universität Stuttgart*, p. 17, 2008.

[69] S. Katayama, Y. Kawahito and M. Mizutani, *Physic Procedia*, vol. 5, pp. 9-17, 2010.

[70] T. Moscicki, J. Hoffman and Z. Szymanski, *Journal of Physics D (Applied Physics)*, vol. 39, pp. 685-692, 2006.

[71] S. David, S. Babu and J. Vitek, *JOM*, vol. 55, no. 6, pp. 14-20, 2003.

[72] B. Chalmers, Principles of Solidification, New York: Wiley, 1964.

[73] H. F. Bishop and W. S. Pellini, *Foundry*, vol. 80, no. 2, pp. p 86-93, 253-261, 1952.

[74] J. A. Brooks, *Trends in Welding Research. 4th International Conference; Gatlinburg, Tennessee; USA; 5-8 June*, pp. 123-134, 1995.

[75] J. Macha and J. Scully, *Corrosion*, vol. 65, no. 7, pp. 472-490, 2009.

[76] T. Iamboliev, A. Zumbilev, L. Kalev, S. Christov, V. Ianev and R. Stang, *Welding Journal (Miami, Fla)*, vol. 78, no. 7, pp. 245s-252s, 1999.

[77] W. F. Savage, E. F. Nippes and G. M. Goodwin, *Welding Journal (Miami, Fla)*, vol. 56, no. 8, pp. 245s-253s, 1977.

[78] G. J. Davies and J. G. Garland, *International Metallurgical Reviews*, vol. 20, pp. 83-106, 1975.

[79] F. Matsuda, H. Nakagawa and K. Sorada, *Trans. JWRI*, vol. 11, no. 2, pp. 67-77, 1982.

[80] F. Matsuda, H. Nakagawa, H. Kohmoto, Y. Honda and Y. Matsubara, *Trans. JWRI,* vol. 12, no. 1, pp. 73-80, 1983.

[81] E. Cicala, G. Duffet, H. Andrzejewski, D. Grevey and S. Ignat, *Materials Science and Engineering A,* vol. 359, no. 1-2, pp. 1-9, 2005.

[82] D. Krenz, A. Egbewande, H.-R. Zhang and O. Ojo, *Materials Science and Technology,* vol. 27, no. 1, pp. 268-274, 2011.

[83] W. A. Owczarski, D. S. Duvall and C. P. Sullivan, *Welding Journal,* vol. 45, no. 4, pp. 145-s-155, 1966.

[84] L. Karlsson, H. Norden and H. Odelius, *Acta Metallurgica,* vol. 36, no. 1, pp. 1-12, 1988.

[85] R. Faulkner, *Journal of Material Science,* vol. 16, no. 2, pp. 373-383, 1981.

[86] D. Mclean, Grain Boundaries in Metal, Oxord: Clarendon Press, 1957, p. 116.

[87] S. Song, Z. Yuan and T. Xu, *Journal of Materials Science Letters (UK),* vol. 10, no. 20, pp. 1232-1234, 1991.

[88] J. H. Westbrook and K. T. Aust, *Acta Metallurgica,* vol. 10, no. 11, pp. 1151-1163, 1963.

[89] K. T. Aust and J. H. Westbrook, *United States Atomic Energy Commission -- Lattice Defects in Quenched Metals*, pp. 771-778, 1965.

[90] K. T. Aust, R. E. Hanneman, P. Niessen and J. H. Westbrook, *Acta Metallurgica,* vol. 16, no. 3, pp. 291-302, 1968.

[91] T. Anthony, *Acta Metallurgica,* vol. 17, no. 5, pp. 603-9, 1969.

[92] J. Pepe and W. F. Savage, *WELD. J.,* vol. 46, no. 9, pp. 411S-422S, 1967.

[93] J. J. Pepe and W. F. Savage, *WELD J,* vol. 49, no. 12, pp. 545S-553S, 1970.

[94] K. R. Vishwakarma, N. L. Richards and M. C. Chaturvedi, *Superalloys 718, 625, 706 and Derivatives - Proceedings of the 6th International Symposium on*

Superalloys 718, 625, 706 and Derivatives, pp. 637-647, 2005.

[95] H. R. Zhang and O. A. Ojo, *Philosophical Magazine Letters,* vol. 89, no. 12, pp. 789-794, 2009.

[96] B. Radhakrishnan and R. G. Thompson, *Metallurgical Transactions A (Physical Metallurgy and Materials Science),* vol. 24A, no. 6, pp. 1409-22, 1993.

[97] O. A. Ojo, N. L. Richards and M. C. Chaturvedi, *Scripta Materialia,* vol. 50, no. 5, pp. 641-646, 2004.

[98] O. A. Ojo, N. L. Richards and M. C. Chaturvedi, *Metallurgical and Materials Transactions A: Physical Metallurgy and Materials Science,* vol. 2, pp. 421-433, 2006.

[99] R. G. Thompson, D. E. Mayo and B. Radhakrishnan, *Metallurgical Transactions A (Physical Metallurgy and Materials Science),* vol. 22A, no. 2, pp. 557-67, 1991.

[100] Y. Nakao, H. Ohshige, S. Koga, H. Nishihara and J. Sugitani, *J. Jpn. Weld. Soc.,* vol. 51, no. 12, pp. 21-27, 1982.

[101] B. Radhakrishnan and R. G. Thompson, *Metallography,* vol. 21, no. 4, pp. 453-71, 1988.

[102] R. Thompson, J. Dobbs and D. Mayo, *Welding Journal (Miami, Fla),* vol. 65, no. 11, pp. 299s-304s, 1986.

[103] W. Miller and G. Chadwick, *Acta Metallurgica,* vol. 15, no. 4, pp. 607-614, 1967.

[104] R. Thompson, J. Cassimus, D. Mayo and J. Dobbs, *Welding Journal (Miami, Fla),* vol. 64, no. 4, pp. 91. s-96. s, 1985.

[105] J. A. Williams and A. R. E. Singer, *Journal of the Institute of Metals,* vol. 96, pp. 5-12, 1968.

[106] M. Qian and J. C. Lippold, *Acta Materialia,* vol. 51, no. 12, pp. 3351-61, 2003.

[107] M. C. Chaturvedi, *ICAMMP-2002: International Conference on Advances in Materials Processing; Kharagpur; India; 1-3 Feb,* pp. 3-9, 2002.

[108] S. Wang, Q. Ma and Y. Li, *Materials and Design,* vol. 32, no. 2, pp. 831-837, 2010.

[109] J. M. Vitek, S. A. David, J. A. Johnson, H. B. Smartt and T. DebRoy, *Trends in Welding Research: Proceedings of the 5th International Conference,* 1998.

[110] N. L. Richards, R. Nakkalil and M. C. Chaturvedi, *Metallurgical and Materials Transactions A (Physical Metallurgy and Materials Science),* vol. 25A, no. 8, pp. 1733-45, 1994.

[111] R. Fabbro, S. Slimani, F. Coste and F. Briand, *26th International Congress on Applications of Lasers and Electro-Optics, ICALEO 2007 - Congress Proceedings,* pp. 382-390, 2007.

[112] C. Kwok, S. Fong, F. Chen and H. Man, *Journal of Materials Processing Technology,* vol. 176, no. 1-3, pp. 168-178, 2006.

[113] S. David, J. Vitek and T. Hebble, *Welding Journal (Miami, Fla),* vol. 10, pp. 289. s-300. s, 1987.

[114] S. Olovsjö, A. Wretland and G. Sjöberg, *Wear,* vol. 268, no. 9-10, pp. 1045-1052, 2010.

[115] S. Ernst, W. Baeslack III and J. Lippold, *Weld. J.,* vol. 68, no. 10, pp. 418s-430s, 1989.

[116] J. C. Adams, *Welding Journal,* vol. 37, no. 5, pp. 210s-215s, 1958.

[117] P. Jhaveri, W. Moffatt and J. C. Adams, *Welding Journal,* vol. 41, no. 1, pp. 12s-16s, 1962.

[118] J. Choi and J. Mazumder, *Trends in Welding Research. 4th International Conference; Gatlinburg, Tennessee; USA; 5-8 June,* pp. 75-86, 1995.

[119] N. L. Richards, X. Huang and M. C. Charurvedi, *Materials Characterization,* vol. 28, no. 3, pp. 179-187, 1992.

[120] O. Idowu, O. Ojo and M. Chaturvedi, *Materials Science and Engineering A,* Vols. 454-455, pp. 389-397, 2007.

[121] A. Matsunawa and S. Katayama, *ASM Conference Proceedings: Joining of Advanced and Specialty Materials,* pp. 8-15, 2001.

[122] A. G. Paleocrassas and J. F. Tu, *Journal of Materials Processing Technology,* vol. 210, no. 10, pp. 1411-1418, 2010.

[123] A. Egbewande, R. Buckson and O. Ojo, *Materials Characterization,* vol. 61, no. 5, pp. 569-574, 2010.

[124] C. Boucher, D. Varela, M. Dadian and H. Granjon, *Revue de Metallurgie. Cahiers D'Informations Techniques,* vol. 73, no. 12, pp. 817-832, 1976.

[125] K. Shinozaki, X. J. Lou, H. Ariyoshi and H. Kuroki, *Trends in Welding Research: Proceedings of the 5th International Conference,* pp. 775-780, 1998.

[126] G. Zhiguo and O. A. Ojo, *Journal of Materials Science Research,* vol. 1, no. 2, pp. 42-55, 2012.

[127] X. Huang, N. Richards and M. Chaturvedi, *Materials and Manufacturing Processes,* vol. 19, no. 2, pp. 285-311, 2004.

[128] W. S. Pellini, *Foundry,* vol. 8, no. 11, pp. 192-199, 1952.

[129] P. P. Puzak, W. R. Apblett and W. S. Pellini, *Welding Journal,* vol. 35, no. 1, pp. p 9s-17s, 1956.

[130] L. Karlsson and H. Norden, *Acta Metallurgica,* vol. 1, pp. 13-24, 1988.

[131] X. Huang, M. Chaturvedi, N. Richards and J. Jackman, *Acta Materialia,* vol. 45, no. 8, pp. 3095-107, 1997.

[132] O. Idowu, O. Ojo and M. Chaturvedi, *Welding Journal (Miami, Fla),* vol. 88, no. 9, pp. 179s-187s, 2009.

[133] M. Qian and J. C. Lippold, *Welding Journal (Miami, Fla),* vol. 82, no. 6, pp. 145s-150s, 2003.

[134] W. A. Baeslack III and D. E. Nelson, *Metallography,* vol. 19, no. 3, pp. 371-379, 1986.